AD-A199 592 CLOUD/MESOSCALE MODEL DEVELOPMENT AND APPLICATION STUDIES(U) COLORADO STATE UNIV FORT COLLINS DEPT OF ATMOSPHERIC SCIENCE W R COTTON ET AL. 30 SEP 87 1/2

UNCLASSIFIED AFGL-TR-87-0219 F19628-84-C-0005 F/G 4/2 NL

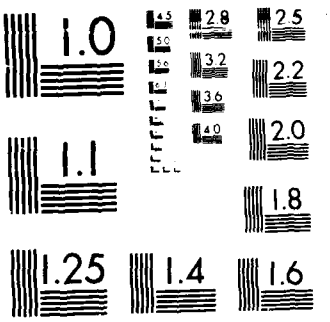

AFGL-TR-87-0219

Cloud/Mesoscale Model Development and Application Studies

William R. Cotton
Gregory J. Tripoli

Contributors:
Piotr Flatau
Craig Tremback
Jerry Schmidt
Kevin Knupp

Colorado State University
Department of Atmospheric Science
Ft. Collins, Colorado 80523

September 30, 1987

Final Report
21 October 1983 - 20 June 1987

AIR FORCE GEOPHYSICS LABORATORY
AIR FORCE SYSTEMS COMMAND
UNITED STATES AIR FORCE
HANSCOM AIR FORCE BASE, MA 01731

"This technical report has been reviewed and is approved for publication"

ROBERT M. BANTA
Contract Manager

ARNOLD A. BARNES, JR.
Branch Chief

FOR THE COMMANDER

ROBERT A. McCLATCHEY
Division Director

This document has been reviewed by the ESD Public Affairs Office (PA) and is releasable to the National Technical Information Service (NTIS).

Qualified requestors may obtain additional copies from the Defense Technical Information Center. All others should apply to the National Technical Information Service.

If your address has changed, or if you wish to be removed from the mailing list, or if the addressee is no longer employed by your organization, please notify AFGL/DAA, Hanscom AFB MA 01731-5000. This will assist us in maintaining a current mailing list.

Do not return copies of this report unless contractual obligations or notices on a specific document requires that it be returned.

REPORT DOCUMENTATION PAGE

1a REPORT SECURITY CLASSIFICATION: Unclassified	1b RESTRICTIVE MARKINGS
2a SECURITY CLASSIFICATION AUTHORITY	3 DISTRIBUTION AVAILABILITY OF REPORT: Approved for public release; Distribution unlimited
2b DECLASSIFICATION/DOWNGRADING SCHEDULE	
4 PERFORMING ORGANIZATION REPORT NUMBER(S)	5 MONITORING ORGANIZATION REPORT NUMBER(S): AFGL-TR-87-0219
6a NAME OF PERFORMING ORGANIZATION: Colorado State University; 6b OFFICE SYMBOL (If applicable)	7a NAME OF MONITORING ORGANIZATION: Air Force Geophysics Laboratory
6c ADDRESS (City, State, and ZIP Code): Department of Atmospheric Science, Ft Collins, Colorado 80523	7b ADDRESS (City, State, and ZIP Code): Hanscom AFB, Massachusetts 01731
8a NAME OF FUNDING/SPONSORING ORGANIZATION; 8b OFFICE SYMBOL (If applicable)	9 PROCUREMENT INSTRUMENT IDENTIFICATION NUMBER: F19628-84-C-0005
8c ADDRESS (City, State, and ZIP Code)	10 SOURCE OF FUNDING NUMBERS: PROGRAM ELEMENT NO: 61102F; PROJECT NO: 6670; TASK NO: 12; WORK UNIT ACCESSION NO: DA

11 TITLE (Include Security Classification)
Cloud/Mesoscale Model Development and Application Studies

12 PERSONAL AUTHOR(S)
William R. Cotton, Gregory J. Tripoli

13a TYPE OF REPORT	13b TIME COVERED	14 DATE OF REPORT (Year, Month, Day)	15 PAGE COUNT
FINAL REPORT	FROM 10/21/83 TO 6/20/87	1987 September 30	150

16 SUPPLEMENTARY NOTATION

17 COSATI CODES			18 SUBJECT TERMS (Continue on reverse if necessary and identify by block number)
FIELD	GROUP	SUB-GROUP	Numerical cloud model; Ice parameterization; High level clouds; Aircraft icing

19 ABSTRACT (Continue on reverse if necessary and identify by block number)

The report summarizes research accomplishments in the following areas:

- Task 1: A 2D and/or 3D model study to define potential for aircraft icing.
- Task 2: A 1D version of the turbulence closure model and development of a cirrus cloud model.
- Task 3: Forecasting and diagnosis of extreme windshear and turbulence associated with thunderstorms.
- Task 4: Summary of CSU RAMS development.

20 DISTRIBUTION/AVAILABILITY OF ABSTRACT	21 ABSTRACT SECURITY CLASSIFICATION
☐ UNCLASSIFIED/UNLIMITED ☐ SAME AS RPT ☐ DTIC USERS	Unclassified
22a NAME OF RESPONSIBLE INDIVIDUAL: Robert Banta	22b TELEPHONE (Include Area Code): (617) 377-2948; 22c OFFICE SYMBOL: AFGL/LYC

DD FORM 1473, 84 MAR — 83 APR edition may be used until exhausted. All other editions are obsolete.

19. ABSTRACT (Continued)

In the case of Task 1 we show that supercooled liquid water in winter orographic clouds varies with the passage of cyclonic storms, the depth of the cloud system, and proximity to mountain slopes. Liquid water is also found near the tops of the cloud system and at temperatures between -10 and -12°C where liquid water depletion processes are not very efficient. There is also evidence of multiple layering of liquid water in orographic clouds.

Sensitivity studies with the RAMS cloud microphysical module reveals the extreme nonlinearity of the microphysical system. A seemingly innocent adjustment in crystal concentration prediction can lead to a large response in aggregation rates. Large changes in aggregation rates, in turn, affect liquid water content since liquid water is the residual between production of condensate by wet adiabatic ascent (as radiational cooling) and loss by vapor deposition and accretional growth of ice crystals. Aggregation plays an indirect, though important, role in tipping that balance. We have made substantial leaps toward the understanding of what factors and parameterizations are of significance to the prediction of supercooled liquid water content. At this time, however, we do not have the capability of skillfully predicting supercooled liquid water in a variety of cloud situations. We also note that it may be necessary to predict liquid water in the size-range 50-100 μm in order to predict aircraft icing conditions reliably.

In the case of Task 2, a 1D higher order closure model has been developed and we have reviewed the literature regarding the properties of upper-level clouds. A major focus in the recent work has been on formulating a new radiation parameterization suitable for ice-phase, high-level clouds. The microphysical module has also been modified to accomodate the unique properties of cirrus clouds. As a first step in this direction the microphysical model has been formulated in a unified approach which allows the use of a number of different basic functions for the size-distributions of drops and ice particles and well as predict the concentrations of hydrometeor species.

In the case of Task 3, we have identified two convective storm downdraft branches which contribute to strong low-level shears and turbulence. One branch called the mid-level branch is predominant during the mature storm phase. The strength of the latter branch is controlled by the stability of the atmospheric boundary layer air ahead of the storm. Other factors, such as precipitation size and phase, exert a strong control on downdraft strengths. In some environments, melting can account for 60% of the cooling of downdraft air. We have also found that as much as 30% of all MCC events produce severe winds with the strongest events exceeding 45 ms^{-1}.

In Task 4, we describe major changes in the CSU RAMS. Some of the most significant changes include implementation of flexible interactive-nested grid scheme allowing an indefinite number of nests, implementation of hydrostatic option, revision of the preprocessor into Fortran 77 standard allowing greater model portability, and alteration of the vectorization permitting faster execution time on computers requiring long vectors. The application of the hydrostatic version of RAMS to mesoscale convective complexes is also described.

TABLE OF CONTENTS

A-1

1.0 INTRODUCTION

In this report we summarize research accomplishments supported by AFGL under contract # F19628-84-C-0005. The report summarizes research accomplishments in the following areas:

- Task 1: A 2D and/or 3D model study to define potential for aircraft icing.
- Task 2: A 1D version of the turbulence closure model and development of a cirrus cloud model.
- Task 3: Forecasting and diagnosis of extreme windshear and turbulence associated with thunderstorms.
- Task 4: Summary of CSU RAMS development.

During the course of this contract, emphasis was shifted from one task to another in response to changes in Air Force needs, changes in project staff, and changes in staffing resulting from a slow-down in project spending. Initially Task 1 was perceived as a high priority item but as we progressed through our research, this area was perceived to be of lesser importance to the Air Force than other tasks. Likewise Task 3 was a major focus of this research during Kevin Knupp's dissertation study. Since completing his thesis this task has received lesser emphasis, though our analysis of Derecho-type events associated with MCCs suggests that it should remain an area of concern to the Air Force. Task 2 has undergone considerable evolution during this project. It initially started out with the intent of developing a simplified 1D model to predict cumulus cloud cover and middle and high clouds. The emphasis has shifted more to the physics (radiative properties and microphysics) of cirrus-type clouds and middle-level stratiform cloud using RAMS as the dynamic model. The shift in emphasis in Task 2 was in

response to a perceived change in Air Force interests and also the change in focus of Piotr Flatau's research interests. We hope to continue a focus in Task 2 under Air Force support. Task 4 is only briefly summarized here as the objective of this task was to keep AFGL personnel informed about changes and developments in RAMS on a regular basis. This has been accomplished through regular quarterly reports and personal discussions.

2.0 MODEL AND OBSERVATIONAL STUDIES RELATED TO DEFINING POTENTIAL AIRCRAFT ICING CONDITIONS

2.1 Introduction

As part of several ongoing research projects, using the RAMS modelling system as an investigation tool, we have studied the microphysical development of several different classes of cloud forms. As a result, we have been led to greatly improve our bulk microphysics parameterization and become aware of some of the more fundamental issues concerning aircraft icing. In this section, we review the progress we have made.

Our test bed for microphysics studies are observed orographic clouds. In particular, we have used results of the COSE (Colorado Orographic Seeding Experiment) run by Dr. L. O. Grant, of Colorado State University. This ongoing observational program has provided us with a substantial data base against which we can test our microphysics hypotheses. The overwhelming advantage of studying orographic clouds is that their dynamics are relatively stationary and deterministic; a simple function of the mean ambient wind. Parcel history can be observed spatially, varying as distance from the orographic barrier. With minimum uncertainty, we are thus able to compare our model

predictions directly to observations. This task is rather elusive when one considers the case of non-steady convective clouds.

2.2 Review of Previous Research

The liquid water content at any location in a cloud is the integrated consequence of several liquid water production processes (FP) and liquid water depletion processes (FD). Liquid water production is determined by the cooling rate of the air as it rises. The cooling rate, in turn, is primarily due to adiabatic ascent. Net radiative cooling is also a factor, at least in weaker wind situations in the mountains and in the more stratiform cloud systems. The major liquid water depletion processes below 0C are vapor depositional growth of ice crystals and riming by cloud droplets. The depletion rates are therefore a function of the concentration of ice particles, the temperature and habits of the ice particles, the cloud supersaturation and liquid water content.

Whenever FP $>$ FD, liquid water will accumulate in the cloud to levels that can be collected on airframe surfaces. If, however, FP $\leq$ FD, liquid water will be depleted so rapidly that only solid precipitation elements will be detectable. As a simple example of the competition between FP and FD, consider the diagram shown in Fig. 2.1 obtained by Chappell (1970) for orographic clouds. The figure illustrates estimated water production rates for airflow over the Climax, Colorado mountain barrier as a function of the 500 mb temperature in that region. Chappell used the 500 mb temperature as a crude index of the cloud top temperature in that region. As the cloud top temperatures and also cloud bases (because the bases are limited by the terrain height) become colder, saturation mixing ratios diminish,

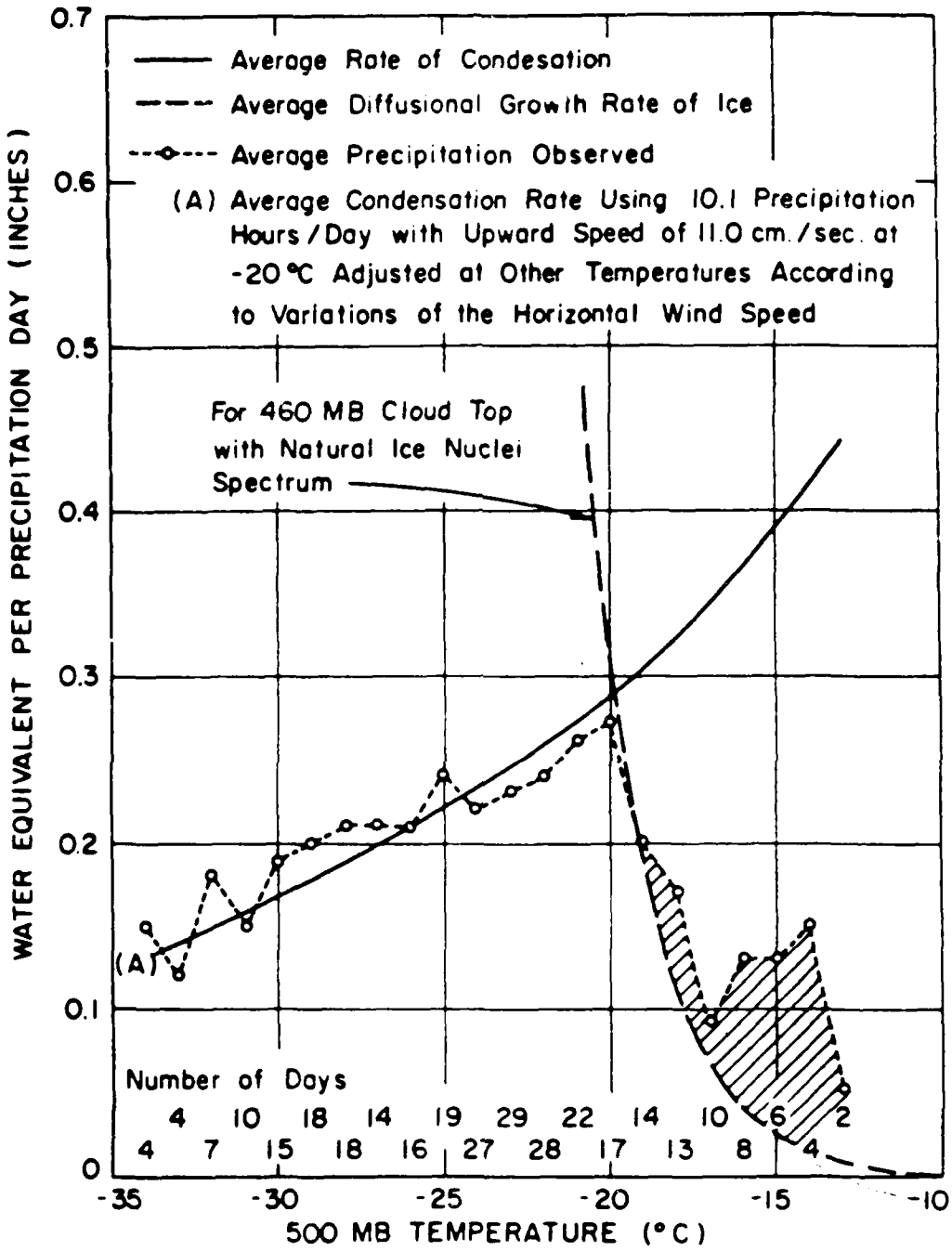

Fig. 2.1. Distribution of non-seeded precipitation at HAO as a function of 500 mb temperature compared to a theoretical distribution computed using the mean diffusional model. Precipitation data are from Climax I sample (251) and values are a running mean over a two-degree temperature interval. [From Chappell, 1970.]

thereby decreasing FP. The long-dashed curve illustrates Chappell's estimate of FD. Chappell assumed that the major depletion process was vapor deposition growth of ice particles. He also assumed that the concentration of ice crystals could be determined by the Fletcher ice nucleus spectrum. This figure illustrates that at temperatures warmer than -20 C, FP >> FD, thus the opportunities for significant liquid water production are large. At temperatures colder than -20 C, the more numerous ice crystals are able to deplete liquid water at a rate faster than it is being produced. Also shown in Fig. 2.1 are the observed surface precipitation rates. At temperatures colder than -20 C, the observed precipitation is comparable in magnitude to the calculated FP. This simply shows that at colder temperatures, FD is limited by FP and little excess liquid water is produced. At temperatures warmer than -20 C, the observed precipitation rate is considerably less than Chappell's estimate of FP, showing an opportunity for production of considerable liquid water. Note that the observed precipitation rate exceeds Chappell's estimate of FD. This is probably because Chappell assumed only vapor deposition contributed to FD whereas riming growth of ice crystals could have been significant at these warmer temperatures where high liquid water contents are likely. Also Chappell used the Fletcher ice nucleus curve which, as discussed below, is frequently a poor estimate of observed ice crystal concentrations at warmer temperatures because it does not consider the effects of ice multiplication.

The observed structure of the supercooled liquid water region in orographic clouds is quite variable and depends on the particular dynamical properties of the cloud system. As we shall see, the detection of supercooled water also depends on the particular water

sensing system.

Stable orograhic clouds

The simplest cloud system in which to interpret the behavior of supercooled water, is the "pure" orographic cloud system. This cloud system occurs over mountainous regions during periods when large-scale frontal activity is absent. They typically occur when a strong cross-barrier pressure gradient is present driving strong barrier-normal winds containing moist air. These are the cloud systems that are often well simulated by linear orographic flow models. As found by Hobbs (1973) over the Cascade Mountains of Washington, and Rauber (1985) over the Park Range of northern Colorado, supercooled liquid water is largest in regions of strong orographic forcing on the windward side of steep rises in topography. Rauber also noted that in some cases liquid water was observed to vary uniformly through the depth of the orographic cloud layer without any discernable changes in the dynamical properties of the cloud system. The only detectable change in cloud structure was a reduction in precipitation rate which indicated that variations in ice crystal concentrations may be responsible. The causes of such concentration variations are not well known, but the evidence presented by DeMott et al. (1986) suggests that enhanced nucleation of ice particles occurs in localized regions of high supersaturations associated with upward motions near cloud top.

Supercooled liquid water in orograhically-modified cyclonic storms

Variations in the distribution of liquid water in orographic clouds are frequently associated with variations in thermodynamic stratification, flow and vertical motion as cyclonic storm systems pass over the mountain barrier. Based on aircraft observations of liquid

water and microphysical structure of orographic clouds over the San Juan mountains of southern Colorado, Marwitz (1980) and Cooper and Marwitz (1980) identified four stages in thermodynamic stratification of a passing storm system. Unfortunately they did not identify these regimes with frontal boundaries or features of the Norwegian Cyclone model. This may be due to the fact that extra-tropical cyclones are so strongly altered in structure by the terrain features that classical warm fronts and cold fronts could not be unambiguously identified.

Nonetheless, they identified four stages in the evolution of the thermodynamic structure of the storm system shown in Fig. 2.2, which can roughly be identified with the passage of a cyclonic storm. Fig. 2.3 illustrates a conceptual model of the liquid water distribution for three of the four stages. During the "stable stage" which generally corresponds to the pre-frontal stage of a cyclonic storm, moisture supplied by the rising warm "conveyor belt" contributes to a deep stable cloud layer with cold tops. The cloud system is nearly completely glaciated, owing to the high ice crystal concentrations associated with the very cold cloud tops. Liquid water was observed only in short-lived patches where gravity waves penetrate transient regions of rapid ascent. Any liquid water that is produced is small, being less than 0.1 g/m^3. As can be seen from Fig. 2.3a, substantial blocking of the low-level flow is indicated during this period. As a cyclonic storm advances across the mountain barrier, the atmosphere transforms to near neutral stability through much of the depth of the troposphere. Liquid water contents rise to values on the order of 0.3 g/m^3 (see Fig. 2.3b). Following the passage of the 500 mb level trough and in some cases a discernable front, the atmosphere transformed to be

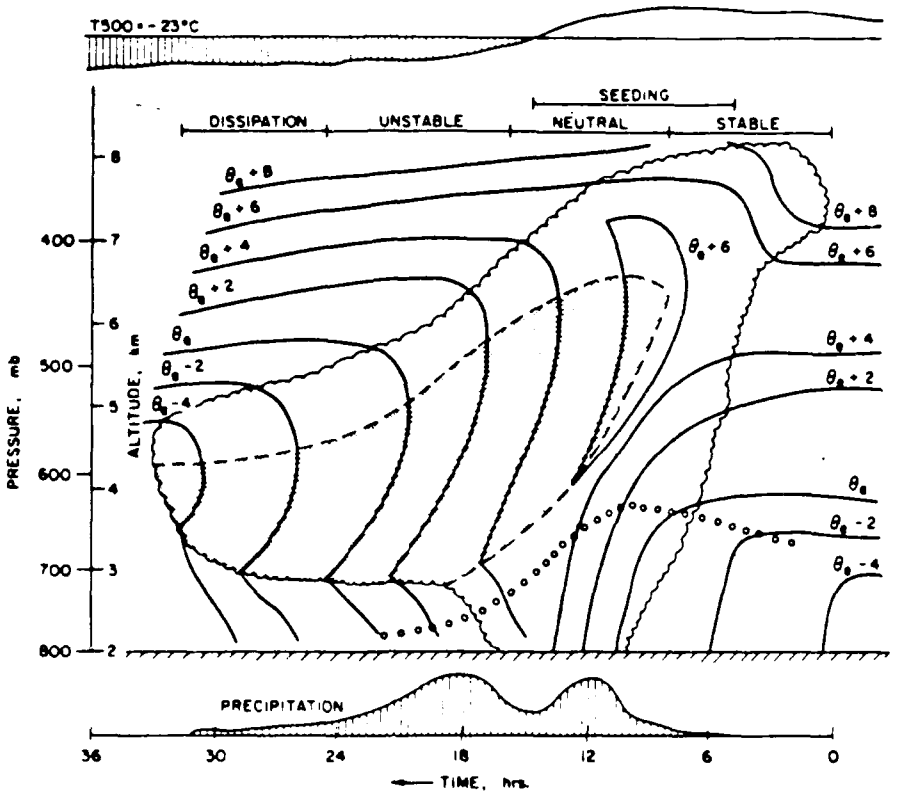

Fig. 2.2. Schematic height-time cross section for a typical storm over the San Juans. The solid lines are lines of constant equivalent potential temperature (θ_e), and the shaded area indicates convective instability. The typical sequence of 500 mb temperature is shown at the top. The reference baseline is -23°C. The level below which the wind directions are < 160° is indicated by circles and is defined as blocked flow. The four stages of the storm and a typical seeding period are indicated. [From Cooper and Marwitz, 1980.]

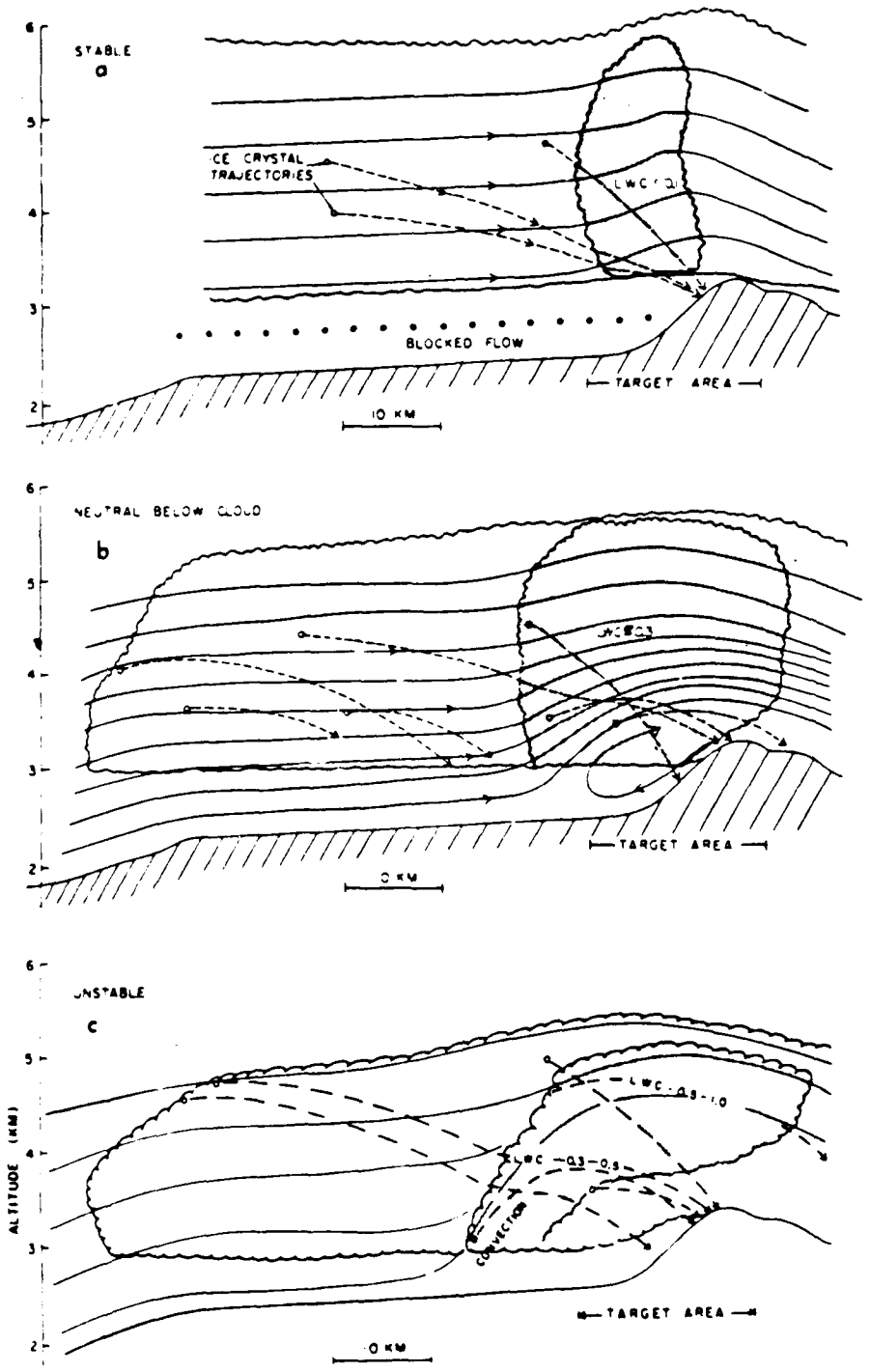

Fig. 2.3. Typical appearance of San Juan storms during the (a) stable, (b) neutral, and (c) unstable storm stages. The airflow is from the left at ~ 15 m s^{-1}. The shaded regions are regions where liquid water is generally found, and some typical liquid water contents (g m^{-3}) are indicated. Solid lines with arrows show air trajectories, and the irregular lines indicate cloud boundaries. Some typical ice crystal trajectories are also shown as dashed lines. The farthest downwind trajectory shows the fall of a hydrometeor with a terminal velocity of 1 m s^{-1}. [From Cooper and Marwitz, 1980.]

convectively unstable at lower levels upwind of the mountains where a surface zone of convergence was observed. Cooper and Marwitz reported that liquid water contents were highest during this stage of the storm system, approaching 1.0 g/m^3 in the upper cloud levels. Hobbs (1975) and Heggli et al. (1983) also found the highest liquid water contents in post-frontal convective clouds observed over the Cascade mountains of the state of Washington and the California Sierras, respectively. Like Cooper and Marwitz, their observations were primarily obtained by aircraft penetrations. One deficiency of aircraft observations is that for safety reasons, aircraft are limited to flying at heights 600 m to 1000 m above mountain tops. Also in the case of convective cells imbedded in stratiform cloud, time continuity of the convective cells cannot be obtained. Recently remote probing systems such as microwave radiometers (Hogg, et al., 1983) and polarization diversity lidar (Sassen, 1984) are providing an opportunity to sense the presence of liquid water in regions previously inaccessible by aircraft. We shall see that data obtained with these new observational systems is substantially altering our view of the distribution of liquid water in orographic clouds.

Using a combination of aircraft observations and passive microwave radar observations, Rauber (1985), Rauber et al. (1986) and Rauber and Grant (1986) have described the distribution of supercooled liquid water observed in the Park Range of northern Colorado during passage of extra-tropical cyclones. They noted that in the region just ahead of and during frontal passage, clouds are characterized by wide area stratiform regions with frequently superimposed deeper clouds and heavier precipitation. Many of the heavier precipitating regions are

convective but some occur in a stably stratified or neutral atmosphere. Liquid water production in the more stratiform region of the pre-frontal environment is strongly influenced by the orientation of the approaching front relative to the orientation of the mountain barrier. In the case of the Park Range, mid-level flow with a strong westerly component generates strong orographic lifting and is generally of higher moisture content. Convection was often observed in the pre-frontal environment. It was sometimes organized into a banded structure. Liquid water was found in the convective clouds during their initial stages of development. However, the liquid water was rapidly depleted by very efficient precipitation processes. In general, liquid water amounts reached a minimum within 15-20 minutes after the onset of convection.

The post-frontal clouds over the Park Range were also characterized by wide area stratiform regions. Orographic forcing is particularly strong because the typically strong westerly to northwesterly mid-level winds are normal to the barrier orientation. The highest liquid water amounts were found 10-15 km upwind of the barrier crest and reach a maximum over the windward slopes where the condensation supply rates are at maximum due to orographic lifting. Two regions of convective instability were observed in the post-frontal region. The first occurred just after frontal passage, and the second during the passage of the 500 mb level trough as the system dissipated. The distribution of liquid water in the post-frontal zone was complicated by the fact that superimposed on steady orographic production of liquid water was the more transient convective activity. Again the convection produced liquid water early in its lifecycle but rapidly produced substantial numbers of ice crystals that depleted liquid water in the convective

regions as well as the lower-level feeder regions.

Fig. 2.4 is a schematic illustration of the observed distribution of supercooled liquid water in (a) shallow orographic clouds, (b) deep stratiform cloud systems, and (c) convective region imbedded in a shallow stratiform cloud system. In all cloud systems liquid water was observed in the "feeder" zone directly upwind and over the barrier crest. A second region of liquid water was inferred between cloud base and the -10 C level. In this region, planar crystals falling into it do not grow rapidly by vapor deposition growth. Also the more rapidly growing needles and columnar form of crystals were characteristically absent. Thus the liquid water depletion mechanisms (FD) were at a minimum, yet water production (FP) at these warmer temperatures was quite high. A third region near the tops of the clouds illustrated in Fig. 2.4 is also a region of frequent liquid water occurrence. Rauber and Grant (1986) argued that this zone of liquid water is a result of an imbalance between liquid water production by adiabatic cooling and depletion by vapor deposition. They argued that large ice crystals capable of extracting large quantities of vapor as they grow (and hence depleting liquid water by the Bergeron-Feindeisen process) rapidly settle out of the cloud top layer. Left behind are numerous small ice crystals which are incapable of extracting water substance at the rates being supplied by adiabatic ascent. Another possible contribution to the observed liquid water near cloud top is that liquid water production could be intensified by radiative cooling. Radiative cooling rates estimated with the Chen and Cotton (1986) stratocumulus model suggest that it can approach 200^{o}C/day in a layer of 5 mb thickness near cloud top. For moist adiabatic ascent, the cooling rate (CR) is

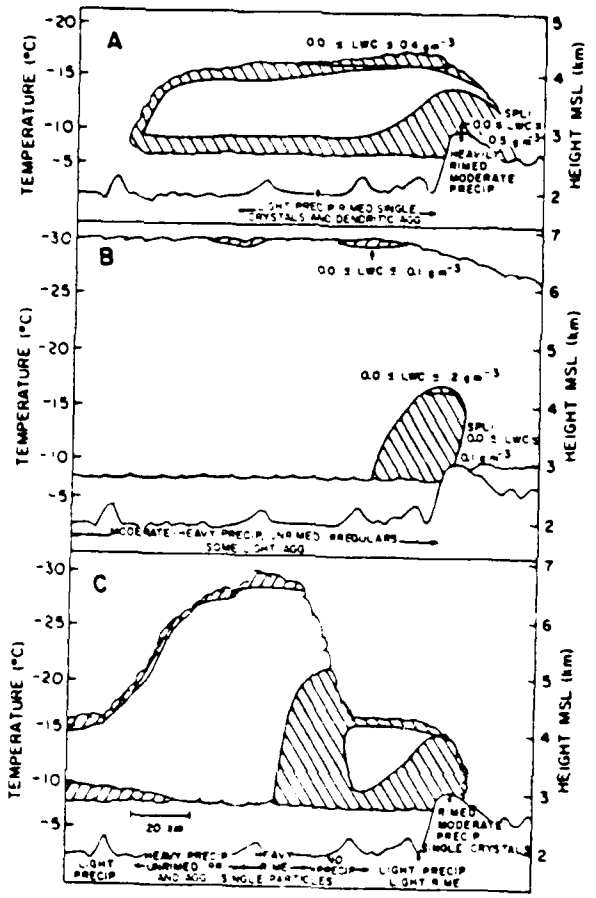

Fig. 2.4. Conceptual models of supercooled liquid water distribution in Park Range cloud systems for (A) a shallow stratiform cloud system with a warm cloud top temperature (CTT > -22°C); (B) a deep stratiform system with a cold cloud top temperature; and (c) a deep convective region embedded in a shallow stratiform system. The characteristic precipitation type is listed for each case along the bottom of the figure. Magnitudes of liquid water contents measured with aircraft or at SPL are shown on the figure. [From Rauber and Grant, 1986.]

$$CR = 665w \ ^{o}C/day,$$

where w is the vertical motion in meters per second. Thus an updraft of 0.3 m/s is required to produce the same amount of cooling and liquid water as cloud top radiation. Cloud top radiative cooling can therefore contribute to an imbalance between FP and FD. Radiative cooling is probably relatively more important in the more stratiform cloud region that blankets the upwind side of the barrier.

Observations of supercooled liquid water over the Sierra Nevada

Aircraft observations of supercooled liquid water in winter cloud systems over the Sierra Nevada (Heggli et al., 1983; Lamb et al., 1976) suggested that the largest amounts of supercooled liquid water resided in convective towers. More recent observations using passive microwave radiometers as well as observations of heavily rimed ice crystals from shallow orographic clouds led Reynolds and Dennis (1986) to conclude that the shallow non-convective clouds contain substantial amounts of supercooled liquid water. Heggli (1986) noted that about 75% of the time saturated clouds, possibly containing liquid water, existed below minimum aircraft flight altitudes. Heggli noted that the vertical distribution of liquid water was bi-modal. A low-level maximum was observed between -2 and -4 C and a secondary maximum similar to that observed by Rauber and Grant (1986) occurred between -10 and -12 C. Heggli also noted that supercooled liquid water did not always occur in single layers. They often observed that supercooled liquid water occurred in multiple layers which were separated by 100m or more of unsaturated air. The mechanisms responsible for such layering of the liquid water zones, however, have not been identified.

Heggli and Reynolds (1985) and Reynolds and Dennis (1986)

interpreted the behavior of liquid water variations during the passage of cyclonic storms over the Sierra Nevada in terms of Browning and Monk's (1982) split-front model shown in Fig. 2.5. Following the passage of the frontal rainband where the heaviest precipitation was observed, a shallow orographic cloud, often of the form of a stratocumulus cloud, prevails. It is in the shallow orographic cloud layer that the highest sustained liquid water contents are observed. Reynolds (1986) attributed this rise in supercooled liquid water to the disappearance of ice crystals settling from higher clouds. In terms of the "seeder-feeder" mechanism, the deep clouds which prevail during the passage of the elevated frontal band yield an environment that is very favorable for the operation of the seeder-feeder process. High-level feeder crystals readily deplete liquid water being generated by the lower-level, imbedded orographic feeder clouds. Following the passage of the frontal rainband, only shallow cloud layers prevail thus essentially shutting down the seeder-feeder process. This is consistent with Kuciauskas' (1986) observation that substantial supercooled liquid water content amounts occurred several hours following the passage of the elevated cloud layer.

In summary, we have seen in this section, that supercooled liquid water in winter orographic clouds is quite variable in its spatial and temporal distribution. It varies with the passage of cyclonic storm systems, the depth of the cloud system, and proximity to mountain slopes. Liquid water is also found near the tops of the cloud system and at temperatures between -10 and -12 C where liquid water depletion processes are not very efficient. There is also evidence of multiple layering of liquid water in some orographic clouds. The mechanisms

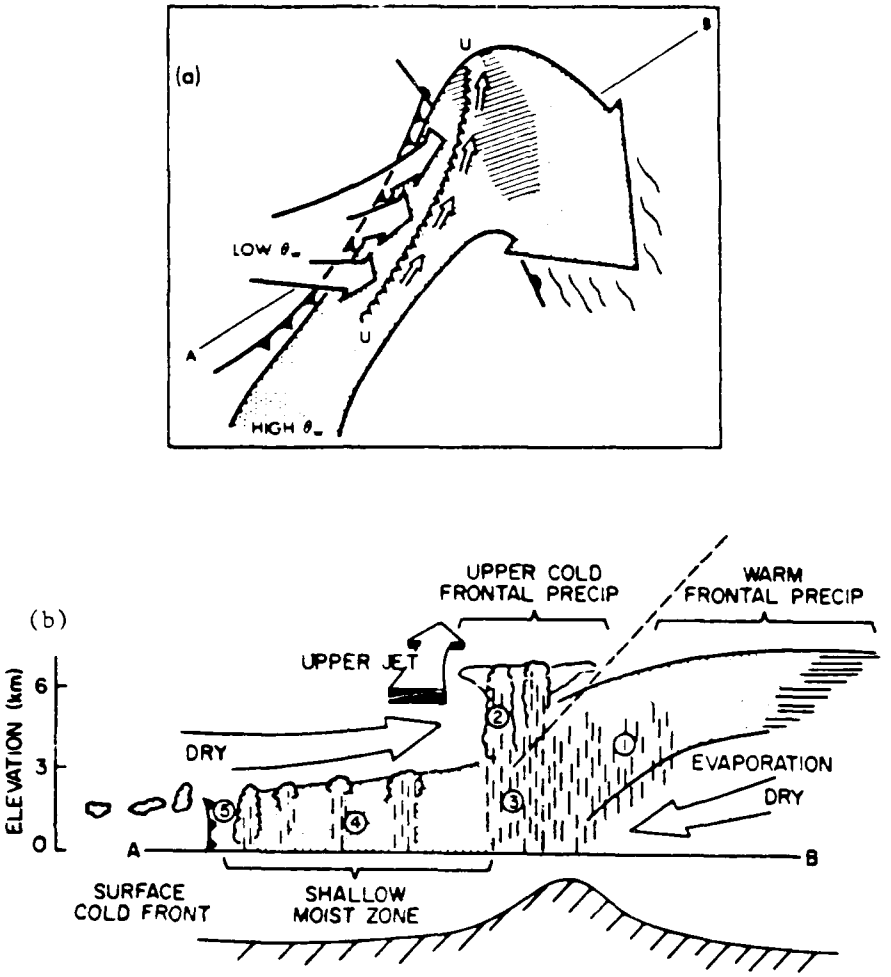

Fig. 2.5. Schematic portrayal of a split-front with the warm conveyor belt undergoing forward sloping ascent, but drawing attention to the split front characteristic and the overall precipitation distribution: (a) plan view, (b) vertical section along AB in (a). In (a) UU represents the upper cold front. The hatched shading along UU and ahead of the warm front represents precipitation associated with the upper cold front and warm front, respectively. Numbers in (b) represent precipitation type as follows: 1, warm frontal precipitation; 2, convective precipitation-generating cells associated with the upper cold front; 3, precipitation for the upper cold frontal convection descending through an area of warm advection; 4, shallow moist zone between the upper and surface cold fronts characterized by warm advection and scattered outbreaks of mainly light rain and drizzle; 5, shallow precipitation at the surface cold front itself. [Adapted from Browning and Monk, 1982, Browning, 1985, and Reynolds and Dennis, 1986.]

responsible for such layering of liquid water are not known at the present time, however.

2.3 RAMS Model Development Appropriate to Aircraft Icing Studies

In the past several years, we have centered our microphysical work around the investigation of the aggregation process. Rauber (1985) concluded in his study of COSE data that aggregation was a highly misunderstood but extremely important phenomena which greatly modulates the precipitation process. Our work investigating MCCs (Mesoscale Convective Complexes) also reveals a great importance of aggregation in extensive stratiform anvil-like clouds to the overall precipitation process (Yeh et al., 1987).

Our need to model the aggregation process led us to develop a crystal concentration and aggregation prediction scheme published by Cotton et al. (1986). Our attempt to adjust the prediction scheme to match observations proved difficult. As part of this investigation, we participated in the International Cloud Modeling Workshop, held in Irsee, F.G.R. in 1985. As part of that workshop we attempted to simulate a "blind" observed orographic seeding case in order to demonstrate the true skill of our prediction scheme. Rauber selected a blind case where aggregates did not form in order to see if we could properly sense the conditions for aggregation. Although we were able to adjust the model to match an open case study, our attempts at the blind case study met with failure in that aggregates were predicted. At this time, we are attempting to learn more about aggregation so that we can build the needed skill into our parameterization.

This ongoing study has illustrated the great non-linearity of this microphysical process. A seemingly innocent adjustment in crystal

concentration prediction can lead to a large response in aggregation. The reactions to the changes we make are seldom intuitively obvious until investigated in detail. As was shown in section 2.2, liquid water content is a residual between production of condensate cooling of moist air and loss by depositional and accretional growth of ice crystals. Aggregation plays an indirect but significant role in tipping that balance. We find that aggregation rapidly depletes the number of ice crystals so that despite increased riming, less depositional ice growth leads to the existence of greater liquid water. From observations, Rauber (1985) demonstrated that liquid water tends to form at cloud top. He hypothesized this may be due to the depletion of ice crystals by precipitation at cloud top again tipping the balance toward growth of cloud water. More recently, Cotton (see Cotton and Anthes, 1987) suggested that longwave radiation divergence at cloud top may also assist in tipping the balance toward production of liquid water there. This is currently being investigated.

Our recent observational studies of MCC stratiform rain have suggested that aggregation may be occurring far more frequently than we have yet realized. Yeh et al. (1987) have found a significant aggregation process at temperatures colder than -12C. Passarelli (1978) and later Rauber (1985) suggested mechanical interaction of dendrite crystals to be the dominant production mechanism, confining the process to the dentritic zone between -12 and -15 C. However, Rauber pointed out an important contribution by spatial dendrites at temperatures below -12 C in initiating the process.

We have become convinced that aggregation is a key element needed to predict all facets of microphysical structure. Perhaps supercooled liquid water content is the most sensitive to its prediction. The prediction of aggregation itself is highly sensitive to two primary factors. The first is the aggregation efficiency. The second is the distribution and number of crystals. This brings the ice crystal nucleation into the problem in a big way. Our best guess on sorption/depositional nucleation rates is an assumed movement along the empirically-derived Fletcher curve, which is only a function of temperature. We know little about how the nucleation rates vary with pressure, altitude, air mass, supersaturation, etc. Grant (personal communication) has pointed out that ice nucleus measurements during the CLIMAX experiment generally departed significantly from the Fletcher curve, being substantially less at temperatures colder than -20 C. Contact nucleation at least using Young's (1974) model also does not appear to be adequate. Thus, one of the central most important parameters to the aggregation process, i.e. crystal production by nucleation, still cannot be predicted within several orders of magnitude routinely. We suggest that more resources be placed toward the formation of theoretical and laboratory studies of models for all microphysical processes and, in particular, primary and secondary ice crystal production.

In studying our crystal concentration parameterization, we have selected several major problems in need of immediate attention. The most important is that we assume a single category for all pristine crystals. Because of the non-linear production rates with temperature suggested by the Fletcher curve, a numerical model rapidly becomes

dominated by the large numbers of small ice crystals initiated at temperatures colder than -25 C. In an updraft this essentially shrinks crystals which should be growing, ultimately inhibiting precipitation sedimentation back into lower levels. We have decided to improve the parameterization by further subdividing pristine crystals into snow-like crystals of relatively large size and terminal velocity and very small pristine crystals. This allows the coexistence of small and large crystals at cold temperatures, enabling the continuous growth of crystals in the updraft. Also, instead of a constant size distribution, we will assume a variable size distribution for the snow. Hence, we are now planning to consider crystals in their pristine form, mature precipitating form, aggregated forms as well as graupel particles.

At this point in the development of our microphysical model, we have found that the formulation has matured to the point where we are in need of a totally new approach to the code emphasizing user-friendliness, flexibility, and parallels between all of the formulations. We also found a need for transportability so that the code can be used with other dynamical models outside of our system. We are therefore now completing the development of a new generalized microphysical code capable of quick and significant changes in the scheme, and incorporating the newer physics described above. This parameterization will be defaulted to the original parameterization reported by Cotton et al. (1986), but is capable of instant modifications by the addition of new hydrometeor categories, alternate size distribution assumptions, alternate diagnostic and prognostic schemes for distribution parameters, and other physics modules. This

code became operational during the fall of 1987. We expect that it will greatly accelerate our rate of development.

In summary, our work in microphysics over the past several years has demonstrated that the existence of supercooled water and thus the potential for aircraft icing is perhaps one of the most difficult of all microphysical paramters to predict, primarily because it tends to exist as a residual of large rates of water production and large rates of precipitation removal processes. We have made substantial leaps toward the understanding of what factors are of significance. At this time, we do not have the capability to skillfully predict supercooled water, however we are continuing to work, both through observation and modelling, to achieve that goal. We also recognize that prediction of the amount of supercooled water is not the only requirement for aircraft icing conditions. The droplet spectra, particularly the presence of droplets in the size range 50-100 μm greatly aggrevates aircraft icing conditions. Unfortunately, this is precisely the size range that our model has the least skill in predicting the amounts of supercooled water. Another approach such as the multiple log-normal basis function approach of Clark and Hall (1983) may be required.

3.0 A 1D VERSION OF THE TURBULENCE CLOSURE MODEL AND DEVELOPMENT OF A CIRRUS CLOUD MODEL

3.1 Introduction

Research in this section began as an extension of the Chen and Cotton (1983) closure model to middle and high-level cloud systems. As a first step Flatau (1985) attempted to develop a level 2 or level 2.5 version of the model so that the number of predictive equations in a mixed-phase cloud system could be minimized. A paper entitled

"Comments on Realizability Conditions for the Mellor and Yamada Level 2.5 and 3.0 Model's" by Flatau and Cotton, has been accepted for publication (see Appendix 1).

Since this stage of research, the work has shifted more to refinements in the microphysics and radiation schemes in RAMS to make it more suitable for simulating cirrus clouds. The results of that work are described below.

3.2 Introduction and Background

Upper level clouds and large scale dynamics

Clouds composed of ice crystals (cirrus) occur frequently in the upper troposphere. They are related to a large scope of atmospheric phenomena. These phenomena include systems of convective origin such as Mesoscale Convective Systems (Chen, 1984; Maddox, 1981, 1983; Wetzel et al., 1983), anvils of severe thunderstorms in mid-latitudes (Heymsfield, 1986; Benetts and Ouldridge, 1984), and tropical anvils (Ackerman et al., 1987).

Cirrus clouds related to large scale synoptic-type situations are well-known to occur in a variety of situations. Jet-stream cirrus have been investigated (Conover, 1960), and the classical pre-frontal ice cloud conditions were studied by many (Starr and Cox, 1980; Heymsfield, 1977). A summary of such extratropical cyclone cloud systems is given in Cotton and Anthes (1987).

Morphology

Not only are high-level clouds related to different synoptic scales of motion, but they exhibit a wide range of morphological characteristics. Stratiform ice clouds associated with Mesoscale Convective Systems are quite common, but they are often inhomogeneous in

both the vertical and horizontal (Yeh et al., 1986), with varying degrees of embedded convection. Such embedded convective cells are probably most strikingly exhibited in cirrus uncinus, clouds which were subject of several studies (Heymsfield, 1972; 1975a,b). The convective nature of some high level clouds makes description of their bulk properties more complex, requiring modelling of smaller scale phenomena within an otherwise uniform, stratified system (e.g., Starr and Cox, 1985a,b). Idealized cases of stratified and uniform upper level clouds were modeled by Ramaswamy and Detwiler, 1986.

Microphysics

Variations in morphological characteristics are closely related to the microphysical constitution of such clouds. Cotton and Anthes (1987) in their forthcoming book on cloud physics summarized the microphysical properties as found by different authors. This is presented in Table I.

As summarized in Table I, cirrus clouds contain ice crystals of typical length 0.5 mm and in concentrations which vary widely from 10^4 to 10^6 m^{-3}. The terminal velocity of the ice crystals is about 50 cm s^{-1}, which is of the same order of magnitude as the updraft speeds. The ice water content of cirrus clouds is typically 0.2 g m^{-3}.

Just how representative these properties are of a typical cirrus cloud is uncertain as there is much natural variability in ice cloud structure. For example, it appears now that ice clouds exhibit quite complex structure as far as ice crystal spectrum: Platt (1987) investigated cirrus crystals in the 2.5 μm to 200 μm size range and showed that there is an abundance of the smaller particles. Heymsfield and Platt (1984) attribute up to 50% of cirrus extinction to very small particles (Fig. 3.1). The increasing abundance of remote sensing and in

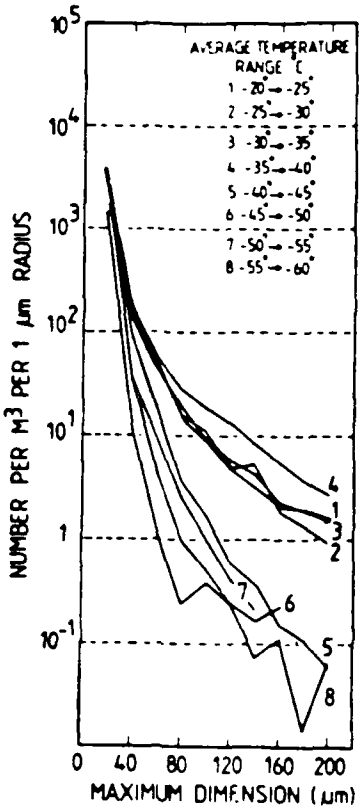

Fig. 3.1a. Average particle spectra in different temperature ranges for the 20-300 crystal maximum dimension. (From Heymsfield and Platt, 1984).

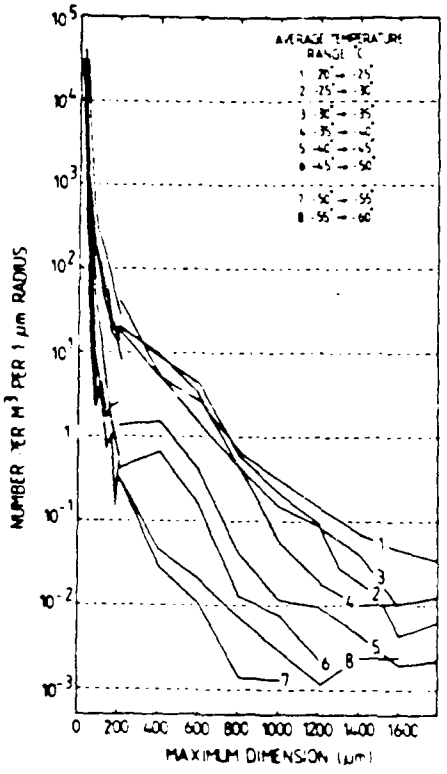

Fig. 3.1b. As in Fig. 3.1a, but for 20-1800 μm maximum dimension. (From Heymsfield and Platt, 1984).

situ measurements suggest that sub-visible ice elements may play a more important role than previously thought (Radke and Hall, 1983). Barnes

Table I. Microphysical characteristics of middle and high clouds.

Property or variable	Value	Reference
Concentration of ice crystals [m^{-3}]	10^5 - 10^6	Braham and P. Spyers-Duran (1967)
	$2x10^5$ - $5x10^5$	Heymsfield (1975a)
	$1.0x10^4$ - 2.5×10^4	Heymsfield and Knollenberg (1972)
	$6.0x10^5$ - 38.0×10^5	Ryan et al. (1972)
	$2.0x10^4$ - 8.0×10^4	Houze et al. (1981)
Length of crystals	up to 0.17 mm	Braham and P. Spyers-Duran (1967)
	0.6-1.0 mm	Heymsfield and Knollenberg (1972)
	length 0.35-0.9 mm	Heymsfield (1975a)
Terminal velocity of crystals	Typically 50 cm s^{-1} Max 120 cm s^{-1}	Heymsfield (1975a)
Ice water content (g m^{-3})	0.15-0.25	Heymsfield and Knollenberg (1972)
	0.15-0.30	Heymsfield (1975a)
	0.20-0.50	Rosinski et al. (1970)
Precipitation rate	0.5-0.7 mm/h	Heymsfield and Knollenberg (1972)
	0.1-1.0 mm/hr	Heymsfield (1975a)
Updraft velocity	1.0-1.5 m s^{-1} (in cirrus uncinus)	Heymsfield (1975a)
	2.0-10.0 cm s^{-1} (warm front overrunning)	Heymsfield (1977)
	20 cm s^{-1} (warm front occlusion)	Heymsfield (1977)
	25-50 cm s^{-1} (closed low aloft)	Heymsfield (1977)
Lifetime of individual cloud	15-25 min	Heymsfield (1975a)

(1982) finds two distinct types of thin cirrus at mid- and upper-tropospheric levels. The first type is very common and consists of concentrations of 10^3 - 10^4 m^3 and no particles larger than 100 μm. He found this type of size distribution 70% of the time while flying in

"clear" air at cirrus altitudes. Figure 3.2 shows large concentrations of small ice crystals in the cirrus clouds. Liquid water contents in thin cirrus can be expected to be about an order of magnitude less than those in Table I.

The crystal habits are of complex structure (Hemysfield and Knollenberg, 1972), with columnar, bullet-like crystal and bullet rosettes dominant. In the small crystal range, Platt (1987) notices that "there are suprisingly few differences between individual flights and between tropical and midlatitude cirrus, considering the wide range in locations and temperatures in which sampling took place." He observed Shimizu (1963) columns, needles, bullets and 'rimed' group crystals. Although there is much similarity between crystals shapes, the existing diversity poses formidable difficulty as far as calculating their single scattering radiative properties (see Section 2.2 for more details).

Despite the difficulty involved, some microphysical parameterizations of ice clouds have been attempted. For example, Cotton and his collaborators in the series of papers (Stephens, 1979; Tripoli and Cotton, 1982; Cotton et al., 1982; Cotton et al., 1986;) developed a parameterization scheme for ice processes which is in routine use in the RAMS cloud/mesoscale model. Other groups use a similar bulk microphysics approach (Hsie et al., 1980; Lin et al., 1980). This subject is discussed in detail in Cotton and Anthes (1987). Heymsfield (personal communication) developed a technique for diagnosing the ice water content and precipitation rate of stratiform clouds from radiosonde data. Such a scheme is currently being tested for use in NCAR's Community Climate Model.

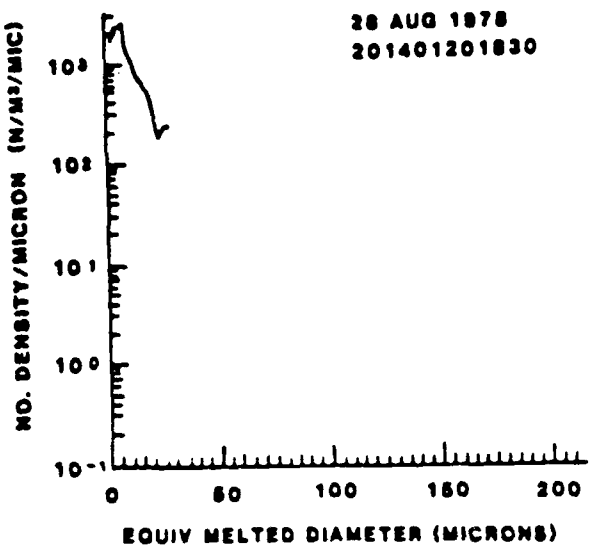

Fig. 3.2. Size distribution in Type 1 subvisible cirrus. The sampling instrumentation had good sensitivity for particles > 100 μm, but none were found. (After Barnes, 1982).

Figure 3.3 is a schematic of the complex microphysical interactions that come into play between different water classes. This interaction diagram is from Cotton and Anthes (1987) and shows how aggregates, graupel, ice, cloud droplets, and rain droplets interact through various physical processes. Recently, Tripoli et al. (1987) attempted to formulate a more general microphysical parameterization scheme for use in the new RAMS structure where all these interactions could be considered in a consistent way.

Radiative characteristics

Cirrus radiative properties influence incoming solar and outgoing planetary radiation (Freeman and Liou, 1979; Ou and Liou, 1984; Stephens, 1980a,b; Ramanathan et al., 1983), thus influencing the earth climate. It is recognized that a change in cloud cover will have a dramatic effect on the Earth's radiative budget. Even changes in atmospheric gases influence the radiative budget mostly through cloud feedback (Ramanathan et al., 1983).

Radiation plays an important role in clouds, and coupled with turbulence and microphysics, influences the dynamics of cloud systems. This was clearly established for stratocumulus clouds. Flatau (1985) and Chen and Cotton (1983), as well as other investigators, simulated off-shore California stratus with the coupled radiative, turbulence, and microphysical model, and they have shown radiation influences on heat and momentum fluxes. In another modelling study by Cotton's group, Chen (1984) and Chen and Cotton (1987) analyzed the instability on the top of the stratiform cloud and linked it with strong radiative forcing. It was found that cloud top entrainment is triggered by the vertical transport of turbulence kinetic energy and is further enhanced by

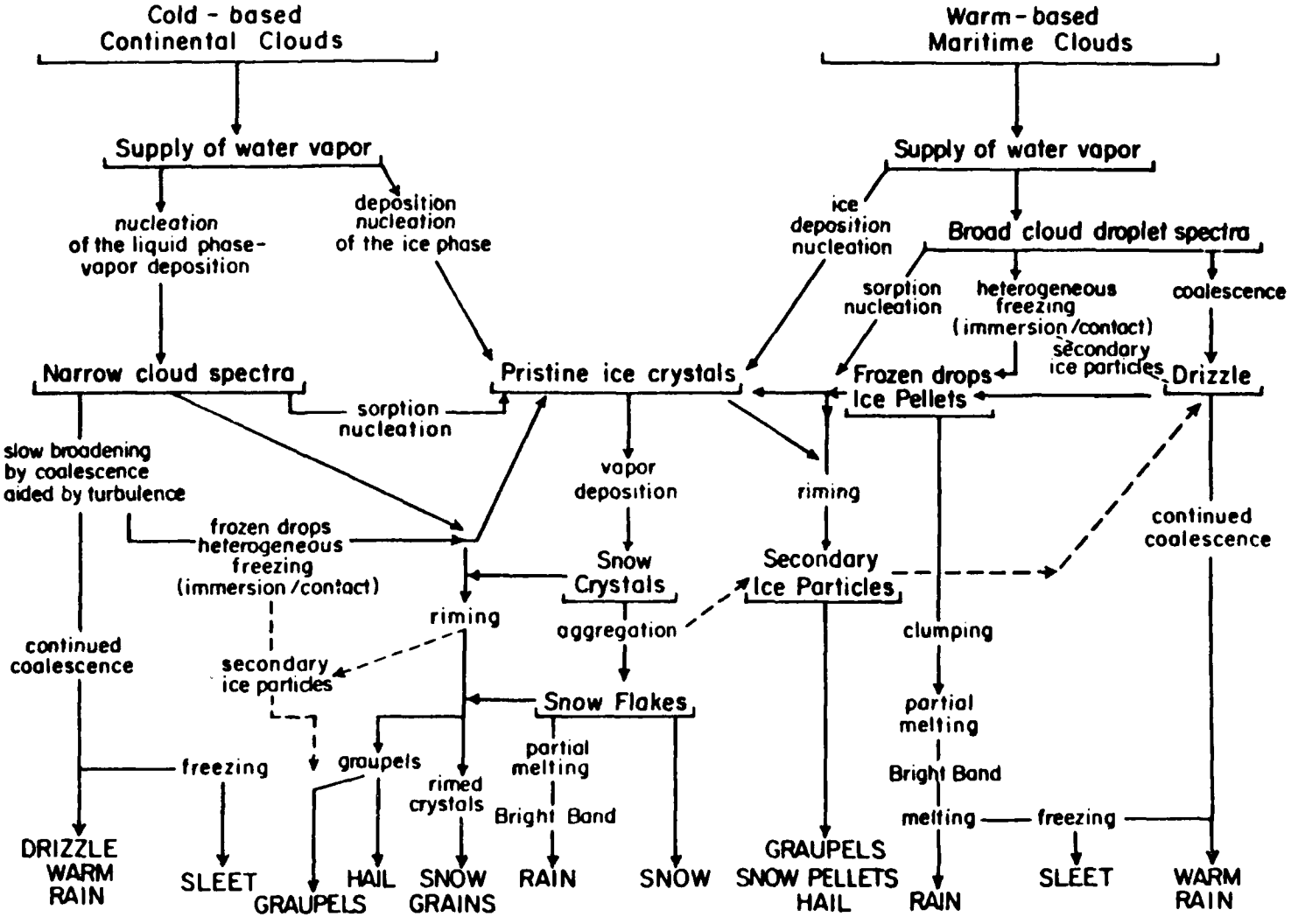

Fig. 3.3. Schematic flow diagram of RAMS microphysics parameterization scheme.

evaporative cooling. The energy driving the entrainment was initially produced by cloud-top destabilization caused by long-wave radiative cooling. In addition, it was found that the competition between shear and radiative cooling is the key to determining whether the cloud layer is shear-driven or buoyancy-driven. For the case with strong shear, the cloud top radiative cooling was found to be balanced by entrainment heating. Furthermore, the effect of shear may become important when the cloud top radiative cooling is weakened by large scale subsidence, the presence of high level clouds, or a moist layer above the capping inversion.

Radiation was also linked with strong dynamical effects in Mesoscale Convective Systems through interaction with its extensive, stratiform anvil (Chen, 1986; Chen and Cotton, 1987). Recently, Tripoli (1986; Tripoli and Cotton, 1987) has proposed that cloud-top radiative cooling traps gravity wave energy beneath the cirrus canopy of an MCS. The resultant trapped waves play a crucial role in the up-scale development of a MCS into a mesoscale convective complex.

Clouds also provide a large atmospheric target for backscattering to lidar systems (Radke and Hall, 1983) and will therefore generally play a beneficial role in the operation of wind sensing lidars unless the signal is too strongly attenuated.

Numerical modelling

(a) Radiation models

Up to now, most (but not all) of the cirrus cloud models concentrated on the radiative part of the problem without much consideration to dynamics and microphysics. For example, Stephens (1980a,b) used a doubling and adding model to solve the Radiative

Transfer Equation (RTE) and presented results of radiative properties of cirrus clouds in the IR region. He considered two types of ice particles, cylinders and spheres, but assumed a mono-disperse spectrum for the broad-band calculations. His results indicate that reflectance of cirrus clouds is small, but strongly influence cloud heating profiles. The reflectance itself is governed by cloud microphysics.

Roewe (1977) and Roewe and Liou (1978) used the discrete-ordinate method (DOM) to solve the RTE in cirrus clouds. In their study, the impact of high level cirrus clouds upon the infrared cooling of the atmosphere was investigated. Band by band cooling was calculated for all major gaseous absorption bands including water continuum. In addition, the influence of a low level cloud on the infrared cooling was investigated in the presence of cirrus clouds of varying thickness. DOM is applied to non-isothermal, inhomogeneous cloudy atmospheres. They assumed that cirrus clouds contain a mono-disperse spectrum of randomly oriented crystals in a horizontal plane. The crystals are long circular cylinders with a mean length of 200 μm, 30 μm in radius, and 0.05 cm^{-3} mean concentration.

Liou (1972) used a simple two-stream model to calculate reflection, transmission, and absorption of several cirrus cloud layers as a function of the solar zenith angle in the visible and near infrared portion of the solar spectrum. He used single scattering properties of ice as determined by his earlier works (Liou, 1972a,b).

Welch et al. (1980a,b) used a two-stream model to calculate the variability of ice cloud radiative properties at selected solar wavelengths. The modified gamma distribution

$$n(L) = aL^{\alpha} \exp\left[-\frac{a}{\gamma}\left(\frac{L}{L_c}\right)^{\gamma}\right]$$

was used for crystal size distribution. Several crystal shapes were assumed, but the treatment of non-sphericity was rather approximate in the calculations. One of the conclusions was that the particle size distribution may strongly influence reflectance, transmittance, and absorptance for wavelengths between 1.3 μm and 2.0 μm. They suggest that measurements of reflectance ratios may provide information about size spectra. Welch et al. (1980b) notice that radiative characteristics are extremely sensitive to the asymmetry factor g.

In addition to these detailed radiative studies, high level clouds were studied in relation to climate (Schneider et al., 1978; Stephens and Webster, 1979; Ramanathan et al., 1983).

(b) Coupled Radiative-Dynamical model

To our knowledge, there are two recent models where upper level cloud dynamics and radiation are considered. These are described in papers by Starr and Cox (1985a,b) and Ramaswamy and Detwiler (1986). Ramaswamy and Detwiler (1986) used a 1D model of monodispersed, randomly oriented ice crystals. Transfer of radiation is modeled with the two stream model. Fifty-six spectral intervals are considered. The equivalent sphere assumption was made to obtain single scattering albedo. The cloud is located between 10 and 11 km in a model atmosphere. Simplified thermodynamics was considered with evaporation and condensation processes influencing crystal evolution. One of the findings was that radiative properties are dependent on crystal concentrations and crystal length. The simulated cloud resembles cirrostratus, but the authors note "comprehensive understanding of

cirrus cloud will require detailed treatments of both microphysics and convection."

A two-part paper by Starr and Cox (1985a,b) is probably the most comprehensive to date. The model has four prognostic equations: 1) potential temperature, 2) water vapor specific humidity, 3) ice water content, and 4) vorticity. Phase changes are evaluated every five minutes. Bulk microphysics parameterization is used with only one class of ice. Depending on ice water content this ice class changes its characteristics (terminal fall speed, etc.). Radiation is represented by broadband infrared and broadband shortwave. The environmental vertical velocity can be imposed and different environmental conditions (thermodynamics) are possible. The diurnal cycle is studied. This 2D model with a 100 m grid predicts generating zones for cirrus, and dynamics of generating zones can be quantitatively studied. Crystal habit and size distribution are found to be quite important in determining the overall water budget.

3.3 Summary of Work Accomplished Using RAMS

In this section we summarize work accomplished using RAMS and supported by the AFGL. Two modules, radiation and microphysics, and the work related to their "fine tuning", are described here. First we describe the current radiation module (Section 3.3.1). Next we summarize current work on establishing more reliable reflectance and transmittance information for upper level clouds from knowledge of single-scattering albedo (Section 3.3.2). Subsequently new developments into multiscattering code are described (Section 3.3.3). Finally, the generalized microphysics package (Section 3.3.4).

3.3.1 Current radiation scheme

Details of the present radiation employed in RAMS has been described elsewhere (Chen and Cotton, 1983). We present only a brief outline of that scheme with particular emphasis on how radiation-cloud interactions are treated and on the improvements required to apply the parameterization to ice crystals.

The current radiation scheme is based on the adding method for shortwave and the emissivity approach for longwave radiation. Both molecular gases and water absorption are considered. The reflectance and transmittance parameterization is based on the two-stream solution with empirical modifications (Stephens, 1978b).

(a) Shortwave parameterization

The shortwave radiation parameterization is based on the adding method. Only the net upward F↑ and downward F↓ components of radiation are considered, independent of wavelengths. Fig. 3.4 illustrates a simple layered two-stream model based on a model developed by Stephens and Webster (1979) and Stephens (1978a,b). For such a model, the fluxes can be written as

$$F\downarrow(n+1) = Re(1,n+1)\, F\uparrow(n+1) + V\uparrow(n+1/2) \qquad (3.1)$$

and

$$F\uparrow(n) = \frac{Tr\uparrow(n)\, F\uparrow(n+1)}{1-Re(1,n)Re(n)} + V\uparrow(n+1/2) \quad , \qquad (3.2)$$

where n represents the layer under consideration. The convention that is used has n increasing downward with greater optical depth. Re(n), A(n) and Tr(n) represent, respectively, the reflectance, absorptance and transmittance in the nth layer. The reflectance Re(1,n-1) represents

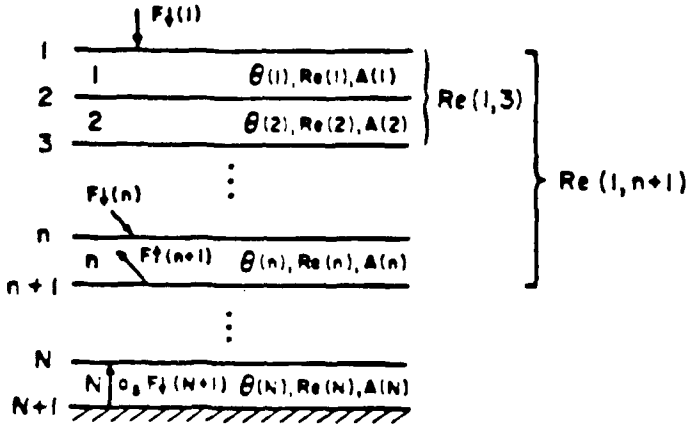

Fig. 3.4. The short-wave radiative model, F↓ and F↑ denote downward and upward fluxes. Re(n) and A(n) represent respectively the reflectance, absorptance at the nth layer. Re(1,n+1) is the multiple reflectance from all layers above the (n+1)th layer. (From Stephens and Webster, 1979).

the combined multiple reflectance contributed by all layers above the (n+1)th layer and the additive terms $V^{\uparrow\downarrow}(n+1/2)$ represent the contributions of sources of radiation multiply scattered by each layer. Details of the algorithms that generate these multiple scattering factors can be found in Stephens and Webster (1979).

The major aspect of the shortwave parameterization is the specification of the individual layer reflectances and transmittances. This is a fairly straightforward task for the clear sky (e.g., Stephens and Webster, 1979), but is more complicated for a cloud layer. The approached used for cloud is based on that of Stephens (1978b) who employed a two stream model as a basis for determining Re(n) and Tr(n).

The most important parameter in such a model is the optical thickness τ_N of the cloud layer. Estimates of τ_N range from $5 < \tau_N < 500$. Formally, the optical thickness varies with wavelength. Thus,

$$\tau_N(x) = \int_0^{\Delta z} \int_0^{\infty} f(r)\, Q(x)\pi r^2 dr dz \quad , \tag{3.3}$$

where $x = 2\pi r/\lambda$, f(r) represents the droplet spectral density function and Q(x) is an efficiency factor for extinction which can be determined from Mie theory. Stephens concluded from his model calculations that the primary factor controlling τ_N is the liquid water content (LWC) of the cloud. Changes in the drop-size distribution were masked by the large variations in LWC. He thus approximated τ_N as

$$\tau_N \simeq 3/2\ W/r_e \quad , \tag{3.4}$$

where r_e (micrometers) is an effective radius of the droplet

distribution defined as

$$r_e = \frac{\int_0^\infty r^3 f(r)dr}{\int_0^\infty r^2 f(r)dr} \qquad (3.5)$$

and W is the liquid water path LWP (gm^{-2}). The LWP is defined as

$$\text{LWP} = W = \int_0^{\Delta\zeta} \rho_o r_c \, dz \quad . \qquad (3.6)$$

where r_c is the cloud water mixing ratio. Two other optical properties (in addition to optical thickness) are required to complete the specification of Re and Tr. They are the single scatter albedo $\bar{\omega}_o$ and backscatter factor. These are also related to cloud liquid water content in the scheme of Stephens (1978b). Therefore the shortwave characteristics of the cloud layer are completely specified by cloud LWC and solar geometry.

(b) Longwave scheme

The longwave scheme is based on the emissivity approach. This method is somewhat traditional for clear sky calculations and the approach used follows that of Rodgers (1967) with the modification suggested by Stephens and Webster (1979) to account for the effects of water-vapor-pressure-dependent absorption in the spectral region $8\mu m < \lambda < 13\ \mu m$. Clouds in the longwave region are treated in the same manner using the concept of effective emissivity. This quantity treats the scattering process as if it were an absorbing process thus providing a

modification to the true emittance of the cloud. Using detailed spectral model calculations of IR transfer through low-level clouds, Stephens (1978) parameterized the effective emissivity as

$$\varepsilon^{\uparrow\downarrow} = 1 - \exp\ (-a_o^{\uparrow\downarrow} W) \quad , \tag{3.7}$$

where W is the liquid water path $W = \int \rho_o\, r_l\, dz$. and r_l represents the mixing ratio of all condensed water. He evaluated the coefficients for upward and downward emissivity as

$$a_o^{\uparrow} = 0.13 m^2 g^{-1} \text{ and } a_o^{\downarrow} = 0.158 m^2 g^{-1} \quad .$$

The coefficients $a_o^{\uparrow}$ and $a_o^{\downarrow}$ correspond to a mass absorption coefficient which may be compared to the values of α_T used by Cliver et al. (1978). As mentioned previously, Stephens found little variation in $a_o^{\uparrow}$ and $a_o^{\downarrow}$ with changes in drop size distributions.

The combined long- and short-wave radiative properties of clouds are thus jointly derived in this scheme from cloud LWP. Therefore both the long- and short-wave radiative properties change in a related manner when LWP is varied. This coupling of the cloud radiative properties through the LWP is an important feature of the scheme enabling the proper evaluation of the total radiative budget of any given cloud layer and the variation of this energy budget with changing cloud properties.

There are a number of complications and uncertainties that arise when applying this scheme to ice clouds. These are:

(1) The relationship of optical thickness and $\bar{\omega}_o$ to ice water path (IWP) has not been established and simple application of these relationships based on liquid water cloud is not appropriate.

(2) The coefficients appearing in the emissivity parameterization (3.7) are uncertain for ice clouds. This uncertainty is aggravated by non-negligible effects of scattering by ice particles in the IR region.

(3) It is not possible to use more complex theory unambiguously to provide the required parameteric relationships as was the case for water clouds. The intrinsic scattering properties of ice crystals in the atmosphere remains uncertain due to complexities in shape, orientation, density, size and concentrations. We thus need to rely more heavily on observations in cirrus and ice clouds (such as will be provided by the FIRE data set) to establish confidence in the scheme.

3.3.2 Single scattering for hexagonal ice crystals

In the previous section we described the radiative code currently used in RAMS and the aspects of the scheme that need to be re-addressed. The vast majority of scattering particles in the upper level clouds are not spherical, most of the current radiation calculations for ice clouds are based on the assumption that the ice particle is a homogeneous sphere. This is not realistic as a wide variety of shapes and sizes have been observed (Heymsfield and Knollenberg, 1972). Plate crystals and columnar crystals of hexagonal cross sections are quite common. In addition, the orientation is not necessarily random, with preferred directions of falling governed by the hydrodynamics of the particle.

Some account of these complexities need consideration in developing the radiation parameterization. In this section we discuss how this problem can be approached using anomalous diffraction theory. A brief account of this approach with the new developments that we have made

will now be presented. The calculations discussed here have direct application to use in more sophisticated radiation models (such as discussed below) which are to be tested using observational data and which provide the ultimate framework for the parameterization.

Until now a rigorous electromagnetic wave solution has not been obtained for hexagonal cylinders. Approximate methods are based on geometrical optics (Cai and Liou, 1982; Jacobowitz, 1971), semi-empirical techniques (Senior and Weil, 1977), and approximate and expensive Extended Boundary Condition Method (EBCM) (Mugnai and Wiscombe, 1980).

The alternative but still approximate theory is based on the principles of geometrical optics and diffraction. This anomalous diffraction theory (ADT) (e.g., Stephens, 1984) holds for particles with a refractive index close to unity

$$(m - 1) \ll 1$$

and ratio of particle size and wavelength $a/\lambda \gg 1$. Since the index of refraction is close to 1, the problem of total scattering in the ADT theory reduces to calculations of the interference between the almost straight transmission and the light diffracted according to Huygens' principle.

Thus, in the anomalous diffraction approximation, the forward scattering amplitude S(0) is given by (Bryant and Latimer 1969)

$$S(0) = \frac{k^2}{2\pi} \int_A (1 - e^{-i\phi^*}) \, dA \qquad (3.8)$$

where $\phi^* = kd(m - 1)$, d is the particle thickness, and m is the complex refraction: $m = n - in'$. The quantity ϕ^* is the complex phase shift of

light passing through the particle relative to that passing around it. The kdn' term contributes to absorptive attenuation.

The extinction and absorption coefficients are defined as

$$C_{ext} = \frac{2}{A} \text{ Re } \int_A (1 - e^{-i\phi^*}) \, dA \tag{3.9}$$

and

$$C_{abs} = \frac{1}{A} \int_A (1 - e^{-2kdn'}) \, dA \tag{3.10}$$

The single scattering albedo

$$\omega = \frac{C_{ext} - C_{abs}}{C_{abs}} \tag{3.11}$$

represents the probability that, if a photon interacts with an elemental volume, it will be scattered rather than truly absorbed.

Here we present calculations of C_{ext}, C_{abs}, and ω for hexagonal crystals.

The geometry of the problem is illustrated in Fig. 3.5.

The sun's rays are coming perpendicular to the 2-3 face ($\alpha = 90^{\circ}$) in case 1 (Fig. 3.6) and perpendicular to face 1-2 ($\alpha = 60^{\circ}$) in case 2. Only two cases are considered, but they represent extreme situations. The length of crystal is c and the length of distance 1-2 is a.

Scattering geometry for Case 1 is presented in Fig. 3.6. We have

$$d(y) = 2\sqrt{3}y \text{ on } d_0d_1 \tag{3.12}$$

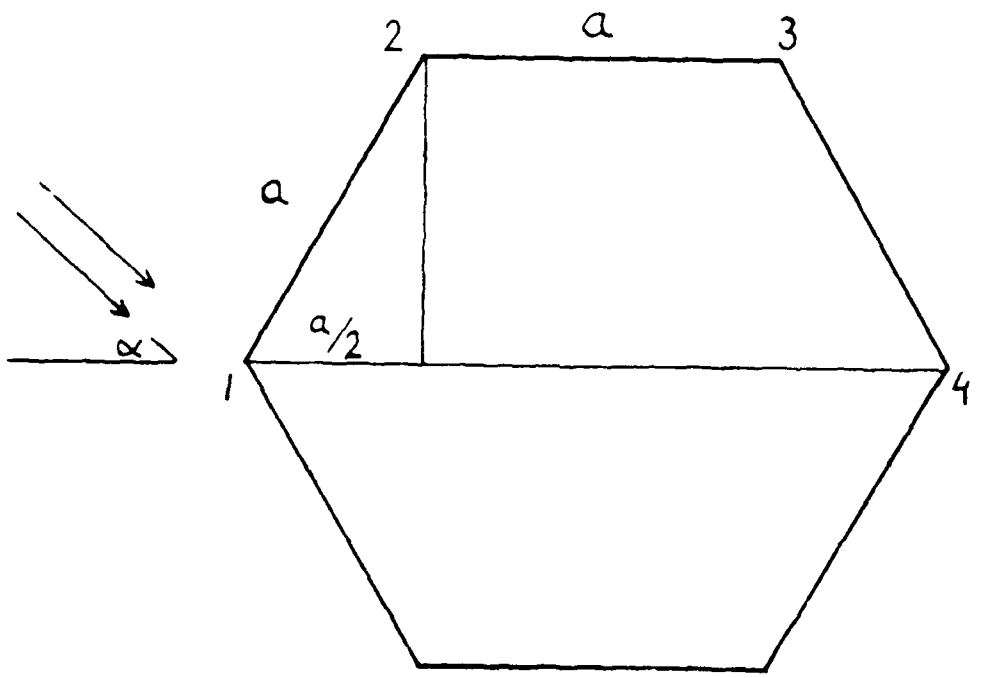

Fig. 3.5. Hexagonal crystal-geometry of light incidence.

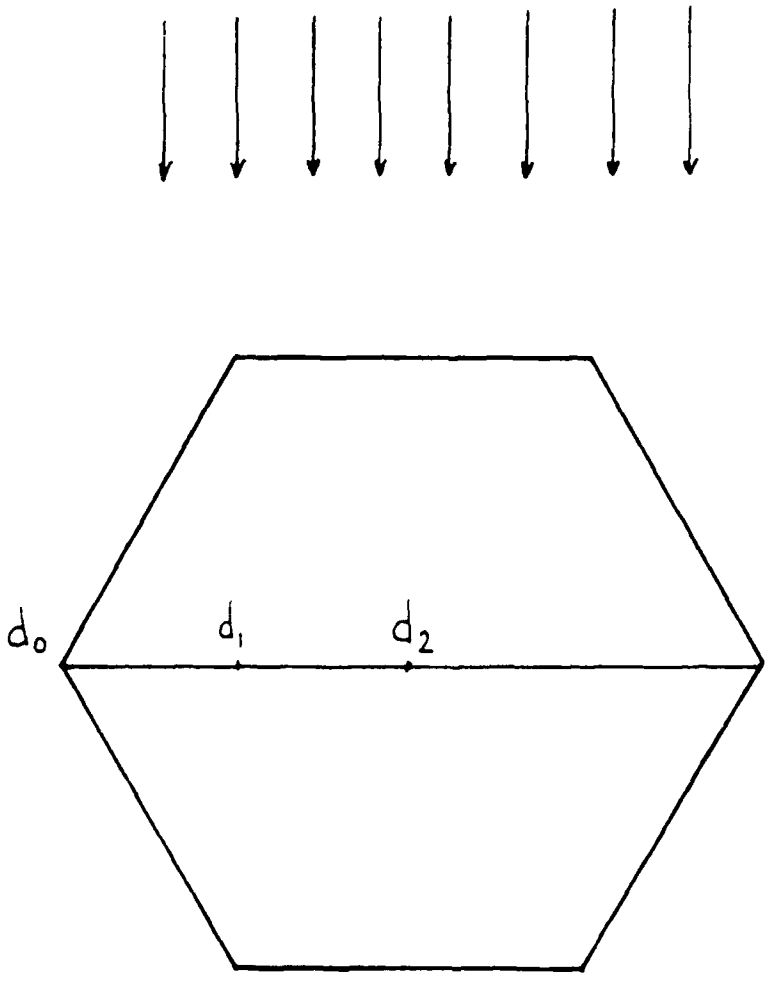

Fig. 3.6. Case 1 geometry.

$$d(y) = 2a \quad \text{on } d_1d_2$$

Extinction efficiency is given by

$$C_{ext} = \frac{2}{A}\, 2c \int_{d_0}^{d_2} f(y)\, dy \,, \tag{3.13}$$

where $f(y) = 1-e^{-kn'd(y)}\cos k(n-1)d(y)$. The factor 2 appears because of symmetry, and the real part of (2) is taken, $A = 2ac$. Length $d(y)$ is one when the sun ray travels inside the crystal.

For case 2 geometry we have on d_0d_1

$$d(y) = a + \frac{2}{\sqrt{3}}\, y \tag{3.14}$$

and extinction efficiency is given by

$$C_{ext} = \frac{2}{A}\, 2c \int_{d_0}^{d_1} f(y)\, dy \,. \tag{3.15}$$

After some algebra, it can be shown that the extinction efficiency factor for case 1 is

$$Q_{ext} = 2 - \frac{2\tan\beta}{\rho\sqrt{3}\sec^2\beta} - \frac{e^{-\rho\tan\beta}}{\sec^2\beta} - e^{-\rho\tan\beta}\cos(\rho)\frac{\tan^2\beta}{\sec^2\beta}$$

$$- \frac{2e^{-1/2\rho\tan\beta\sqrt{3}}}{\sec^2\beta\rho\sqrt{3}}\left[\tan\beta\cos\left(\tfrac{1}{2}\rho\sqrt{3}\right) - \sin\left(\tfrac{1}{2}\rho\sqrt{3}\right)\right] \tag{3.16}$$

The absorption coefficient (case 1) is

$$Q_{abs} = 1 - \frac{1}{2}e^{-2\rho\tan\beta} - \frac{1}{2\rho\tan\beta\sqrt{3}} + \frac{1}{2}e^{-\rho\tan\beta\sqrt{3}}\frac{1}{\rho\tan\beta\sqrt{3}} \quad (3.17)$$

Similarly, for case 2, we have

$$Q_{ext} = 2\left[\frac{2e^{-1/2\rho\tan\beta}}{\rho}\sin\frac{1}{2}\rho - \frac{2e^{-1/2\rho\tan\beta}}{\rho}\cos\frac{1}{2}\rho\tan\beta\right.$$

$$\left. - \frac{2e^{-\rho\tan\beta}}{\rho}\sin\rho + \frac{2e^{-\rho\tan\beta}}{\rho}\cos\rho\tan\rho + \tan^2\beta + 1\right]/(\tan^2\beta+1) , \quad (3.18)$$

and

$$Q_{abs} = -\frac{e^{-\rho\tan\beta}}{\rho\tan\beta} + \frac{e^{-2\rho\tan\beta}}{\rho\tan\beta} + 1 . \quad (3.19)$$

The results are shown in Figs. 3.7-3.10. In Fig. 3.7, Q_{ext} (curves which for large values of ρ converge or oscillate around 2) and Q_{abs} are shown for different values of complex parts of the refractive index. In Fig. 3.8 we compare extinction for both cases and Fig. 3.9 shows averaged coefficients. Fig. 3.10 shows single scattering albedo as a function of phase shift for different values of refractive index.

3.3.3 Multiple scattering code - matrix-exponential method

We now outline the sophisticated method of solving the radiative transfer equation. This method has many advantages over other techniques. On the one hand, it will be employed in its full sophistication to test the appropriateness of the scattering theories against observations. On the other hand and because of the analytic nature of the method, the theory can be simplified down to the level of

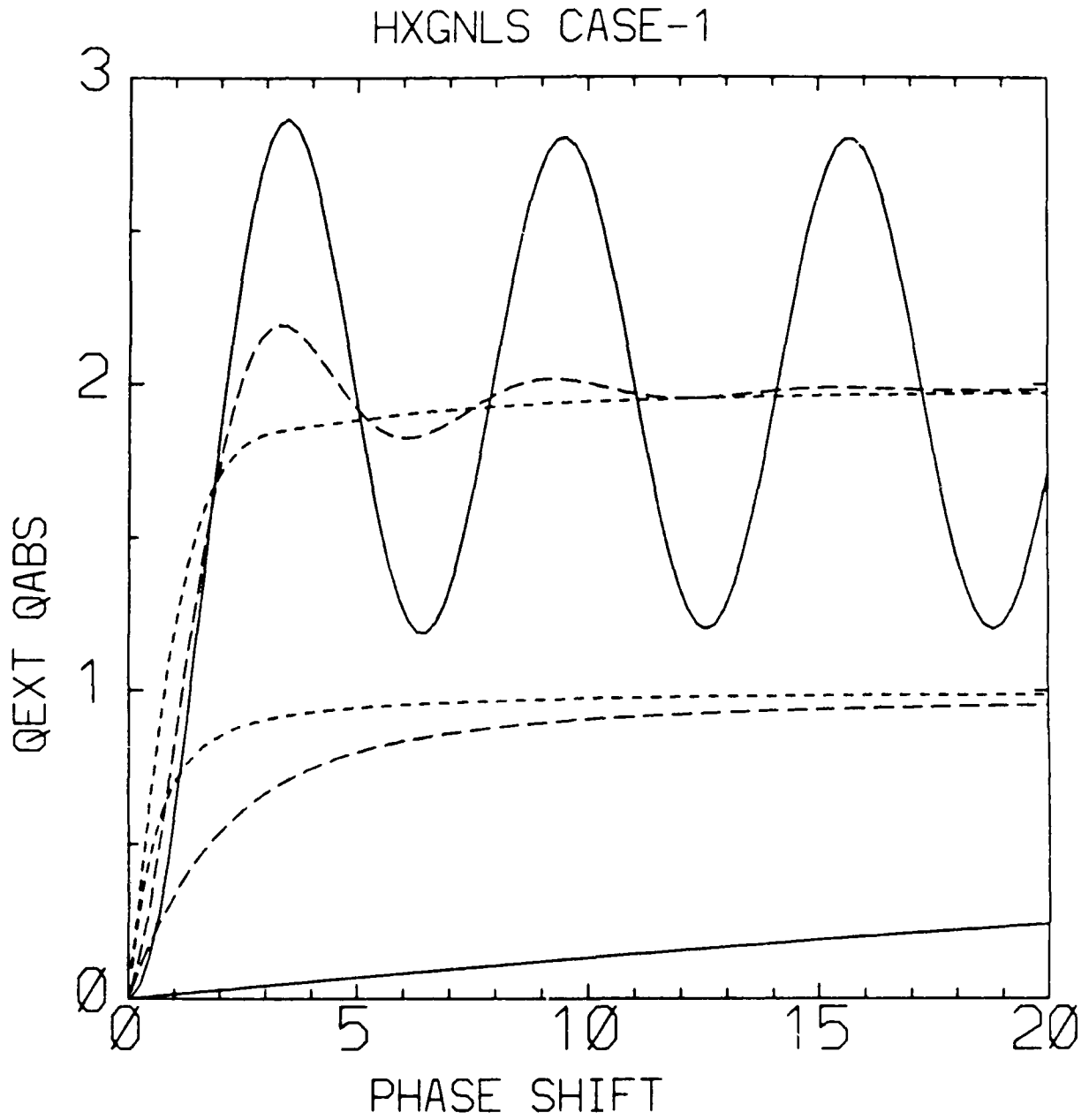

Fig. 3.7. Extinction efficiency Q_{ext} (converging or oscillating around 2 for large phase shift values) and absorption efficiency Q_{abs} for different values of tanβ as a function of phase shift ρ. Solid line for tanβ = 0.05, long-dash line for tanβ = 0.3 and short-dash line for tanβ = 1.

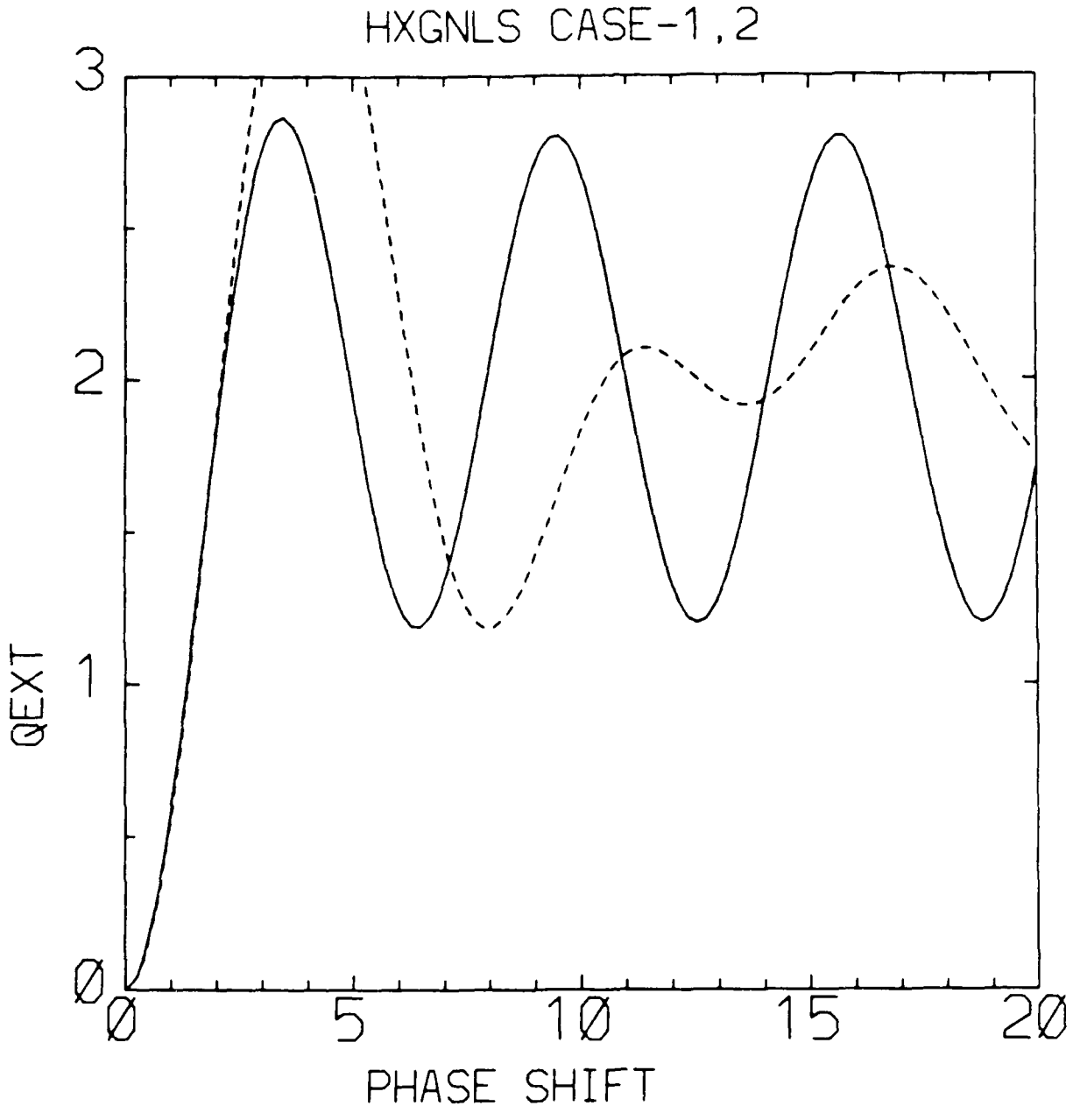

Fig. 3.8. Comparison of Case 1 and Case 2 extinction coefficient for $\tan\beta = 0.05$.

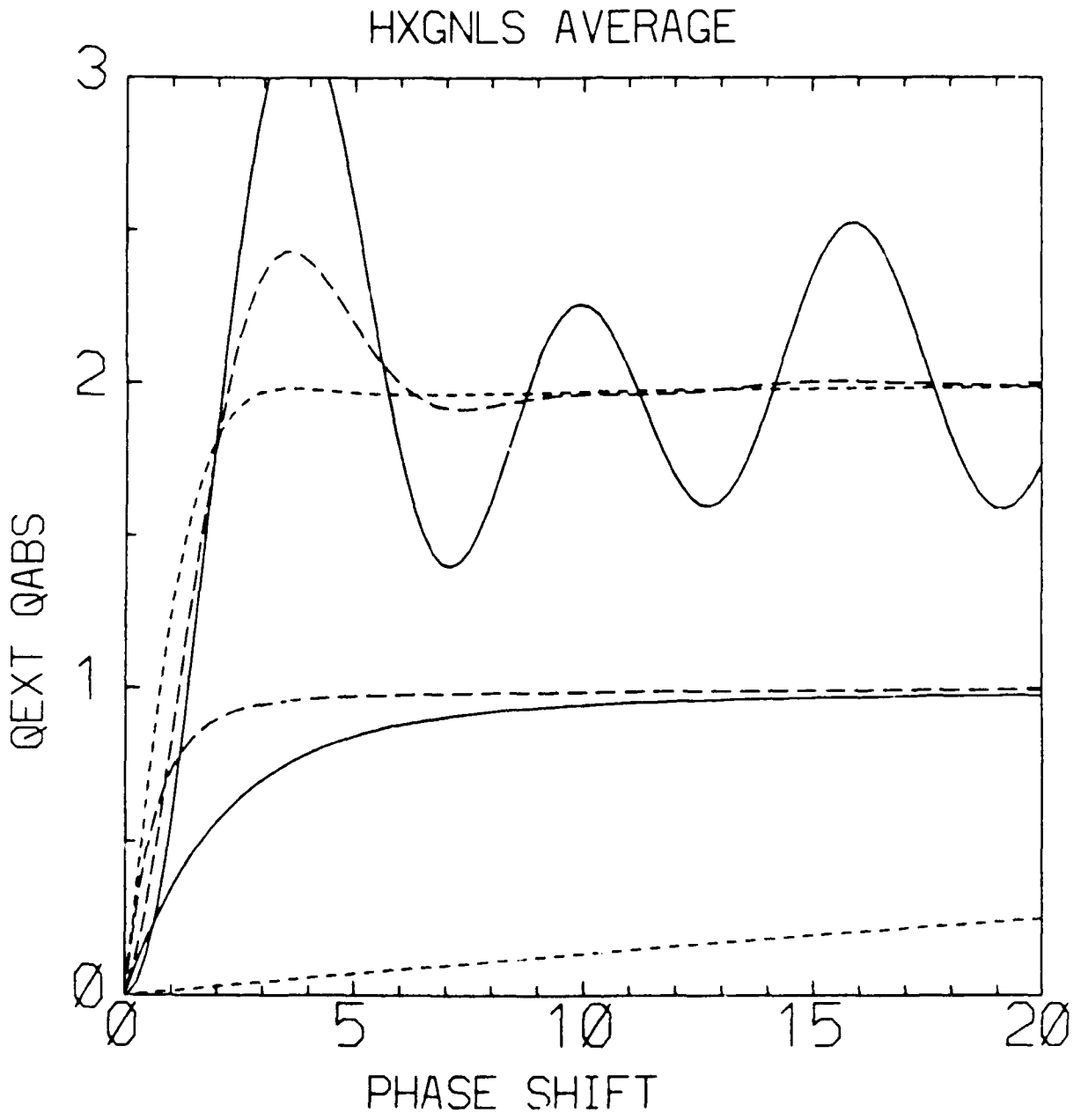

Fig. 3.9. Same as in Fig. 3.7, but for average of Case 1 and Case 2.

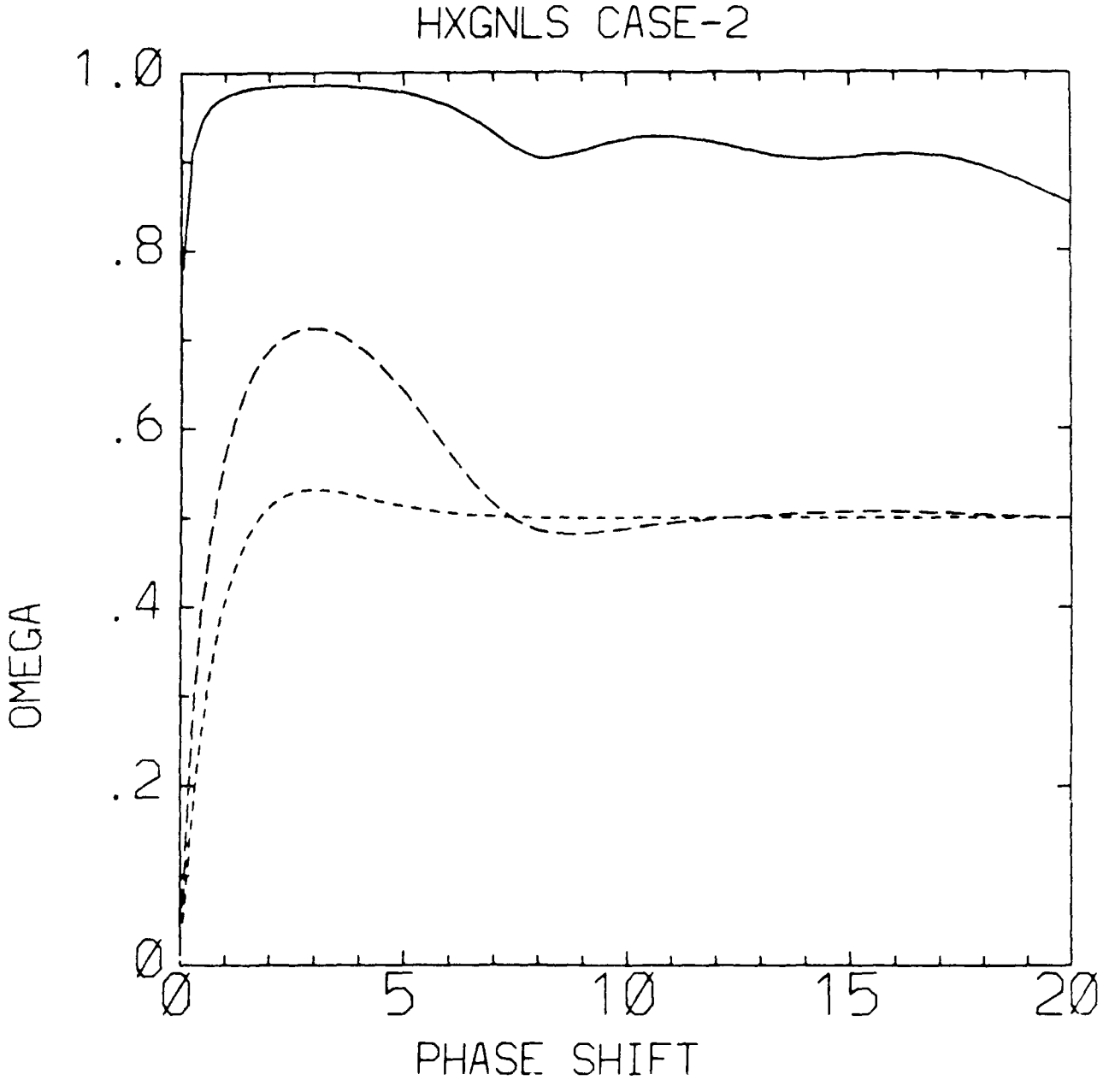

Fig. 3.10. Single scattering albedo ω as a function of phase shift for different values of tan β. Solid line for tan β = 0.05, long-dash line for tan β = 0.3 and short-dash line for tan β = 1. Hexagonals Case 2.

a two stream model as used in the original RAMS scheme. We now outline the method.

Introduction

Recently Flatau and Stephens (1987) reviewed and extended the matrix-exponential technique for solution of the radiative transfer equation (Aronson, 1972; Karp et al., 1980; Waterman, 1981). The matrix-exponential technique allows one to write the solution of radiative transfer equations for the homogeneous layer as

$$\bar{I}(\tau) = e^{A\tau}\,\bar{I}(o) + \bar{I}^{nh} \tag{3.20}$$

In this paper Flatau and Stephens (1987) show how $e^{A\tau}$ can be solved using eigenvector expansion. Detailed analysis of a two-stream (Meador and Weaver, 1980), one-level model is provided and the explicit form of $e^{A\tau}$ is given using bi-linear expansion of A. It is shown how the bi-linear expansion of A can be used to find the inhomogeneous part $\bar{I}^{nh}$. This allows us to formulate, in a fast and an elegant way, the solution for $\bar{I}^{nh}$ for arbitrary source function. Two cases of source function are considered

$$\bar{S}\ e^{-\tau/\mu_o} \tag{3.21}$$

and

$$\bar{S}\ (b_o + b_1\tau) \tag{3.22}$$

but the technique is very general. Two-point boundary conditions are considered using, as an example, the two-stream, one-level model. An algorithm is proposed to solve RTE in terms of matrix multiplication

$$e^{A_1 \Delta\tau_1} e^{A_2 \Delta\tau_2} \ldots . e^{A_n \Delta\tau_n}. \tag{3.23}$$

Such a method avoids finding "continuity" constants, thus saving time and computer memory.

We show that the comutator

$$[A,B] = AB - BA \tag{3.24}$$

plays an important role in RT and that it expresses the fact that the two layers interact (add) in a non-linear way. The doubling technique (Grant, 1969a,b,c) is also discussed, and the identity

$$e^{A2\tau_N} = (e^{A\tau_N})^2 \tag{3.25}$$

is used to formulate the doubling scheme.

The star product is shown to be equivalent to <u>standard</u> matrix multiplication of the form

$$e^{A_1\tau_1} e^{A_2\tau_2}. \tag{3.26}$$

We also hypothesize about the role of matrix operators

$$\exp\left(\int_0^\tau A(\tau)dt\right)$$

and

$$\exp(A_o \int_o^\tau \omega_o(\tau)dt) \tag{3.27}$$

for inhomogeneous layers. It is suggested that they may play an important role in the approximate solution of RTE or RTE's theoretical studies.

Instead we formulate the problem in the short sub-section below.

Matrix-exponential scheme - formulation of the problem

The equation describing the transfer of monochromatic radiation through a plane parallel homogeneous atmosphere is given by (Stamnes, 1986)

$$\mu \frac{dI(\tau,\mu,\phi)}{d\tau} = I(\tau,\mu,\phi) - J(\tau,\mu,\phi), \tag{3.28}$$

where $I(\tau,\mu,\phi)$ is the specific intensity at level τ in a cone of unit solid angle along the direction μ,ϕ, τ is the optical depth, ϕ the azimuthal angle, μ the cosine of the polar angle, and J is a source term.

The discrete ordinate approximation to the zero-order Fourier component of (3.28) can be written as (Stamnes and Swanson, 1981)

$$\mu_i \frac{dI_i(\tau}{dt} = I_i(\tau) - \sum_{j=1}^{n} (C_{i,-j}I_{-j} + C_{ij}I_j) - Q_i(\tau), \tag{3.29}$$

where $I_i(\tau) = I(\tau,\mu_i)$, $Q_i(\tau) = Q(\tau,\mu_i)$, and

$$C_{ij} = 1/2\omega_0 \sum_{i=0}^{2n-1} a_j(2l + 1)g_l P_l(\mu_i)P_l(\mu_j). \tag{3.30}$$

The system (3.29) of 2n coupled differential equations can be written in matrix form as

$$\begin{bmatrix} \frac{dI^+}{d\tau} \\ \frac{dI^-}{d\tau} \end{bmatrix} = \begin{bmatrix} -\alpha & -\beta \\ \beta & \alpha \end{bmatrix} \begin{bmatrix} I^+ \\ I^- \end{bmatrix},$$

$$I^{\pm} = \begin{bmatrix} I(\tau, \pm m_1) \\ I(\tau, \pm \mu_2) \\ \cdot \\ \cdot \\ \cdot \\ I(\tau, \pm \mu_n) \end{bmatrix},$$

where the elements of the n x n matrices α and β are given by

$$\alpha_{ij} = \mu_i^{-1}(C_{ij} - \delta_{ij}) = \mu_i^{-1}(C_{-i,-j} - \delta_{ij})$$

$$\beta_{ij} = \mu_i^{-1}C_{-ij} = \mu_i^{-1}C_{i,-j} \tag{3.31}$$

$\delta_{ij} = 1$ if $i = j$ and $\delta_{ij} = 0$ if $i \neq j$.

We wish to solve the radiative transfer problem for a plane parallel, planetary atmosphere having all its inhomogeneities confined to the vertical direction. Figure 3.4 illustrates the problem and introduces

some of the notation conventions to be used. Each layer in the atmosphere is assumed to be homogeneous but may have an arbitrary optical thickness, $\Delta\tau_i = \tau_i - \tau_{i-1}$. Our goal is to compute the angle-dependent, specific intensity at all points in the atmosphere, $I(\tau; \mu,\phi)$, where μ is the consine of the zenith angle, and ϕ is the azimuth angle measured from the sun's meridian.

We may write the discrete ordinate equations (2.23) as

$$\frac{d\bar{I}}{dt} = A\bar{I} + \bar{S} \tag{3.32}$$

where $\bar{S}$ is the source vector. The form of the matrices appearing in these equations is not important for the current discussion. Writing Eq. (3.32) in the form

$$\frac{d\bar{I}}{dt} - A\bar{I} = \bar{S}$$

and multiplying by $e^{-A\tau}$, we obtain

$$\frac{d}{dt}(e^{-A\tau}\bar{I}) = e^{-A\tau}\bar{S}. \tag{3.33}$$

Integrating between 0 and τ, the above becomes

$$e^{-A\tau}\bar{I}(\tau) = \bar{I}(0) + \int_0^\tau e^{-A\tau}\bar{S}(\tau)dt \tag{3.34}$$

Finally,

$$\bar{I}(\tau) = e^{A\tau}\bar{I}(0) + \int_0^{\tau} e^{A(\tau-t)}\,\bar{S}(t)dt \tag{3.35}$$

Here we assumed that A is constant. In more specific form the general solution (3.35) can be written for one homogeneous layer as

$$\bar{I}(\tau_i) = e^{A_i\Delta\tau_i}\,\bar{I}(\tau_{i-1}) + \bar{I}_i^{nh},$$

where

$$\bar{I}_i^{nh} = \int_{\tau_{i-1}}^{\tau_i} e^{A_i(\tau_{i-1} - t)}\,\bar{S}(t)\,dt \tag{3.36}$$

If we are not interested in the interior radiation, the system of Eq. (3.35) can be simplified immediately to

$$\bar{I}(\tau=\tau_N) = e^{A_N\Delta\tau_N}\,e^{A_{N-1}\Delta\tau_{N-1}}\,\ldots.e^{A_1\Delta\tau_1}\,\bar{I}(0) + \bar{I}^{nh}$$

From the solution (3.35) we can form the matrix equation

$$\bar{I}(\tau) = Q\bar{I}(0) + \bar{I}^{nh}$$

where

$$Q = e^{A\tau}. \tag{3.37}$$

Using definition (3.37) of transfer array Q we can introduce Q-matrix for the entire atmosphere as

$$Q = Q_n \ldots\ Q_2\ Q_1 \quad . \tag{3.38}$$

where

$$Q_i = e^{A_i \Delta\tau_i} \quad . \tag{3.39}$$

A most aggravating property of the matrix exponential is that the familiar additive law fails unless we have commutativity (Moler and van Loan, 1978), i.e.,

$$e^{\tau A} e^{\tau B} = e^{\tau(A+B)}$$

if and only if

$$[A,B] = AB - BA = 0.$$

It is evident that if

$$[Q_i,\ Q_j] = 0 \tag{3.40}$$

for every combination of i,j then Q in Eq. (3.38) could be expressed by

$$Q = e^{\int_c^{\tau_N} A\ dt} \quad . \tag{3.41}$$

Because (3.40) is not satisfied it is equally evident that commutators will play an important role in the solution to RTE. Indeed it is known that adding slab reflectances and transmittances does not follow linear law, which gives a physical meaning to non-commutativity.

It should be emphasized that equation (3.37) is only a formal solution, since we are dealing with a two-point boundary value problem

in which $\overline{I}^{-}(0)$ and $\overline{I}^{+}(\tau_N)$ are to be determined. However, we can overcome this problem and show equivalence of the matrix-exponential technique with the doubling and adding scheme.

3.3.4 Unified approach to microphysics scheme

Radiation properties as described in Section 3.3.2 are related to single crystals only. To use it in the RAMS model we have to weight the single scattering albedo with the crystal size distribution to obtain the bulk radiation characteristics. Currently the microphysics scheme is based on the Marshall-Palmer distribution, but we expect that some other distributions may fit the experimental results better. For example recent experimental results (FIRE data) as well as new analysis by Heymsfield and Platt (1984) indicate that small crystals may contribute up to 50% of overall radiative characteristics of ice clouds. It strongly indicates the necessity of introducing a two-modal distribution function with the primary mode describing small ice crystals, numerous in concentration but small in water content, and a secondary mode, containing large crystals with small concentrations but large ice water content. Below we summarize a new, unified approach to the bulk microphysics scheme. We give examples how to efficiently calculate the generalized moments for four different distributions. It is then easy to obtain a formal solution for the bi-modal parameterization.

This summary is an outgrowth of several previous works by Cotton and his co-workers. These include rain parameterization from Manton and Cotton (1977) and Tripoli and Cotton (1980); ice parameterization from Cotton et al. (1982) and Stephens (1979); and aggregation parameterization from Cotton et al. (1986).

Several suggestions as to the type of distribution to be expected in the clouds are considered here. The Marshall-Palmer function is used because it is a basis of current implementation. AFGL's truncated distribution (Eerthel and Plank, 1983) is discussed as well as Clark and Hall's (1983) log-normal function. The gamma-type function is also considered.

Size spectra

Several empirical formulas have been proposed for the spectra of various water categories. The spectral density function n(D) is defined such that n(D)dD is the total number concentration of particles, whose diameter is between D and D+dD, per unit volume of air. Hence,

$$N(D) = \int_0^D n(D)dD, \tag{3.42}$$

is the total concentration of particles of diameters smaller than D, per unit volume of air.

(a) Gamma distribution

A family of gamma distributions was considered by several authors (see e.g. Scott (1968)). The defining equation for this family is

$$N(D) = \frac{N_t\, a^{\nu+1}}{\Gamma(\nu+1) D_m} \left(\frac{D}{D_m}\right)^{\nu} \exp\left(-\frac{aD}{D_m}\right) \tag{3.43}$$

where D is the diameter of particle, N_t the is total concentration, D_m is mean diameter, a and ν are coefficients and Γ is the gamma function

(b) Marshall-Palmer distribution

The special case of (3.43) is often used in cloud physics. Assuming a = 1, ν = 0 we have

$$N(D) = \frac{N_t}{D_m} \exp(-\frac{D}{D_m}) \tag{3.44}$$

The mean diameter is related to the slope of the distribution - (λ),

$$\lambda = \frac{1}{D_m} \tag{3.45}$$

(c) Doubly-truncated Marshall-Palmer distribution

AFGL measurements (Berthel and Plank, 1983; Berthel et al., 1987) indicate that it is often advantageous to approximate the spectral size distribution with the Marshall-Palmer probability but truncated on both sides of the spectrum, i.e.,

$$N(D) = \frac{N_t}{SD_m} \exp(-\frac{D}{D_m}) \tag{3.46}$$

for $D_{min} < D < D_{max}$, and 0 otherwise, where

$$S = e^{-D_{min}/D_m} - e^{-D_{max}/D_m}$$

(d) Log-normal distribution

Clark (1976) and Nickerson et al. (1986) have advocated use of an asymmetrical distribution of the log-normal type. It is defined by

$$N(D) = \frac{N_t}{\sqrt{2\pi}\sigma D} \exp[-(\ln D - \mu)^2/(2\sigma^2)] \tag{3.47}$$

where μ and σ^2 are the mean and variance of lnD, respectively. For example,

$$\mu = \ln D_m = \overline{\ln D} \tag{3.48}$$

where D_m is the geometric mean of the D's. We also have

$$\sigma^2 = (\ln\sigma_m)^2 = \overline{(\ln D - \ln D_m)^2} \tag{3.49}$$

Moments and distribution-weighted functions

In the development of the bulk parameterization scheme, such as we are pursuing here, one is interested in the average properties of a hydrometeor class. For example, such a property can be the average fall velocity that is "typical" for all size droplets, typical collection efficiency, etc. Therefore we would like to be able to calculate averages $\bar{f}$

$$\bar{f} = \int_{D_{min}}^{D_{max}} f(D)N(D)dD. \tag{3.50}$$

Such integration, for an arbitrary f(D) and N(D), is difficult. For f of the form

$$f(D) = KD^{\alpha}, \tag{3.51}$$

where K and α are constants, and four distributions considered previously, it can be done in closed form.

If the most general form of f is (3.51) or the linear combination of such functions, the problem reduces to finding the generalized moment of distribution N(D)

$$M^{\alpha} = \int_{D_{min}}^{D_{max}} D^{\alpha} N(D)dD. \tag{3.52}$$

(a) Moments and averages of Γ-distribution

From (3.52) and (3.43) we have

$$M^{\alpha} = \int_{0}^{\infty} D^{\alpha} \frac{N_t a^{\nu+1}}{\Gamma(\nu+1) D_m} \left(\frac{D}{D_m}\right)^{\nu} \exp\left(-\frac{aD}{D_m}\right)dD \tag{3.53}$$

Let $y = \frac{aD}{D_m}$, then (3.53) can be written as

$$M^{\alpha} = N_t \left(\frac{D_m}{a}\right)^{\alpha} \frac{1}{\Gamma(\nu+1)} \int_{0}^{\infty} y^{\alpha+\nu} \exp(-y)dy \tag{3.54}$$

From table of integrals

$$M^{\alpha} = N_t D_m^{\alpha} \frac{\Gamma(\nu+\alpha+1)}{a^{\alpha}\Gamma(\nu+1)} \tag{3.55}$$

For f of the specific form

$$f = KD^{\alpha}$$

we get

$$\bar{f} = N_t f(D_m) F(\alpha), \tag{3.56}$$

where

$$F(\alpha) = \frac{\Gamma(\nu+\alpha+1)}{a^{\alpha}\Gamma(\nu+1)} \tag{3.57}$$

(b) Moments and averages of Marshall-Palmer distribution

Setting $\nu = 0$ and $a = 1$ in the expression for the gamma distribution (3.56) we get

$$M^{\alpha} = N_t D_m^{\alpha}\, \Gamma(\alpha+1) \tag{3.58}$$

and

$$\bar{f} = N_t f(D_m) F(\alpha), \tag{3.59}$$

where

$$F(\alpha) = \Gamma(\alpha + 1)$$

(c) Moments and averages of doubly-truncated Marshall-Palmer distribution

From (3.46) and (3.52) we have

$$M^{\alpha} = \int_{D_{min}}^{D_{max}} D^{\alpha} \frac{N_t}{SD_m} \exp(-\frac{D}{D_m})dD. \tag{3.60}$$

Let $y = \frac{D}{D_m}$. We can write (3.60) as

$$M^{\alpha} = N_t D_m^{\alpha} \frac{1}{S} \int_{D_{min}}^{D_{max}} y^{\alpha} \exp(-y)dy \tag{3.61}$$

and integrating we get

$$M^{\alpha} = N_t D_m{}^{\alpha} \frac{1}{S} \left[\gamma\left(\alpha+1, \frac{D_{max}}{D_m}\right) - \gamma\left(\alpha+1, \frac{D_{min}}{D_m}\right)\right] \tag{3.62}$$

The distribution-averaged f is

$$\bar{f} = N_t f(D_m) F(\alpha), \tag{3.63}$$

where

$$F(\alpha, D_{max}, D_{min}, D_m) = \frac{\gamma\left(\alpha+1, \frac{D_{max}}{D_m}\right) - \gamma\left(\alpha+1, \frac{D_{min}}{D_m}\right)}{S}$$

If D_{max}/D_m is large and D_{min}/D_m is small, further simplification is possible:

$$\gamma(\alpha+1, \infty) \rightarrow \Gamma(\alpha+1)$$

and

$$\gamma(\alpha+1, 0) \rightarrow 0$$

i.e.,

$$F(\alpha) = \Gamma(\alpha+1) \tag{3.64}$$

It seems (Ranta, private communication) that conditions where D_{min}/D_m is small are often satisfied.

(d) Moments and averages of log-normal distribution

From the definition (3.52) we have

$$M^{\alpha} = \int_0^{\infty} D^{\alpha} \frac{N_t}{\sqrt{2\pi}\sigma D} \exp[-(\ln D - \mu)^2/(2\sigma^2)]dD \tag{3.65}$$

and let

$$y = \frac{\ln D - \mu}{\sqrt{2}\sigma}.$$

After substitution we get

$$M^{\alpha} = \int_{-\infty}^{+\infty} \exp(\sqrt{2}\sigma y\alpha + \mu\alpha - y^2) \frac{N_t}{\sqrt{\pi}} dy. \tag{3.66}$$

Using the expression for the above integral we have

$$M^{\alpha} = N_t e^{\mu\alpha} \exp(\frac{\sigma^2\alpha^2}{2}) \tag{3.67}$$

Using the above expression we obtain the distribution-averaged function of the general form $f = K D^{\alpha}$.

$$\bar{f} = N_t K e^{\mu\alpha} \exp(\frac{\sigma^2\alpha^2}{2}) \tag{3.68}$$

But from (3.48) we have $D_m = e^{\mu}$, i.e.

$$Ke^{\mu\alpha} = KD_m^{\alpha}.$$

Finally, we can express $\bar{f}$ by

$$\bar{f} = N_t f(D_m) F(\alpha,\sigma), \tag{3.69}$$

where N_t is total concentration, $f(D_m)$ is a function evaluated for the geometric mean of particle diameter, $F(\alpha,\sigma)$ is a function depending on α and variance σ of distribution

$$F(\alpha,\sigma) = \exp(\frac{\alpha^2\sigma^2}{2}) \tag{3.70}$$

Summary of distribution functions and their moments

We considered up to now four different distributions: gamma, Marshall-Palmer, truncated Marshall-Palmer and log-normal. We were able to derive distribution-averaged formula for the $f = KD^{\alpha}$, where K and α are constants to the general expression

$$\bar{f} = N_t f(D_m) F(\alpha), \tag{3.71}$$

where N_t is total concentration, $f(D_m)$ is the value of the function at the mean diameter, and $F(\alpha)$ function of α and possibly some other parameters. The form of the F-function is summarized below.

GAMMA DISTRIBUTION

$$F(\alpha) = \frac{\Gamma(\nu+\alpha+1)}{a^{\alpha}\Gamma(\nu+1)}$$

MARSHALL-PALMER

$$F(\alpha) = \Gamma(\alpha+1)$$

DOUBLY-TRUNCATED MARSHALL-PALMER

$$F(\alpha, D_{max}, D_{min}, D_m) = \frac{\gamma(\alpha+1, \frac{D_{max}}{D_m}) - \gamma(\alpha+1, \frac{D_{min}}{D_m})}{S}$$

where

$$S = e^{-D_{min}/D_m} - e^{-D_{max}/D_m}$$

LOG-NORMAL DISTRIBUTION

$$F(\alpha, \sigma) = \exp(\frac{\alpha^2 \sigma^2}{2})$$

It follows from (3.71) that, if f is proportional to D^{α} or if it is a linear combination of such functions, we can formally perform the calculation for one of the distributions and substitute a different $F(\alpha)$ when a different size spectra are needed.

This generalized approach was already used to develop a unified approach to microphysics parameterization (Tripoli et al., 1987).

In summary, the foundations of the turbulence, radiation, and microphysical modules have been developed to extend RAMS to the simulation of cirrus clouds. Much work remains to complete this model, however.

4.0 FORECASTING AND DIAGNOSIS OF EXTREME WIND SHEARS AND TURBULENCE

A summary of work completed relating to extreme wind shears by severe convective storms is presented here. Over the course of the contract the focus has gradually shifted from the convective scale downdraft structure and its influence on severe wind shear to the upper end of the meso-β (20-200 km) scale. It is now apparent that long lived

severe surface outflow events lasting on the order of six to nine hours may accompany a large percentage of mesoscale convective complexes (approximately 30 percent of the MCCs studied thus far). Because these systems generally peak in intensity after midnight this represents a genuine concern for the general public, local forecasters and aircraft concerns, such as aircraft tied down at airport facilities, in the affected areas. A natural question that arises then is why do some systems continue to produce severe surface winds through the early morning hours while others peak in the early evening and then rapidly subside? Also are there signatures in the synoptic environment which may allow one to accurately predict these events in time to give ample advice to those who may need the data to either protect vulnerable machinery or alter planned activities?

Insights to the above questions have been provided through both the numerical and observational studies conducted under the current contract. A series of numerical studies performed by Knupp (1985) provided information on the structure of downdrafts during the developing and mature stages. He identified the major downdraft circulation branches in Fig. 4.1 as consisting of both a mid-level and an up-down downdraft branch. The mid-level branches are thought to predominate in the early stages of the downdraft when large shears and strong surface outflows my exist. The up/down downdraft branch may become a more prominent feature during the mature storm stage. A factor controlling the strength of this downdraft branch is the stability of the ABL lying ahead of the storm. The stability in turn my be affected by outflow layers from previous storm systems or cloud shadowing and/or evaporation of precipitation falling into inflow layer ahead of the

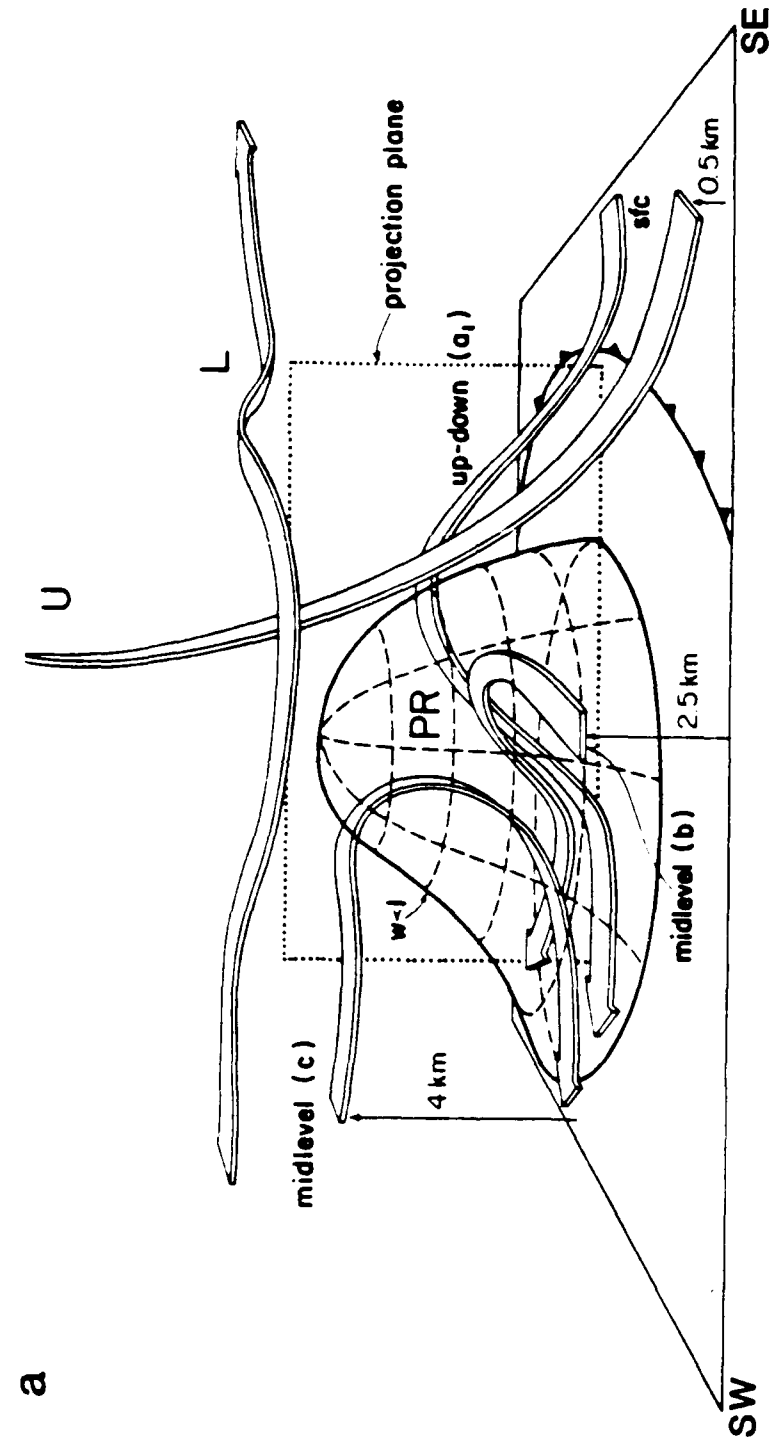

Fig. 4.1. (a) Schematic illustrating primary relative flow branches comprising the low-level precipitation-associated downdraft located along the upshear flank with respect to the updraft.

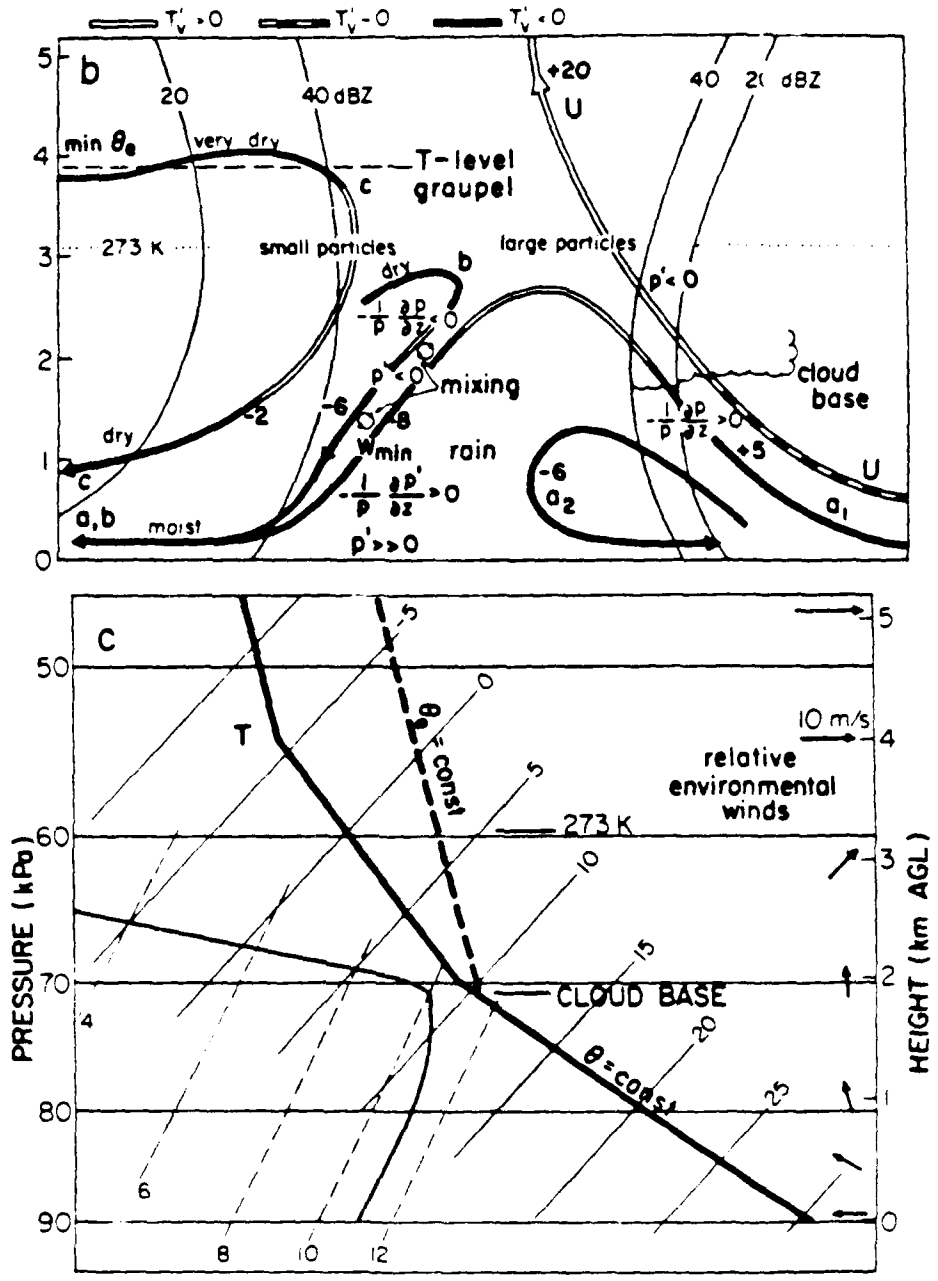

Fig. 4.1. Continued - (b) Projection of primary downdraft flow branches onto a vertical east-west plane. Physical processes along each branch are portrayed. (c) Sounding illustrating the relationship of downdraft properties to environmental structure.

storm. He showed that downdraft speeds along this branch may attain downburst intensity.

Other factors controlling downdraft intensity were also documented. The cloud model results indicate that precipitation size and phase exerted a strong control on the modeled downdraft strengths. Knupp reported that melting accounted for approximately 60 percent of the cooling in environments supporting low cloud bases. As cloud base height increased, the relative cooling by melting decreased in importance. Sensitivity to the characteristic size of the precipitation was shown when downburst type outflows were produced by merely quartering the precipitation size used in the simulation. Other controls on outflow strength may arise due to the modification in the ABL from either short-or-long lived convective elements. Knupp and Jorgensen (1985) suggest that convective scale perturbations on a resoscale surface flow field produced by a convectively induced meso-high may be one mechanism which could sustain downburst type outflows over a long period of time.

It has long been recognized that certain radar echo configurations such as bow echoes tend to be associated with downburst activity (Fujita, 1978). A Doppler radar observation of a bow echo system on the 2nd of August that occurred in Montana showed that the system had both the mid-level and up/down sources to the downdrafts. This system had peak reflectivities of 70 dBZ and peak outflows exceeding 30 m/s. On the storm's upshear flank at mid-levels was a well defined inflow toward the storm, shown in Fig. 4.2, that was initially thought to contribute significantly to the surface outflow through the vertical transport of the higher momentum air to the surface within the predominate downdraft

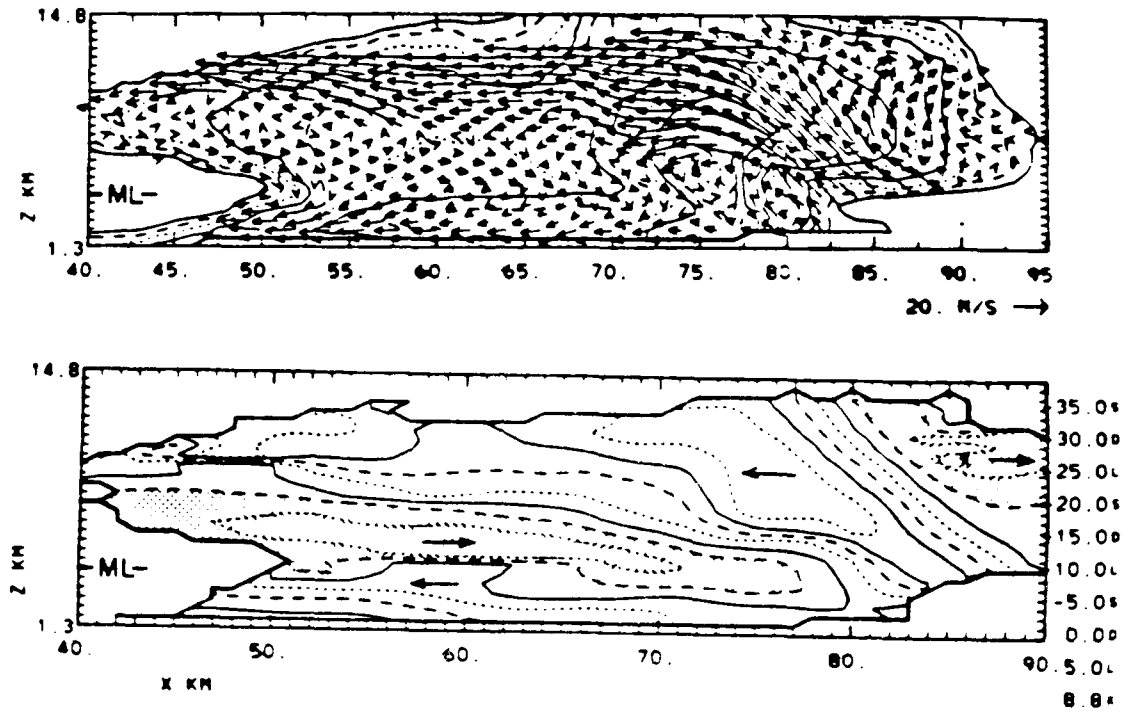

Fig. 4.2. Vertical east-west cross-section taken normal to the squall line along the inflow jet into the rear of the rear flank of the storm. ML refers to the melting level. (a) Storm relative flow along the plane of the cross-section reflectivity contours are in 5 dBZ intervals beginning with 10 dBZ. (b) The u component of flow in (a) contoured in 5 m/s intervals indicating vertical wind shear present upshear of the convective cores.

zones. Later trajectory work indicated however, that the primary source region for the downdraft air was from the downshear region of the storm. The analysis indicated that the "rear inflow jet" was a mixture of parcels from several different locations within the storm including the leading edge of the system. Tajectories released in the rear inflow did not reach the surface nor did they approach the leading edge of the storm. We thus concluded that strong surface winds associated with organized squall lines may not initially require mid-level transport from the upshear portion of the storm system. The analysis indicated that the areal extent and the strength of the rear inflow increased with time and may have had a more direct impact on the surface flow momentum at a later time in the storm's life cycle.

The surface analysis indicated a large meso-high of nearly 6 mb behind the squall line. The strongest winds at the surface were located on the southeast flank of the meso-high and to the north of the strongest cell with the squall line. The Doppler analysis placed a large 15 m/s downdraft on the northern flank of this cell. Thus, in this case, the strongest surface winds occurred in a region where convective scale perturbations were superimposed on a background flow provided by the meso-high, supporting the hypothesis given by Knupp and Jorgenson (1985).

The storm of 2 August was unusual in the sense that it propagated into the cold stable outflow wake of a previous meso-β system (see Fig. 4.3). Aircraft measurements taken ahead of the squall line revealed a elevated inflow source existed above the low-level stable layer. The elevated inflow layer in turn was a remnant of the pre-storm atmospheric boundary layer and was being continually replenished by the

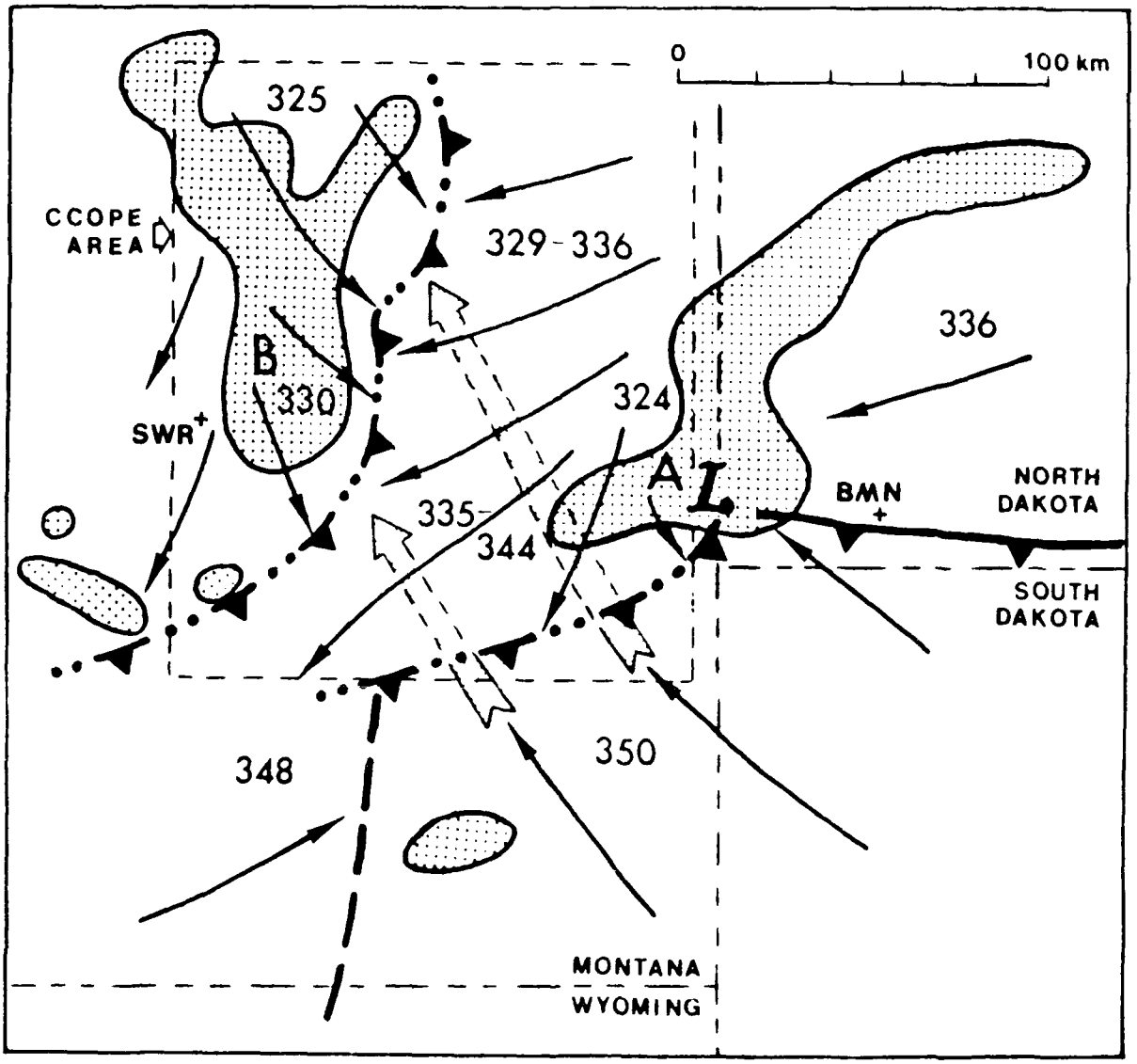

Fig. 4.3. Surface mesoscale features at 2030 MDT 2 August 1981. Thin arrows represent surface flow while broad dashed arrows represent synoptic flow above the surface cold dome produced by the storm labeled A. Stippling denotes 30 dBZ storm contours. Storm B is the squall described in the text and the numbers are representative surface θ_e values.

synoptic/regional-scale flow. This is one mechanism by which storms may maintain their intensity and could remain a threat long after the peak daily heating has subsided.

The strongest cell was located near the vertex in the bow echo and nearly 80 km from the surface-based high θ air seen in Fig. 4.3. A more complete analysis of the convective structure indicated that the strongest cell was an example of a weakly evolving supercell (Foote and Frank, 1983). The overall structure of the squall line suggests that the rotational characteristics extended beyond the single supercell within the line to include the ordinary cells located along the southern 50 km of the line. It is suggested that subclasses of convective organization on length scales of 50 to 100 km may exist along a squall line depending on the environmental conditions such as the strength of the wind shear and perhaps the resultant shape of the outflow produced by different cells along the line. These subclasses may be a combination or ordinary and supercell type storms acting as a coherent entity. It appears that the bow echo may represent one such subclass or arrangement of convection along a squall line.

A recent paper by Rotunno et al. (1987) indicates that a controlling factor in the behavior of the squall line is the degree of cancellation between the horizontal vorticity produced by the solenoid associated with the cold outflow and the horizontal vorticity present due to wind shear in the inflow layer. The optimal situation for long-lived lines occurs when the two sources completely cancel each other. Extending their analysis to a curved outflow pool one might then expect the optimal situation to exist only in a relatively narrow zone since the horizontal vorticity vector associated with a circular cold pool

rotates through 360 degrees while the inflow horizontal shear vector retains its initial orientation. Thus one might expect a spectrum of convective behavior along a curved outflow pool with the longest lived features occurring in the region where the vorticity vectors from each source lie opposite to each other. We speculate that this may have had a control in locating the supercell in the 2 August case near the vertex in the bow echo where the tightest gradient was observed in the circular surface cold pool that accompanied this system.

The 2nd of August squall line was an integral component of a MCC that moved southeastward over the Dakotas during the early morning hours of the 3rd. The resultant MCC was accompanied by severe wind reports throughout the period. We have begun to compile statistics on other MCCs that also produce severe winds into the early morning hours. Preliminary findings are that roughly 30 percent of the MCC episodes produce severe winds for several hours after midnight with the strongest wind events exceeding 45 m/s in non-tornadic activity.

It is our hope to construct a useful conceptual model of these events based on the work completed in part by the funding provided to date from the current contract. Any successful model will need to incorporate the multi-scale aspects of the problem as touched on above. These include the controls on downdraft strength due to environmental and microphysical framework within which the storm evolves as presented by Knupp (1985). Mesoscale organization of large outflow pools and the storms ability to decouple from the surface may also be important factors in long lived events. A better understanding of the rear inflow jet and it's ultimate control on the surface outflow is also needed. Doppler studies performed to date indicate that a common characteristic

of bow echo squall lines is the enhanced mid-level inflow on the storms upshear flank. The sequence of events in the 2 August squall line suggest that this feature developed in response to a strong downdraft and thus the severe surface winds preceeded the development of a strong rear inflow jet at mid-levels. The question remains whether this is a typical or atypical sequence of events and as such will be the subject of further inquiry. Finally the dynamics of storm systems such as bow echo squall lines and other subclasses of convective organization that may form in an ensemble of convective cells (particularly those conducive to severe wind events) need to be better defined and hopefully predicted. It is hoped that these brief reports provide some guidance for future research and understanding.

5.0 SUMMARY OF RAMS DEVELOPMENT

RAMS has been undergoing a major overhaul and enhancement to allow several new features to be added to the system and to correct for some old deficiencies. Some reasons for the major changes in the system are:

- to allow for the implementation of two-way nesting capabilities in the model
- to add the computational schemes of the "Pielke" model to the RAMS system
- to allow for faster execution time on computers which require longer vector lengths
- to conform as closely to the FORTRAN 77 standard as possible to facilitate portability

To accomplish these goals, several changes needed to be made:

- A new preprocessor was written, itself in the FORTRAN 77 standard, to correct many of the problems with the old PP1. Obsolete features of

PP1 were removed (e.g., IF block processing which FORTRAN 77 can handle). The new preprocessor also is much faster executing, taking only about 1/6 as long as PP1.

- The old RAMS was run with a "slab" I/O scheme where all the variables of a subset of the domain was kept in central memory. Because of this, most of the model was vectorized only in vertical loops. These short loops were relatively efficient on a CRAY, but were much too short to be efficient on a CYBER 205. The I/O structure for the new RAMS was changed to keep the whole domain in memory but only a subset of the model's 3-D variables. This scheme allows full 3-D loops to be used in the code where a CYBER can vectorize the code across all three loops. This also eliminates the necessity of the macro capabilities of PP1, making development of the code much easier.
- The new I/O structure of the new RAMS makes the implementation of both the two-way nesting algorithms and the inclusion of the "Fielke" schemes much easier. For the nesting, it is necessary to interpolate the boundary conditions of the fine nests from the coarser nests. This process is much easier if the whole domain of a variable is in core at once. For the "Fielke" schemes, each variable is updated after every term is calculated. This would have been economically infeasible in the slab I/O scheme. In addition, there are some numerical schemes which require the entire domain in core (e.g., cubic spline advection, Long's filter). Lengthy scratch arrays would have been needed with the slab I/O scheme.
- With the desire to conform to the FORTRAN 77 standard, many of the individual physical computational routines such as the microphysics

and radiation parameterizations have been rewritten in a very general form so that they could be transported to even a different model in the future if desired. A summary of RAMS is given in Appendix 2.

Test simulations have recently begun with the new system. Comparison runs with the old "Pielke" model have had favorable results with only a few minor discrepancies remaining. A two-way nested sea breeze simulation, both hydrostatic and non-hydrostatic, has been run to exercise the nesting algorithms and again reasonable results were produced. It is anticipated that a preliminary "production" version of the new RAMS will be available within a few months. A preprint of a paper presented at the Envirosoft '86 conference in Los Angeles in November 1986 which gives further details of the new system and its options is reproduced as Appendix 3.

The hydrostatic nested regional scale version of RAMS is being evaluated by simulating mesoscale convective complexes observed during the CCOPE and SPACE field programs. The simulations are being run using version 6 of RAMS, the hydrostatic model with forward-backward time differencing. Each case is set up similarly, a coarse grid is run with about a 110 km resolution and a Kuo-type convective parameterization over a domain of about 4500 km. A finer grid of about 40 km is then one-way nested within the coarser grid. A Fritsch-Chappell type convective parameterization is used on this higher resolution grid. Sensitivity experiments are run on the finer grid testing the sensitivity to various physical and numerical processes. From the results so far, several statements can be inferred from the model results.

- The development of the mesoscale circulation of the convective

system is dependent on the convective heating which, in turn, is dependent on many of the more arbitrary aspects of the convective parameterizations.

- For the development of the mesoscale anvil circulation, the convective heating must be widespread and persistent, not necessarily very strong. The heating must be projected on a scale larger than the Rossby radius of deformation and over a longer timescale than that of an individual cumulus cloud to form a quasi-balanced circulation.
- For the convection to be that long-lived and widespread, the synoptic and meso-α scales must provide support (conditional instability, low-level convergence, upper-level divergence, etc.) for the continued convection.
- The inclusion of a resolvable scale ice phase and the associated increase in the amount of latent heat released helps to "spin up" the resolvable scale circulation and increases the magnitude of the mesoscale circulation.
- The propagation of the simulated MCC is dependent on the behavior of the low-level jet, even in this baroclinic environment. As the night progressed and the jet veered, the system moved toward the east (at approximately the observed speed) along with the maximum convergence zone at the nose of the simulated jet.
- The timing, location, and strength of the modelled convective systems is sensitive to the model initial conditions, especially to the initial state of the soil moisture (which is not routinely observed). Variations in the soil moisture can dramatically affect the PBL structure and therefore affect the atmospheric circulation

in the vicinity of gradients in PBL characteristics.

Other simulations, testing the sensitivity of the convective systems to radiation, microphysical parameters, and precipitation will be run in the near future.

REFERENCES

Ackerman, T.P., K-N Liou, F.P.J. Valero, and L. Pfister, 1987: Heating rates in tropical anvils. To be submitted to J. Atmos. Sci.

Aronson, R., 1972: Traveling mode solution of transport-theory problems by inspection. Transport Theory and Statistical Physics, 2, 181-196.

Barnes, A., 1982: The cirrus and subvisible cirrus background. Preprints, 2nd Conference on the Nonurban troposphere, Williamsburg, VA, May 25-28, American Meteorological Society, Boston, MA., 170-175.

Bennets, D.A., and M. Culdridge, 1984: An observational study of the anvil of a winter maritime cumulonimbus cloud. Quart. J. R. Met. Soc., 110, 85-103.

Berthel, R.C., R.M. Banta, and V.G. Plank, 1987: The application of doubly-truncated hydrometeor distributions to numerical cloud models. AFGL-TR-87-0050, Air Force Geophysics Laboratory, Hanscom AFB, MA, 21 pp.

Berthel, R.C., and V.G. Plank, 1983: A model for the estimation of rain distributions. AFGL-TR-83-0030, Environmental Research Papers, No. 822, Meteorology Division, Air Force Geophysics Laboratory, Hanscom AFB, MA, NTIS #ADA130080.

Braham, R.R., Jr., and P. Spyers-Duran, 1967: Survival of cirrus crystals in clear air. J. Appl. Meteor., 6, 1053-1061.

Browning, K.A. and G.A. Monk, 1982: A simple model for the synoptic analysis of cold fronts. Quart. J. R. Meteor. Soc.,108, 435-452.

Bryant, F.P., and P. Latimer, 1969: Optical efficiencies of large particles of arbitrary shape and orientation. J. Coll. Interface Sci., 30, 291-304.

Cai, Q., and K-N. Liou, 1982: Polarized light scattering by hexagonal ice crystals: Theory. Appl. Optics, 21, 3569-3580.

Chappell, C.F., 1970: Modification of cold orographic clouds. Atmos. Sci. Paper #173 (Ph.D. Dissertation), Dept. of Atmos. Sci., Colorado State University, Fort Collins, CO 80523.

Chen, C., 1984: The physics of the marine stratocumulus-capped mixed layer. Colorado State Univ., Dept. of Atmospheric Science, Ft. Collins, CO 80523, Ph.D. Dissertation.

Chen, C., and W.R. Cotton, 1983: Numerical experiments with a one-dimensional higher order turbulence model: Simulation of the Wangara Day 33 Case. Boundary-Layer Meteorol., 25, 375-404.

Chen, C., and W.R. Cotton, 1987: The physics of the marine stratocumulus capped mixed layer. Submitted to J. Atmos. Sci.

Chen, S., 1986: A simulation of the stratiform region of a mesoscale convective system - a study of longwave radiation and melting influences. M.S. Thesis, Colorado State University, Fort Collins, CO 80523,

Chen, S., and W.R. Cotton, 1987: The simulation of a mesoscale convective system and its sensitivity to physical parameterizations. Submitted to J. Atmos. Sci.

Clark, T.L., and W.D. Hall, 1983: A cloud physical parameterization method using movable basis functions: Stochastic coalescence parcel calculations. J. Atmos. Sci., 40, 1709-1728.

Clark, T.L., 1976: Use of log-normal distributions for numerical calculations of condensation and collection. J. Atmos. Sci., 33, 810-821.

Conover, J. H., 1960: Cirrus patterns and related air motions near the jet stream as derived by photography. J. Meteor., 17, 532-546.

Cooper,W.A. and J.D. Marwitz, 1980: Winter storms over the San Juan Mountains. Part III: Seeding potential. J. Appl. Meteor., 19, 942-949.

Cotton, W.R., and R.A. Anthes, 1987: The Dynamics of Clouds and Mesoscale Meteorological Systems. Chapter II "Middle- and high-level clouds." To be published by Academic Press.

Cotton, W.R., and G.J. Tripoli, 1983-1986: Cloud/Mesoscale Model Development. Quarterly Reports to Air Force Geophysics Laboratory on Contract F19628-84-C-0005. (Available from Colorado State University, Dept. of Atmospheric Science, Fort Collins, CO 80523, 14 reports).

Cotton, W.R., M.A. Stephens, T. Nehrkorn and G.J. Tripoli, 1982: The Colorado State University three-dimensional cloud/mesoscale model -1982, Part II: An ice parameterization. J. Rech. Atmos., 16, 295-320.

Cotton, W.R., G.J. Tripoli, R.M. Rauber and E.A. Mulvihill, 1986: Numerical simulation of the effects of varying ice crystal nucleation rates and aggregation processes on orographic snowfall. J. Clim. Appl. Met., 25, 1658-1680.

DeMott, P.J., R.M. Rauber, and L.O. Grant, 1986: Ice nucleation in wintertime orographic cloud systems. J. Atmos. Sci., in review.

Flatau, P.J., 1985: Study of second-order turbulence closure technique and its application to atmospheric flows. Colorado State Univ., Dept. of Atmospheric Science, Fort Collins, CO 80523, Atmos. Sci. Paper No. 393.

Flatau, P.J., and G.L. Stephens, 1987: On the fundamental solution of the radiative transfer equation. Submitted to J. Geophys. Res.

Foote, G.B. and H.W. Frank, 1983: Case study of a hailstorm in Colorado. Part III: Airflow from triple-Doppler measurements. J. Atmos. Sci., 40, 686-707.

Freeman, K.P., and K-N Liou, 1979: Climatic effects of cirrus clouds. Advances in Geophysics, 21, 231-287.

Fujita, T.T., 1978: Manual of downburst identification for project NIMROD. Satellite and Mesometeorology Research Paper No. 156, Dept. of Geophysical Sciences, Univ. of Chicago, 104 pp. [NTIS No. N78-30771/7GI].

Grant, I.P., and G.E. Hunt, 1969a: Discrete space theory of radiative transfer: I. Fundamentals. Proc. Roy. Soc., A313, 199-216.

Grant, I.P., and G.E. Hunt, 1969b: Discrete space theory of radiative transfer. II. Nonnegativity and stability. Proc. Roy. Soc., A313.

Grant, I.P., and G.E. Hunt, 1969c: Discrete Space theory of radiative transfer and its application to problems in planetary atmospheres. J.Atmos. Sci., 26, 963-972.

Heggli, Mark, 1986: A ground based approach used to determine cloud seeding opportunity. 10th Conference on Weather Modification. May 27-30, 1986, Arlington, Virginia, AMS, Boston, MA.

Heggli, Mark F. and David W. Reynolds, 1985: Radiometric observations of supercooled liquid water within a split front over the Sierra Nevada. J. Atmos. Sci., 24, 1258-126.

Heggli, M.F., L. Vardiman, R.E. Stewart and A. Huggins, 1983: Supercooled liquid water and ice crystal distributions within Sierra Nevada winter storms. J. Clim. Appl. Meteor., 22, 1875-1886.

Heymsfield, A. J., 1972: Ice crystal terminal velocities. J. Atmos. Sci., 29, 1348-1356.

Heymsfield, A.J., 1975a: Cirrus uncinus generating cells and the evolution of cirriform clouds. Part I: Aircraft observations of the growth of the ice phase. J. Atmos. Sci., 32, 799-808.

Heymsfield, A.J., 1975b: Cirrus uncinus generating cells and the evolution of cirriform clouds. Part II: The structure and circulations of the cirrus uncinus generating head. J. Atmos. Sci., 32, 809-819.

Heymsfield, A.J., 1977: Precipitation development in stratiform ice clouds: A microphysical and dynamical study. J. Atmos. Sci., 34, 367-381.

Heymsfield, A.J., 1986: Ice particle evolution in the anvil of a severe thunderstorm during CCOPE. To be published in J. Atmos. Sci.

Heymsfield, A.J., and R. G. Knollenberg, 1972: Properties of cirrus generating cells. J. Atmos. Sci., 29, 1358-1368.

Heymsfield, Andrew J. and C.M.R. Platt, 1984: A parameterization of the particle size spectrum of ice clouds in terms of the ambient temperature and the ice water content. J. Atmos. Sci., 41, 846-855.

Hobbs, P.V., 1973: Anomalously high ice particle concentrations in clouds. Invited review paper, 8th International Conference on Nucleation, Leningrad, September, 1973.

Hobbs, P.V., 1975: The nature of winter clouds and precipitation in the Cascade Mountains and their modification by artificial seeding. J. Appl. Met., 14, 783-858.

Hogg, D.C., F.O. Guiraud, J.B. Snider, M.T. Decker, and E.R. Westwater, 1983: A steerable dual-channel microwave radiometer for measurement of water vapor and liquid in the troposphere. J. Appl. Met., 22, 789-806.

Houze, R.A., Jr., S.G. Geotis, F.D. Marks, Jr., and A.K. West, 1981: Winter monsoon convection in the vicinity of North Borneo. Part I: Structure and time variation of the clouds and precipitation. Mon. Wea. Rev., 109, 1595-1614.

Hsie, E-Y, R.D. Farley, and H.D. Orville, 1980: Numerical simulation of ice-phase convective cloud seeding. J. Appl. Metorol., 19, 950-977.

Jacobowitz, H., 1971: A method for computing the transfer of solar radiation through clouds of hexagonal ice crystals. J. Quart. Spectrosc. Radiat. Transfer, 11, 691-695

Karp, A. H., J. J. Greenstadt, and J. A. Filmore, 1980: Radiative transfer through an arbitrarily thick, scattering atmosphere. J. Quant. Spectro. Rad. Trans., 24, 391-406.

Knupp, Kevin R., 1985: Precipitating convective cloud downdraft structure: A synthesis of observations and modeling. Ph.D. dissertation, Colorado State University, Department of Atmospheric Science, Fort Collins, CO, 80523. (Atmospheric Science Paper No. 387)

Knupp, Kevin R. and David P. Jorgensen, 1985: Case study analysis of a large-scale and long-lived downburst-producing storm. 14th Conference on Severe Local Storms, 29 Oct - 1 Nov, 1985.

Kuciauskas, Arunas P., 1986: Use of radar in forecasting seedable conditions for the SCPP. 10th Conference on Weather Modification. May 27-30, 1986, Arlington, Virginia, AMS, Boston, MA.

Lamb, D., K.W. Nielsen, H.E. Klieforth and J. Hallett, 1976: Measurements of liquid water content in winter cloud systems over the Sierra Nevada. J. Appl. Meteor., 15, 763-775.

Lin, Y-L., R.D. Farley, and H.D. Orville, 1980: The addition of a snow content field to a cloud model. Inst. of Atmos. Sci., S. Dakota School of Mines and Technology, Rapid City, SD, 75 pp.

Liou, K.N., 1972a: Electromagnetic scattering by arbitrarily oriented cylinders, Appl. Optics, 11, 667-674.

Liou, K.N., 1972b: Light scattering by ice clouds in the visible and infrared: a theoretical study, J.Atmos.Sci., 29, 525-536.

Maddox, R.A., 1981: The structure and life-cycle of midlatitude mesoscale convective complexes. Atmospheric Science Paper No. 336, Dept. of Atmospheric Science, Colorado State University, Fort Collins, Colorado, 80523, 311 pp.

Maddox, R.A., 1983: Large-scale meteorological conditions associated with midlatitude, mesoscale convective complexes. Mon. Wea. Rev., 111, 1475-1493.

Manton, M.J., and W.R. Cotton, 1977. Parameterization of the atmospheric surface layer. J. Atmos. Sci., 34, 331-334.

Marwitz, John D., 1980: Winter storms over the San Juan mountains: Part II: Dynamical processes. Journal of the Atmospheric Sciences, 19, 913-926.

Meador, W. E., and W.R. Weaver, 1980: Two-stream approximation to radiative transfer in planetary atmospheres: A unified description of existing methods and a new improvement. J. Atmos. Sci, 37, 630.

Moler, C. B., and C. F. Van Loan, 1978: Nineteen dubious ways to compute the exponential of a matrix. SIAM Review, 20, 801-836.

Mugnai, A., and W.J. Wiscombe, 1980: Scattering of radiation by moderately nonspherical particles. J. Atmos. Sci., 37, 1291-1307.

Nickerson, E.C., E. Richard, R. Rosset, and D.R. Smith, 1986: The numerical simulation of clouds, rain, and airflow over the Vosges and Black Forest Mountains: A meso-β model with parameterized microphysics. Mon. Wea. Rev., 114, 398-414.

Cliver, D.A., W.S. Lewellen and G.G. Williamson, 1978: The interaction between turbulent and radiative transport in the development of fog and low-level stratus. J. Atmos. Sci., 35, 310-316.

Ou, S.S., and K-N, Liou, 1984: A two dimensional radiation-turbulence climate model. I: Sensitivity to cirrus radiative properties. J. Atmos. Sci., 41, 2289-2309.

Passrelli, Richard E. Jr., 1978: The evolution of snow size spectra in winter storms. University of Chicago, Technical note 52.

Platt, C.M.R., 1987: Cirrus crystals in the 2.5 m to 200 m size range. Submitted to J. Atmos. Sci.

Radke, L.F., and F.F. Hall, Jr., 1983: Tropospheric clouds and hydrometeors in atmospheric infrared backscatter: Summary of present knowledge and recommendations for future work. F.F. Hall, Jr., Editor, Wave Propagation Lab., Boulder, Colo. NOAA Tech. Memo. ERL WPL-110.

Ramanathan, V., E. J. Pitcher, R. C. Malone, and M. L. Blackmon, 1983: The response of a spectral general circulation model to refinements in radiative processes. J. Atmos. Sci., 40, 605-630.

Ramaswamy, V., and A. Detwiler, 1986: Interdependence of radiation and microphysics in cirrus clouds. J. Atmos. Sci., 43, 2289-2300.

Rauber, R.M., 1985: Physical structure of northern Colorado river basin cloud systems. Ph.D. Thesis, Atmospheric Science Paper No. 390, Department of Atmospheric Science, Colorado State University, Fort Collins, CO 80523.

Rauber, Robert M. and Lewis O. Grant, 1986: The characteristics and distribution of cloud water over the mountains of Northern Colorado during wintertime storms. Part II: Spatial distribution and microphysical characteristics. J. Clim. App. Met., 25, 489-504.

Rauber, Robert M., DaXiong Feng, Lewis O. Grant, and J.B. Snider, 1986: The characteristics and distribution of cloud water over the mountains of Northern Colorado during wintertime storms. Part I: Temporal variations. J. Clim. App. Met., 25, 468-488.

Reynolds, David W., 1986: A randomized exploratory seeding experiment on widespread shallow orographic clouds: Forecasting suitable cloud conditions. 10th Conference on Weather Modification. May 27-30, 1986, Arlington, Virginia, AMS, Boston, MA.

Reynolds, David W. and Arnett S. Dennis, 1986: A review of the Sierra Cooperative Pilot Project. Bulletin American Meteorological Society, 67, 513-523.

Roewe, D.E., 1977: Influence of cirrus clouds on the infrared cooling in the troposphere and lower stratosphere. M. Sc. Thesis, Dept. of Meteorology. University of Utah.

Roewe, D., and K.N. Liou, 1978: Influence of cirrus clouds on the infrared cooling rate in the tropopause and lower stratosphere. J. Appl. Met., 17, 92-106.

Rosinski, J., C. T. Nagamoto, G. Langer, and F. Parungo, 1970: Cirrus clouds as collectors of aerosol particles. J. Geophys. Res., 75, 2961-2973.

Rotunno, Richard, Joseph B. Klemp, and Morris L. Weisman, 1987: A theory for squall lines. To be submitted to Journal of the Atmos. Sci., 1987.

Ryan, B. T., H. Blau, Jr., P. C. von Thuna, M. L. Cohen, and G. D. Roberts, 1972: Cloud microstructure as determined by an optical cloud particle spectrometer. J. Appl. Meteor., 11, 149-156.

Sassen, Kenneth, 1984: Deep orographic cloud structure and composition derived from comprehensive remote sensing measurements. Journal of Climate and Applied Meteorology, 23, 568-583.

Schneider, S.H., W.M. Washington, and R.M. Chervik, 1978: Cloudiness as a climate feedback mechanism: Effect on cloud amounts of prescribed global and regional surface temperatures changes in the NCAR GCM. J. Atmos. Sci., 35, 2207-2221.

Scott, W.T., 1968: Analytic studies of cloud droplet coalescence I. J. Atmos. Sci., 25, 54-65.

Senior, T.B.A. and H. Weil, 1977: Electromagnetic scattering and absorption by thin-walled dielectric cylinders with application to ice crystals. Appl. Optics, 16, 2979-2985.

Shimizu, H., 1963: "Long prism" crystals observed in the precipitation in Antarctica. J. Met. Soc. Japan, 41, 305-307.

Stamnes, K., 1986: The theory of multiple scattering of radiation in plane parallel atmosphere. Reviews of Geophysics, 24, 299-310.

Stamnes, K., and R.A. Swanson, 1981: A new look at the discrete ordinate method for radiative transfer calculations in anisotropically scattering atmospheres. J. Atmos. Sci., 38, 387-399.

Starr, D. O'C., and S. K. Cox, 1980: Characteristics of middle and upper tropospheric clouds as deduced from rawinsonde data. Atmos. Science Paper No. 327, Colorado State University, Ft. Collins, Colorado, 71 pp., US ISSN 0 067-0340.

Starr, D. O'C., and S.K. Cox, 1985a: Cirrus clouds, Part 1: A cirrus cloud model. J. Atmos. Sci., 42, 2664-2681.

Starr, D. O'C., and S.K. Cox, 1985b: Cirrus clouds, Part 2: Numerical experiment on the formation and maintenance of cirrus. J. Atmos. Sci., 42, 2682-2694.

Stephens, M.A., 1979: A simple ice phase parameterization. Dept. of Atmospheric Science, Colorado State Univ., Fort Collins, CO. 80523, Atmos. Sci. Paper 319, M.S. Thesis.

Stephens, G.L., 1978a: Radiation profiles in extended water clouds. I: Theory. J. Atmos. Sci., 35, 2111-2122.

Stephens, G.L., 1978b: Radiation profiles in extended water clouds. II: Parameterization schemes. J. Atmos. Sci., 35, 2123-2132.

Stephens, G.L., 1980a: Radiative properties of cirrus clouds in the infrared region. J. Atmos. Sci., 37, 435-446.

Stephens, G.L., 1980b: Radiative transfer on a linear lattice: Application to anisotropic ice crystal clouds. J. Atmos. Sci., 37, 2095-2104.

Stephens, G.L., 1984: Scattering of plane waves by soft obstacles: Anomalous diffraction theory for circular cylinders. Appl. Optics, 23, 954-959.

Stephens, G.L. and Webster, P.J., 1979: Sensitivity of radiative forcing to variable cloud and moisture. J. Atmos. Sci., 36, 1542-1556.

Tripoli, G.J., 1986: A numerical investigation of an orogenic mesoscale convective system. Ph.D. dissertation, Colorado State University, Dept. of Atmospheric Science, Fort Collins, Colorado 80523. (Atmospheric Science Paper No. 401).

Tripoli, G.J., and W.R. Cotton, 1980: A Numerical Investigation of Several Factors Contributing to the Observed Variable Intensity of Deep Convection Over South Florida. J. Appl. Met., 19, 1037-1063.

Tripoli, G.J., and W.R. Cotton, 1982: The Colorado State University Three-Dimensional Cloud/Mesoscale Model - 1981. Part I: General Theoretical Framework and Sensitivity Experiments. J. Rech. Atmos., 16, 185-220.

Tripoli, G.J. and W.R. Cotton, 1987: A numerical study of an observed orogenic mesoscale convective system. Part 2: Analysis of governing dynamics. To be submitted to J. Atmos. Sci., 1987.

Tripoli, G.J., P.J. Flatau, and W.R. Cotton, 1987: Generalized microphysics parameterization scheme. To be published as Colorado State University Dept. of Atmospheric Science Paper as a technical report.

Waterman, P. C., 1981: Matrix-exponential description of radiative transfer. J. Opt. Soc. Am., 71, 410-422.

Welch, R.M., S.K. Cox, and J.M. Davis, 1980a: Solar radiation and clouds. Meteorological Monographs, 17, 96 pp.

Welch, R.M., S.K. Cox, and W.G. Zdunkowski, 1980b: Calculations of the variability of ice cloud radiative properties at selected solar wavelengths. Appl. Optics, 19, 3057-3067.

Wetzel, P.J., W.R. Cotton and R.L. McAnelly, 1983: A long-lived mesoscale convective complex. Part II: Evolution and structure of the mature complex. Mon. Wea. Rev., 111, 1919-1937.

Yeh, J-D., M.A. Fortune, and W.R. Cotton, 1986: Microphysics of the stratified precipitation region of a mesoscale convective system. Preprints, Conference on Cloud Physics, Snowmass, Colo., AMS, J151-154.

Yeh, Jia-Dong, Bei-Fen Fan, Michael A. Fortune, and William R. Cotton, 1987: Comparison of the microphysics between the transition region and stratiform region in a mesoscale convective complex. 3rd Conference on Mesoscale Processes, Vancouver, BC, Canada, AMS, Boston, MA.

Young, K.C., 1974a: A numerical simulation of wintertime, orographic precipitation: Part I. Description of model microphysics and numerical techniques. J. Atmos. Sci., 31, 1735-1748.

Young, K.C., 1974b: A numerical simulation of wintertime, orographic precipitation: Part II. Comparison of natural and AgI-seeded conditions. J. Atmos. Sci., 31, 1749-1767.

LIST OF PUBLICATIONS SUPPORTED BY THIS CONTRACT

Cotton, W.R., E. Mulvihill, G. Tripoli and R. Rauber, 1985: The simulation of orographic snowfall over the Northern Colorado Rockies--A blind simulation experiment. Proceedings, 4th Conf. on Weather Modification, Honolulu, Hawaii, WMC, 147-148.

Cotton, W.R., G.J. Tripoli, R.M. Rauber, 1984: A numerical simulation of the effects of small scale topographical variations on the generation of aggregate snowflakes. Preprints, 9th International Cloud Physics Conference, 21-28 August 1984, Tallinn, U.S.S.R.

Cotton, W.R., G.J. Tripoli, R.M. Rauber and E.A. Mulvihill, 1986. Numerical simulation of the effects of varying ice crystal nucleation rates and aggregation processes on orographic snowfall. J. Clim. Appl. Met., 25, 1658-1680.

Flatau, P.J., 1985: Study of second-order turbulence closure technique and its application to atmospheric flows. Colorado State Univ., Dept. of Atmospheric Science, Fort Collins, CO 80523, Atmos. Sci. Paper No. 393.

Hindman, E.E., 1986: An atmospheric water balance over a mountain barrier. J. Clim. Appl. Met., 25, 180-183.

Knupp, K.R., 1987: Downdrafts within High Plains cumulonimbi. Part I: General kinematic structure. J. Atmos. Sci., 44, 987-1008.

Knupp, K.R., and W.R. Cotton, 1985: Convective cloud downdraft structure: An interpretive study. Rev. Geophys. and Space Physics, 23, 183-215.

Knupp, K.R., and W.R. Cotton, 1985: Downdraft initiation with precipitating convective clouds. Preprints, 14th Conf. Severe Local Storms, 29 Oct - 1 Nov 1985, AMS.

Tremback, C.J. and R. Kessler, 1985: A surface temperature and moisture parameterization for use in mesoscale numerical models. Preprints, 7th Conference on Numerical Weather Prediction, 17-20 June 1985, Montreal, Canada, AMS.

Tremback, C.J., J. Powell, W.R. Cotton, and R.A. Pielke, 1987: The foward-in-time upstream advection scheme: Extension to higher orders. Mon. Wea. Rev., 115, 540-555.

Tremback, C.J., G. Tripoli, R. Arritt, W.R. Cotton, and R.A. Pielke, 1987: The regional atmospheric modeling system. Proceedings, International Conference on Development and Application of Computer Techniques to Environmental Studies, Los Angeles, CA, November 1986. P. Zannetti, Ed., Computational Mechanics Publication, Southampton, England, 601-607.

AD-A199 592 CLOUD/MESOSCALE MODEL DEVELOPMENT AND APPLICATION STUDIES(U) COLORADO STATE UNIV FORT COLLINS DEPT OF ATMOSPHERIC SCIENCE W R COTTON ET AL. 30 SEP 87 2/2

UNCLASSIFIED AFGL-TR-87-0219 F19628-84-C-0005 F/G 4/2 NL

END
DATE FILMED
11 88

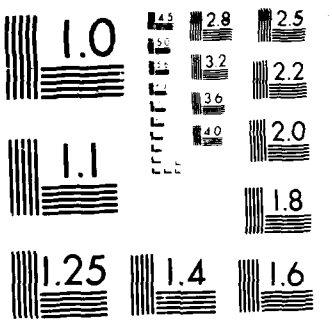

Tripoli, G.J., P.J. Flatau, and W.R. Cotton, 1987: Generalized microphysics parameterization scheme. To be published as Colorado State University Dept. of Atmospheric Science Paper as a technical report.

APPENDIX I

Comments on Realizability Conditions for the Mellor and Yamada Level 2.5 and 3 Models

by

Piotr J. Flatau and William R. Cotton
Department of Atmospheric Science
Colorado State University
Fort Collins, CO 80523

Submitted to Boundary-Layer Meteorology

December 1985

ABSTRACT

In this paper we present some analytical calculations for Level 2.5 and 3 of the well-known Mellor and Yamada (M-Y) hierarchy of second-order turbulence closure models. For Level 2.5 we extend previous calculations by M-Y and show that the requirement of positive-definiteness of the $\overline{u^2}$, $\overline{v^2}$ variances imposes stringent conditions on the possible values of mean flow quantities G_M and G_H (non-dimensional mean flow shear and temperature gradient, respectively).

Two additional parameters that are related to the predictive flow variables $G_T = \frac{l^2}{q^2} \frac{(\beta g)^2}{q^2} \overline{\theta^2}$ and $\alpha = (\frac{\overline{dU}}{dz})^2 / [(\frac{\overline{dU}}{dz})^2 + (\frac{\overline{dV}}{dz})^2]$ are shown to be important to describe the eddy-exchange coefficients and fluxes for the Level 3.0 and 2.5 model. Some of the Level 3.0 functions are presented, and the possible range of model applicability is indicated.

Finally we comment on the problem of realizability conditions and applicability of the Mellor and Yamada models.

1. INTRODUCTION

In a sequence of papers, Mellor and Yamada (Mellor,1973,1977; Mellor and Yamada,1974,1982; Yamada,1975,1983; Yamada and Mellor,1979) (hereafter refered to as M-Y) developed a hierarchy of models based on the second-order closure approach. Different degrees of simplification were employed, and the resulting schemes were defined as levels. Initially, four levels were introduced (Level 4 the most complex and Level 1 the simplest), but soon it became apparent that this classification was too narrow, and now we have levels 1.0, 1.5, 2.0, 2.5, 3.0, 3.5 and 4. The M-Y hierarchy of models gained significant popularity and was applied by many to various atmospheric flows (see Mellor and Yamada 1982 review paper for a virtually complete list of their hierarchy of models applications).

It was recognized by M-Y (1982) and others (Hassid and Galperin, 1983; Helfand and Labraga, 1985) that for some combination of the non-dimensional mean flow parameters (these can be obtained from the prognostic equations) the model predicts negative variances or results in singularities in solutions. Such non-physical behavior appears to be related to highly transitory phenomena such as rapid change from day to night conditions or to the rapid entrainment at the top of the mixed layer.

Mellor and Yamada mention that negative variances appear occasionally in their simulations. In the 1974 paper they state that: "The components $\overline{u^2}$, $\overline{v^2}$, and $\overline{w^2}$ should, of course, be positive definite. This turns out to be true in practice everywhere in the Level 2 calculation and nearly so for Levels 3 and 4 where, however, small negative values appeared between 0700-0800 (after a discontinuity in the

tendency of wall temperature) at a couple grid points."

Recognition of such non-physical behavior lead M-Y and others (Hassid, 1983; Helfand, 1985) to the so-called realizability conditions for possible values of turbulent fluxes and/or mean flow quantities. Simply stated, this means that whenever a model gives non-physical behavior, the clipping approximation (setting a non-physical value to some other, usually arbitrary, value) is employed or change of (predicted) mean flow gradient has to be made. Therefore, it seems to be of importance to predict the possible limits of M-Y hierarchy of models in advance. This provides insight on the range of model applicability and saves one frustration during the code developement.

In Chapter 2 we discuss briefly M-Y Level 2.5 and 3.0 models and resulting eddy exchange coefficients and turbulent fluxes. In Chapter 3 we present some analytical calculations for the Level 2.5 and 3 models. For Level 2.5 we extend previous calculations by M-Y (1982) and show that the requirement of positive-definiteness of the $\overline{u^2}$ and $\overline{v^2}$ variances imposes stringent conditions on the possible values of the mean flow quantities G_M and G_H (non-dimensional mean flow shear and temperature gradient, respectively).

Two additional parameters that are related to the predictive flow variables $G_T = \frac{l^2}{q^2}\frac{(\beta g)^2}{q^2}\overline{\theta^2}$ and $\alpha = (\frac{\bar{dU}}{dz})^2 / [(\frac{\bar{dU}}{dz})^2 + (\frac{\bar{dV}}{dz})^2]$ are shown to be important to describe eddy-exchange coefficients and fluxes for the Level 3.0 and 2.5 model. Some of the Level 3.0 functions are presented and possible range of model applicability is indicated.

Finally, in Chapter 4, we comment on the problem of realizability conditions and applicability of the Mellor and Yamada models.

2. MODEL EQUATIONS

M-Y use departure from isotropy as a small parameter in their analysis of the Reynolds-averaged equations. They show that in the atmospheric boundary layer (ABL) one can neglect diffusion, time and advection terms. Level 3 predicts only variances. In Level 2.5 only the equation for the turbulent kinetic energy (TKE) is retained.

Because of simplifications applied to the theory, the resulting set of Reynolds equations is linear and can be solved analytically. The algebra used in this study is extensive (see Yamada, 1978; Flatau, 1985 for more details). For many algebraic manipulations in this paper we used the symbolic algebra program REDUCE 3 (Hearn,1984). We will present results for the calculations of the dry case (i.e., without cloud microphysics-turbulence covariances). The extension to a moist case is relatively simple.

To make the final formulas more compact, let us introduce several non-dimensional quantities. The non-dimensional eddy exchange coefficients S_M and S_H are defined by the following equations

$$K_M = lqS_M \tag{1}$$

and

$$K_H = lqS_H \tag{2}$$

where K_M and K_H are momentum and heat eddy exchange coefficients, l is turbulent length scale, and q is defined by $q^2 = \overline{u^2} + \overline{v^2} + \overline{w^2}$. The $\overline{u^2}$, $\overline{v^2}$ and $\overline{w^2}$ are velocity variances.

We also define the non-dimensional parameters G_M, G_H, G_T, and α, which are related to the mean flow variables

$$G_M = \frac{l^2}{q^2}\left(\left(\frac{\partial \bar{U}}{\partial z}\right)^2 + \left(\frac{\partial \bar{V}}{\partial z}\right)^2\right) \tag{3}$$

$$G_H = \frac{l^2}{q^2}\beta g\frac{\partial \bar{\theta}}{\partial z} \tag{4}$$

$$G_T = \frac{l^2}{q^2}\frac{(\beta g)^2}{q^2}\overline{\theta^2} \tag{5}$$

$$\alpha = \left(\frac{d\bar{U}}{dz}\right)^2 / \left[\left(\frac{d\bar{U}}{dz}\right)^2 + \left(\frac{d\bar{V}}{dz}\right)^2\right] \tag{6}$$

where $\beta = 1/\theta_o$, θ_o is the basic state potential temperature, $\overline{\theta^2}$ is the potential temperature variance, $\frac{\partial \bar{U}}{\partial z}$, $\frac{\partial \bar{V}}{\partial z}$ are mean flow velocity gradients, and $\frac{\partial \bar{\theta}}{\partial z}$ is the potential temparature gradient. It can be seen that $0 \leq \alpha \leq 1$. Notice that G_M, G_H, G_T, and α are related to the prognostic equations in the model. In other words, if we express all variables in terms of G_M, G_H, G_T, and α, then the problem is solved. After some algebra we can show that S_M and S_H for the Level 3.0 are given by

$$S_M = \frac{S_M^n}{S^d},$$

$$S_H = \frac{S_H^n}{G_H S^d} \tag{7a,b}$$

where

$$S_M^n = 9G_H A_2 A_1 (A_2 + 4A_1 C_1) + A_1(27A_1^2 G_T + 36A_2 A_1 G_T - 3C_1 + 1)$$

$$S_H^n = -9G_H^2 A_2^2 A_1 + 18G_H G_M A_2 A_1^2 C_1 + G_H A_2(-27A_2 A_1 G_T + 1) + 18G_M A_2 A_1^2 G_T + 3A_2 G_T$$

$$S_d = 108G_H^2A_2^2A_1^2 + 54G_HG_MA_2^2A_1^2 - 21G_HA_2A_1 + 6G_MA_1^2 + 1$$

These formulas are the same as those in Mellor and Yamada's (1974) paper (eqs 55,56), although they are written here in the non-dimensional form.

For the Level 2.5 we get the non-dimensional eddy exchange coefficients in the form

$$S_M = \frac{S_M^n}{S^d},$$

$$S_H = \frac{S_H^n}{S^d} \qquad (8a,b)$$

where

$$S_d = (3G_HB_2A_2 + 12G_HA_2A_1 - 1)(6G_MA_1^2 - 9G_HA_2A_1) - G_MG_H(54A_2^2A_1^2 + 72A_2A_1^3) + G_HA_2(3B_2 + 12A_1) - 1$$

$$S_H^n = -(18G_MC_1A_1^2 - 9G_HA_2A_1 + 1)A_2$$

$$S_M^n = -G_HA_1(9C_1B_2A_2 + 36C_1A_2A_1 - 3B_2A_2 + 9A_2^2 - C_1 + 1)$$

For both levels the final set of equations is

$$\overline{u^2}/q^2 = 1/3 + A_1\delta S_MG_M - 2A_1S_HG_H,$$

$$\overline{v^2}/q^2 = 1/3 + A_1\beta S_MG_M - 2A_1S_HG_H, \text{ and}$$

$$\overline{w^2}/q^2 = 1/3 + 2A_1S_MG_M + 4A_1S_HG_H, \qquad (9a,b,c)$$

where $\delta = 2(3a - 1)$ and $\beta = 2(2 - 3a)$.

$$\overline{uv} = 6A_1l^2S_M\frac{\partial\bar{U}\partial\bar{V}}{\partial z\partial z}$$

$$\overline{uw} = -lqS_M\frac{\partial\bar{U}}{\partial z}$$

$$\overline{vw} = -lqS_M \frac{\partial \bar{V}}{\partial z} \qquad (10a,b,c)$$

$$\overline{u\theta} = 3A_2 l(S_H + S_M) \frac{\partial \bar{\theta}}{\partial z} \frac{\partial \bar{U}}{\partial z}$$

$$\overline{v\theta} = 3A_2 l(S_H + S_M) \frac{\partial \bar{\theta}}{\partial z} \frac{\partial \bar{V}}{\partial z}$$

$$\overline{w\theta} = -lqS_H \frac{\partial \bar{\theta}}{\partial z} \qquad (11a,b,c)$$

and for Level 2.5 only

$$\overline{\theta^2} = B_2 lS_H \frac{\partial \bar{\theta}}{\partial z} \qquad (12)$$

The ratio of TKE production to dissipation can be expressed as

$$(P_s + P_b)/\varepsilon = B_1(S_M G_M + S_H G_H) \qquad (13)$$

3. ANALYTICAL RESULTS FOR THE MELLOR AND YAMADA HIERARCHY OF MODELS

In this chapter we discuss some analytical results and realizability conditions for the Mellor and Yamada (1982) hierarchy of models - Levels 2.5 and 3.0. The purpose of such a study is to decide what the possible limitations of the scheme are. Using the typical values of parameters G_H, G_M, G_T, R_f, and α (see Chapter 2), we are able to plot fields of turbulent variances and co-variances. Obvious criteria such as positive-definiteness of variances are used to limit the possible range of mean flow values.

3.1 Level 2.5

The Level 2.5 model depends on three predictive parameters. These are G_H (non-dimensional temperature gradient), G_M (non-dimensional quantity related to the mean flow shear), and α (ratio of shear squares in the x and y directions). See Chapter 2 for their definitions. The

contours of turbulent quantities such as non-dimensional momentum and heat eddy coefficients, turbulent variances $\overline{u^2}$, $\overline{v^2}$, $\overline{w^2}$ and ratio of the turbulent production to the turbulent dissipation are plotted here with G_H and G_M as independent variables. The α-dependence of these turbulent quantities will also be discussed.

Let us start with the Figure 2b where $(P_s + P_b)/\varepsilon$ is plotted. The G_M values are always positive and are shown there for (0.,3.) region. The G_H values can be negative (for stable case) and positive (for unstable case). The (-0.4,0.1) range of G_H values is used here. The isoline $(P_s + P_b)/\varepsilon = 1$ corresponds to the local equilibrium assumption (i.e., it satisfies the Level 2.0 model conditions). On the other hand, for arbitrary G_H and G_M, the $(P_s + P_b)/\varepsilon \neq 1$. This is clearly seen in Figure 2b. In Figure 2b isolines labeled INF-1 represent values of G_H and G_M for which $(P_s + P_b)/\varepsilon$ is singular. Curves labeled P1 and P2 give G_H and G_M values where $(P_s + P_b)/\varepsilon$ goes to zero. Contours are plotted for $(P_s + P_b)/\varepsilon = (0.5,1.0,1.5,2.0,2.5)$.

The P1 isoline originates at $G_M = 0$ and $G_H = 0$. It delimits the region of positive (upper part) and negative (lower part) values of $(P_s + P_b)/\varepsilon$. For the stable case ($G_H < 0$) and small G_M, the buoyancy term P_b becomes negative and is larger than shear generation term P_s. This leads to negative $(P_s + P_b)/\varepsilon$. On the other hand, for the unstable case, values of $(P_s + P_b)/\varepsilon$ are always positive.

Figures 1 and 2a present values of eddy exchange coefficients S_M and S_H. The INF-1 curve is the same as before and represents G_H and G_M values for which S_H and S_M tends to infinity. These large values of exchange coefficients are not physically possible, and the region close to the INF curve has to be somehow excluded. The values to the left of

INF curve are positive, which indicates positive exchange coefficients. On the S_M diagram the SM curve is for $S_M = 0$. In the region between INF and SM curves in Figure 1, the S_M values are negative: however, from other considerations (positive definiteness of velocity variances), we will have to exclude this region. In other words, Level 2.5 is forced to predict positive (down-gradient) values of exchange coefficients. Positive definiteness of velocity variance also leads to some limits on the possible values of G_H and G_M.

Compare now Figures 1 (S_M) and 2b (production/dissipation). Notice that the gradient Richardson number is given by $Ri = -G_H/G_M$. One can then easily obtain S_M as a function of Ri for constant values of $(P_s + P_b)/\varepsilon$. Figure 6 combines plots of the curves discussed above (i.e., S_M, S_H, and $(P_s + P_b)/\varepsilon$) and can be used for tracing S_H, S_M behavior for constant $(P_s + P_b)/\varepsilon$ values. In Figure 6 heavy solid lines are S_M values, S_H values are represented by broken lines, and thin solid lines are $(P_s + P_b)/\varepsilon$ values. For G_M approaching 0 with the constraint $(P_s + P_b)/\varepsilon$ = const. (i.e., traveling down the $(P_s + P_b)/\varepsilon$ isoline), we get a finite value of S_M. This limited value corresponds to infinite (and negative) Richardson number. Notice that $(P_s + P_b)/\varepsilon > 0$ isolines cross the G_H axis for positive, non-zero values of G_H. The above discussion applies to the other turbulent covariances. They all can be expressed as a function of only one mean flow quantity (Richardson number) if a certain constraint on the ratio of the turbulent production to the turbulent dissipation is imposed.

Figures 3-5a,b show turbulent variances of velocity components $\overline{w^2}/q^2$, $\overline{u^2}/q^2$, $\overline{v^2}/q^2$. From Eqs. 9a,b we see that u- and v-variances depend on α. It can be shown that from the point of view of

realizability conditions the $\alpha = 0$ and $\alpha = 1$ give the most stringent limitations on the possible G_H values. Therefore, all the results here are presented for $\alpha = 1$; i.e., for $\frac{\partial \bar{V}}{\partial z} = 0$. The $\overline{w^2}/q^2$ is not dependent on α. Examining Figures 3-5 we see that $\overline{v^2}/q^2$ is positive only for $G_H \leq 0.0288$, and this limit seems to guarantee positive definiteness of all velocity variances.

Finally we present velocity variances and $(P_s + P_b)/\varepsilon$ as a function of S_M and S_H (Figures 7-8a,b). Again $\alpha = 1$. Only positive isolines and those that are smaller than one are plotted for the velocity variances. The isolines are labelled A,B,C,D, and E and correspond to (0.001, 0.2, 0.5, 0.7, 1.0) values. The isotropic case (all variances equal to 1/3) gives approximately the same values of S_M and S_H. The realizable solution follows this patterr for other velocity variances; i.e., the S_H and S_M values are of the same order.

3.2 Level 3.0

This level of simplification was considerably less investigated and used by researchers. We performed analysis of this model and some of the results are presented in Figures 9-14. Here the additional parameter G_T comes to play, which makes analysis more involved. We plot G_M-G_H dependence of turbulent quantities for 2 different values of G_T = (0.1, 3.0). The range of G_M and G_H is from -6 to 6 on all plots. Values of G_M have to be positive, but negative ones are retained here for illustrative purposes. As before, negative values are plotted as dashed lines. Contours for the normalized (by q^2) velocity variances are chosen at 0.05, 0.2, 0.5 and 1.0 (0.12 instead of 0.2 for the vertical velocity variance). By definition, all velocity variances have to be in the (0,1) range. One can see (e.g., in Figure 9) that values

(G_M, G_H) giving realizable solutions for the Level 2.5 may now correspond to negative variances. The solutions are highly variable with G_T. The realizable values are, in general, located close to the $(P_s + P_b)/\varepsilon = 1$ isoline.

We diagnostically calculated (Flatau, 1985) Level 3.0 functions from the numerical results of our runs of the Level 2.5 model. The results indicated that the Level 3.0 produces very stringent conditions on the G_M and G_H values. The picture is still not clear; however, we hope to obtain some diagnostic results from the working Level 3.0 model.

4. CONCLUSIONS

As was mentioned, it seems that the Level 2.5 and 3.0 model does not properly handle transitory phenomena but has the ability to adjust the mean flow and turbulence to consistently physical values. As long as variances are not used explicitly (for example to diagnose triple correlation terms) but are just diagnosed, the fact that they are negative is only annoying. The slowly varying phenomena, e.g., dry boundary layer on a sunny day - as in the Wangara case - are predicted well by the lower-level, second-order closure schemes. The apparent failure of Level 3.0 and 2.5 to predict highly variable flows can probably be traced to the basic assumption of Mellor and Yamada - namely, scaling out the advection and diffusion terms in almost all equations. At the top of the stratocumulus layer where intensive, local (radiative) cooling is distributed mainly through turbulent diffusion and where gradients of stratification are strong, the assumption of the small role of diffusional terms can be a weak one (see e.g. Chen, 1984 simulations of Sc deck). In such a case, when greater definition of the turbulence is important, our results indicate that the

higher-level second-order turbulence closure scheme should be used. It is true, though, that the model is driven towards local equilibrium. Imagine vigorous TKE advected to an otherwise undisturbed region. Parameterization of dissipation provides negative feedback in the TKE equation

$$\frac{\partial q^2}{\partial t} = \ldots - \frac{q^3}{\Lambda_2},$$

and the model will adjust to local equilibrium. This fact is probably the only justification of usage of the Level 2 (which is based on the local equilibrium assumption) model together with a prognostic equation for the TKE (this scheme was used by Yamada (1983)). Such a scheme, by definition, cannot take into account situations which are strongly out of equilibrium. Similiary, we have shown in Chapter 3 that the Level 2.5 and 3.0 give realizable solutions only for the situations close to the local equilibrium.

Probably the simplest and the strongest recommendation that can be inferred from this study is to apply the lower-level second-order schemes in accordance with their assumptions. The Mellor and Yamada hierarchy is based on small parameter scale analysis (departure from isotropy), and if this assumption is not satisfied, the scheme will not work properly. Although the realizability conditions should be checked diagnostically, their use should be limited as much as possible. If the model is consistently not realizeable, the only reasonable solution is to implement the higher-level scheme. If the non-realizable solutions occur sporadically (model spin-up time, transition from day to night, top of the PBL), and if the main emphasis of the model is not on a very detailed physical depiction of these regimes, it can be used with some confidence.

ACKNOWLEDGEMENTS

We would like to thank Mrs. Brenda Thompson for her patience in typing the manuscript and Ms. Judy Sorbie for drafting the figures. Ms. Annette Claycomb contributed significantly in improving this manuscript. Several conversations and letters exchanged with Dr G.L. Mellor were very useful.

This research was supported by the Air Force Geophysics Laboratory, Meteorology Division - Cloud Physics Branch under Contract #F19628-84-C-0005 and under Electric Power Research Institute Contract #RFP 1630-25. Computations were performed on the National Center for Atmospheric Research (NCAR) Cray-1 computer. NCAR is supported by the National Science Foundation.

REFERENCES

Bader, D.C.: 1985, 'Regional Boundary Layer Evolution in Mountainous Terrain', Ph.D. Thesis, Dept. of Atmospheric Science, Colorado State University, Fort Collins, CO, 80523.

Chen, C.: 1984, 'The Physics of the Marine Stratocumulus-Capped Mixed Layer', Ph.D Thesis, Colorado State University, Fort Collins, Colo.

Flatau, P.J.: 1985, 'Study of Second-Order Turbulence Closure Technique and its Application to Atmospheric Flows', M.Sc. Thesis, Dept. of Atmospheric Science, Colorado State University, Fort Collins, CO, 80523.

Hassid, S. and Galperin, B.: 1983, 'A Turbulent Energy Model for Geophysical Flows', Boundary-Layer Meteorol. 26, 397-412.

Hearn, A.C.: 1984, REDUCE User's Manual, Ver. 3.0, The RAND Corp., Santa Monica, Rand Publ. CP78(4/83).

Helfand, H.M. and Labraga, J.C.: 1985, 'Design of a Nonsingular Level 2.5 Second-Order Closure Model for the Prediction of Atmospheric Turbulence', submitted for publication.

Mellor, G.L.: 1973, 'Analytic Prediction of the Properties of Stratified Planetary Surface Layers', J.Atmos.Sci. 30, 1061-1069.

Mellor, G.L.: 1977, 'The Gaussian Cloud Model Relations', J. Atmos. Sci. 34, 356-358 and 1483-1484.

Mellor, G.L., and Yamada, T.: 1974, 'A Hierarchy of Turbulence Closure Models for Planetary Boundary Layers', J.Atmos.Sci. 34, 1791-1806. (Corrigenda: 1977, J.Atmos.Sci. 34, 1482).

Mellor, G.L., and Yamada, T.: 1982, 'Development of a Turbulence Closure Model for Geophysical Fluid Problems', Rev.Geophys.Space Phys. 20,

851-875.

Yamada, T.: 1975, 'The Critical Richardson Number and the Ratio of the Eddy Transport Coefficients Obtained from a Turbulence Closure Model', J. Atmos. Sci. 32, 926-933.

Yamada, T.: 1978, 'A Three-Dimensional, Second-Order Closure Numerical Model of Mesoscale Circulation in the Lower Atmosphere', Topical Rep. ANL/RER-78-1, 67 pp., Radiol. and Environ. Res. Div., Argonne Natl. Lab., Argonne, Ill.

Yamada, T., and Mellor, G.L.: 1975, 'A Simulation of the Wangara Atmospheric Boundary Layer Data', J.Atmos.Sci. 32, 2309-2329.

Yamada, T. and Mellor, G.L.: 1979, 'A Numerical Simulation of the BOMEX Data Using a Turbulence Closure Model Coupled with Ensemble Cloud Relations', Q.J. Roy. Meteorol. Soc. 105, 915-944.

Yamada, T.: 1983, 'Simulations of Nocturnal Drainage Flows by a q^2 l Turbulence Model', J. Atmos. Sci. 40, 91-106.

Figure 1. Level 2.5 functions. Constants of the model are indicated at the top of each plot. They are in the A_1, A_2, B_1, B_2, C_1, C_2, C_3 order. The INF-1 curve indicates values where functions tend to infinity. Here momentum eddy exchange coefficient S_M is plotted.

Figure 2. (a) Same as in Figure 1, but for S_H; (b) same as in Figure 1, but for $(P_s + P_b)/\varepsilon$, P1 curve indicate points where function goes to 0.

Figure 3. (a) Same as in Figure 1, but for $\overline{w^2}/q^2$, VEL-1 is where function goes to 0, (b) same as (a), different G_H, G_M.

Figure 4. (a) Same as in Figure 1, but for $\overline{u^2}/q^2$, VEL-1 is where function goes to 0, (b) same as (a), different G_H, G_M.

Figure 5. (a) Same as in Figure 1, but for $\overline{v^2}/q^2$, VEL-1 is where function goes to 0, (b) same as (a), different G_H, G_M.

Figure 6. Composite of plots presented in Figures 1 and 2. The heavy solid lines indicate S_M functions, broken lines are isolines of S_H, and thin solid lines are isolines of the ratio of turbulent production and dissipation. The INF-1 curve gives singular points for all functions. P1 and P2 curves are for $(P_s + P_b)/\varepsilon = 0$.

Figure 7. Level 2.5 plots as a function of S_M and S_H. (a) For $\overline{u^2}/q^2$, (b) for $\overline{v^2}/q^2$.

Figure 8. Level 2.5 plots as a function of S_M and S_H (a) $\overline{w^2}/q^2$, (b) $(P_s + P_b)/\varepsilon$.

Figure 9. Level 3.0 functions. Constants of the model are indicated at the top of each plot. They are in the A_1, A_2, B_1, B_2, C_1, G_T. The INF-1 curve indicates values where functions tend to infinity. Here $G_T = 0.1$. Numbers at the bottom of each plot indicate G_H values for $G_M = 0$ where the denominator (first two numbers) and numerator (next number or numbers) of the function tend to zero.

Figure 10. (a) Same as in Figure 9, but for $(P_s + P_b)/\varepsilon$, the P1 curve indicates values of G_M and G_H where $(P_s + P_b)/\varepsilon$ goes to zero, (b) same as (a) but, for $\overline{u^2}/q^2$.

Figure 11. (a) Same as in Figure 9, but for $\overline{v^2}/q^2$, (b) same as in Figure 9, but for $\overline{w^2}/q^2$.

Figure 12. Same as in Figure 9, but for $G_T = 3.0$.

Figure 13. Same as in Figure 10, but for $G_T = 3.0$.

Figure 14. Same as in Figure 11, but for $G_T = 3.0$.

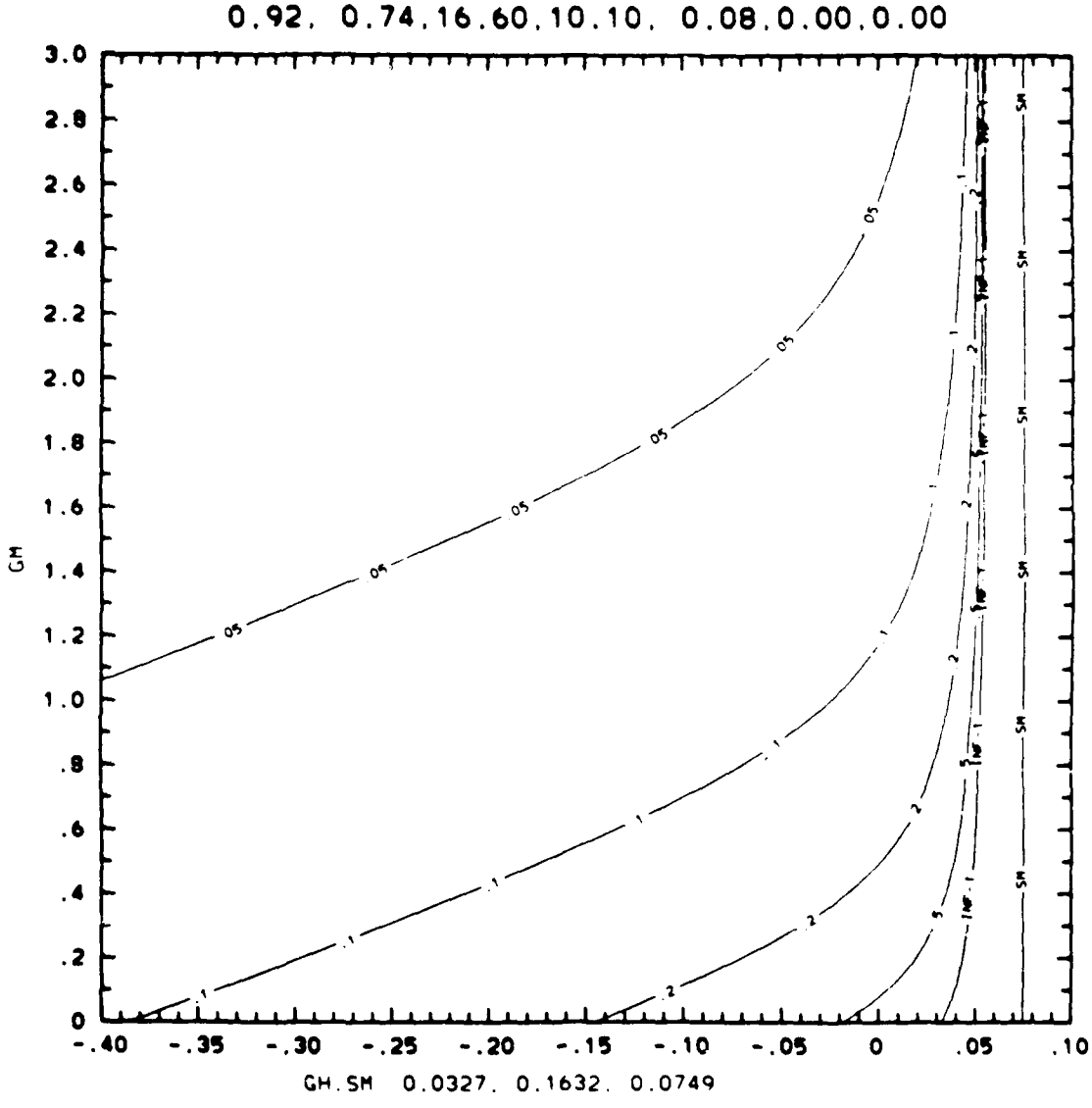
0.92, 0.74,16.60,10.10, 0.08,0.00,0.00
GM
3.0
2.8
2.6
2.4
2.2
2.0
1.8
1.6
1.4
1.2
1.0
.8
.6
.4
.2
0
-.40
-.35
-.30
-.25
-.20
-.15
-.10
-.05
0
.05
.10
GH.SM 0.0327, 0.1632, 0.0749

Figure 1

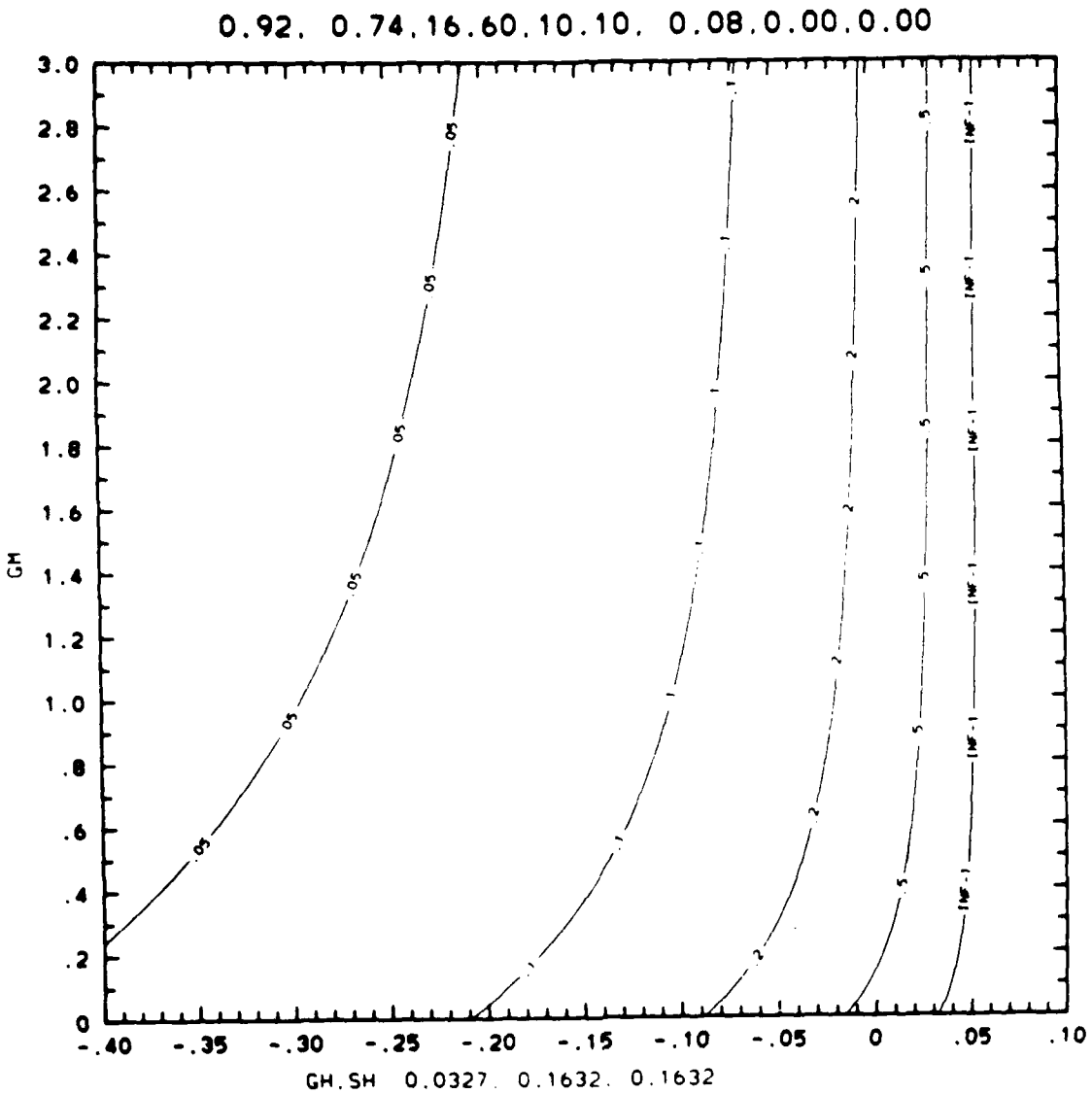

Figure 2a

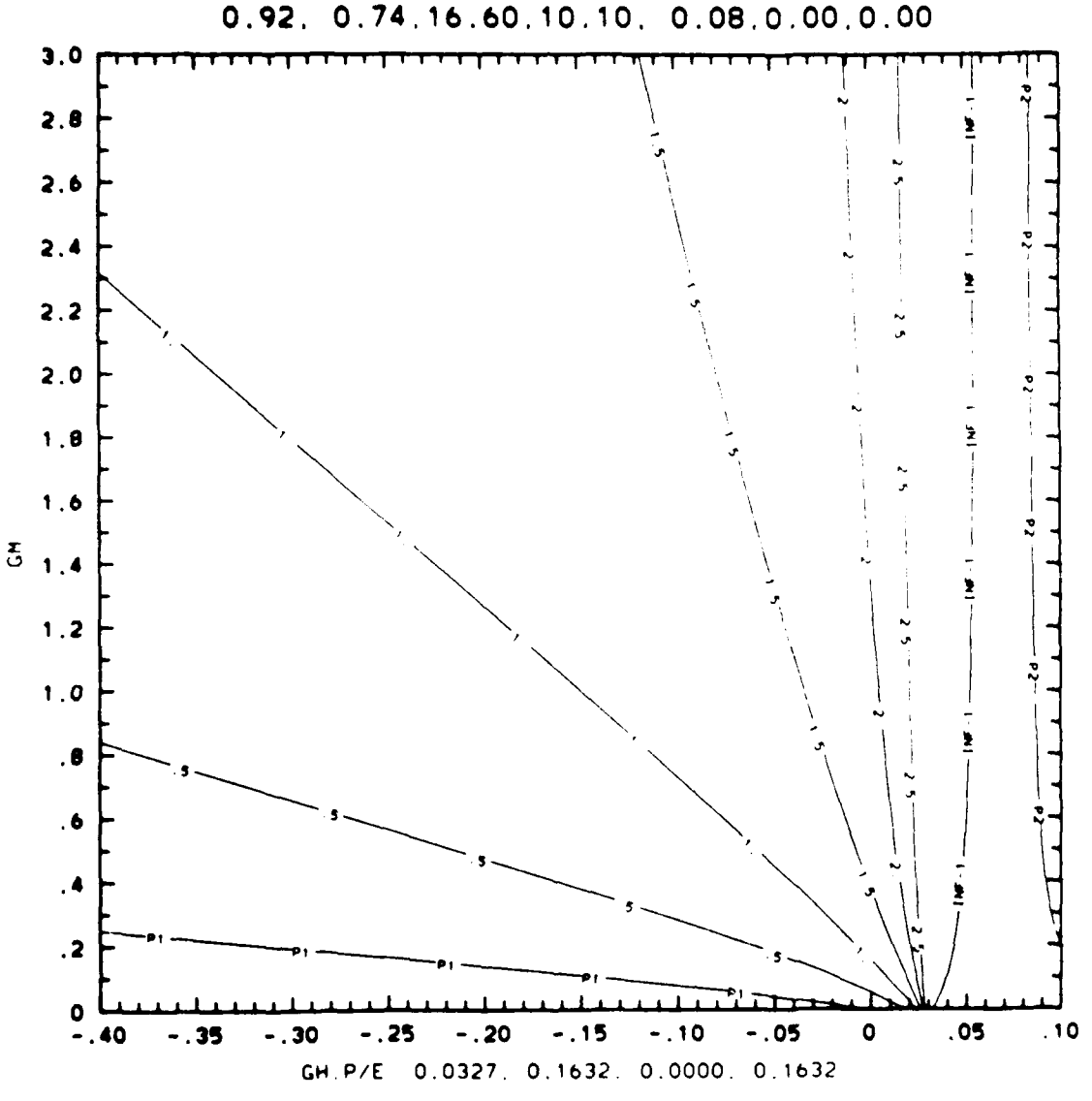
0.92, 0.74,16.60,10.10, 0.08,0.00,0.00
GM
3.0
2.8
2.6
2.4
2.2
2.0
1.8
1.6
1.4
1.2
1.0
.8
.6
.4
.2
0
-.40
-.35
-.30
-.25
-.20
-.15
-.10
-.05
0
.05
.10
GM,P/E 0.0327, 0.1632, 0.0000, 0.1632

Figure 25

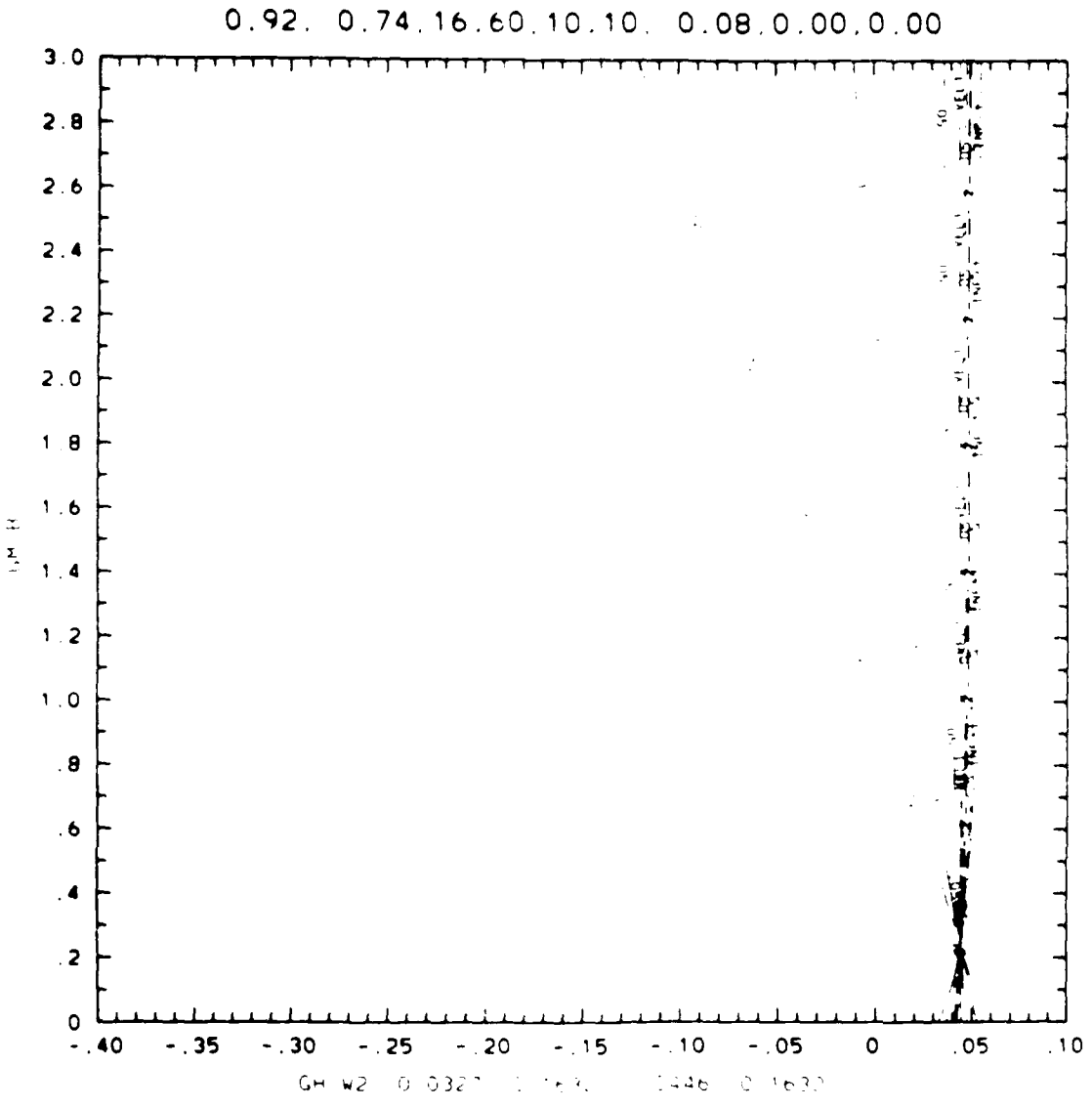
0.92, 0.74,16.60,10.10, 0.08,0.00,0.00
3.0
2.8
2.6
2.4
2.2
2.0
1.8
1.6
1.4
1.2
1.0
.8
.6
.4
.2
0
-.40
-.35
-.30
-.25
-.20
-.15
-.10
-.05
0
.05
.10

Figure 3a

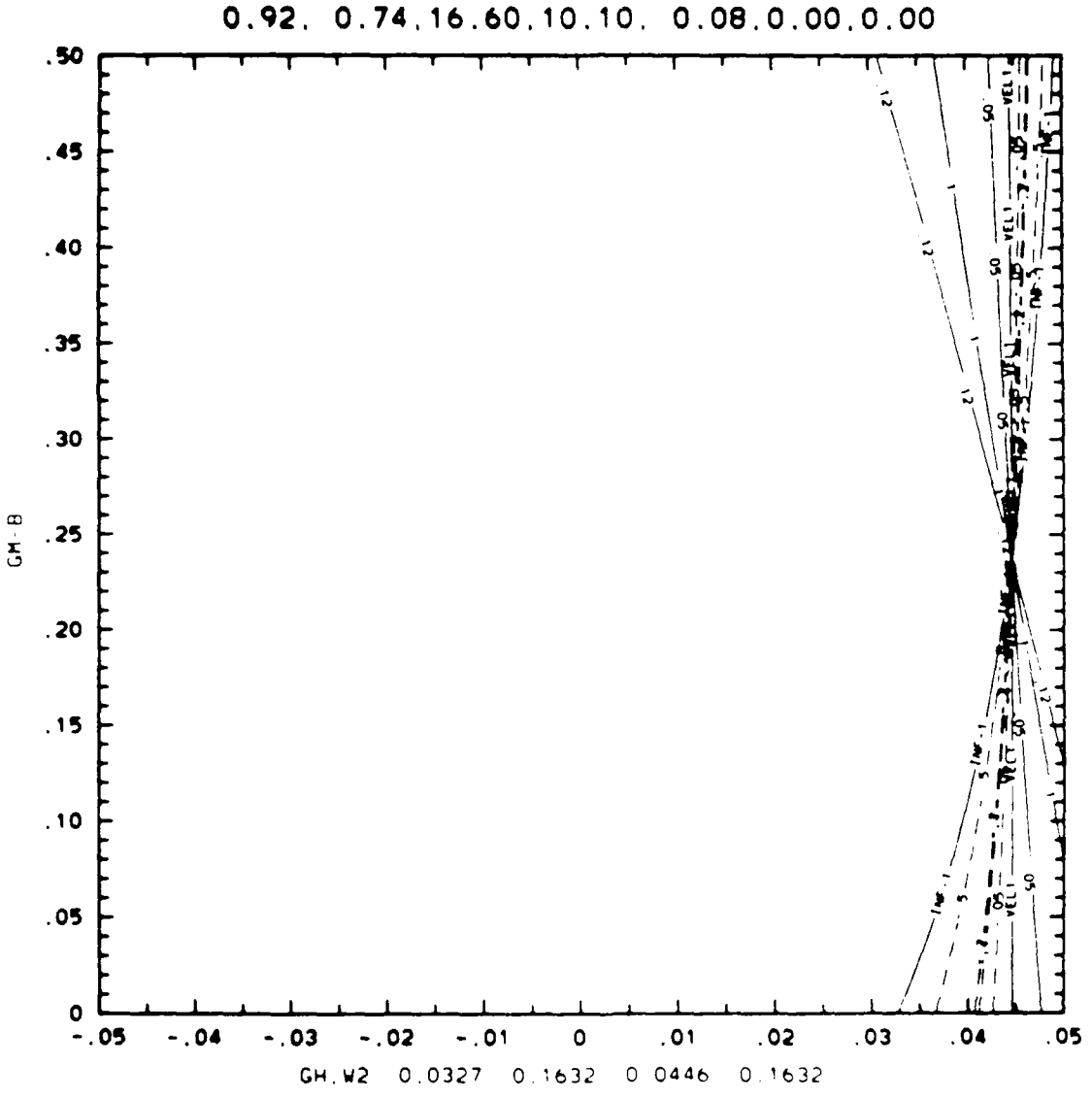
0.92, 0.74,16.60,10.10, 0.08,0.00,0.00
GM-B
.50
.45
.40
.35
.30
.25
.20
.15
.10
.05
0
-.05
-.04
-.03
-.02
-.01
0
.01
.02
.03
.04
.05
GH.W2 0.0327 0.1632 0.0446 0.1632

Figure 4

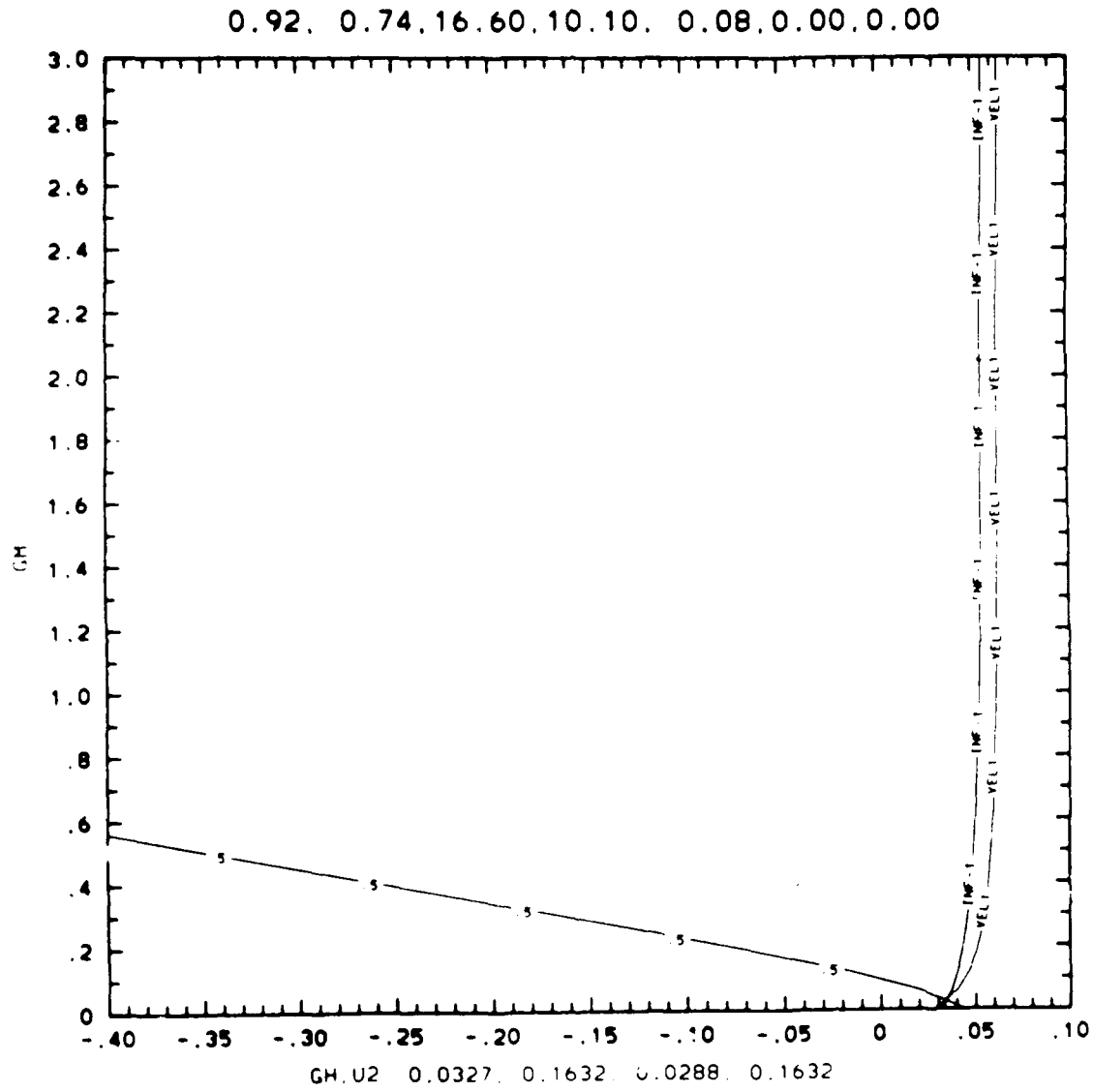
0.92, 0.74,16.60,10.10, 0.08,0.00,0.00
3.0
2.8
2.6
2.4
2.2
2.0
1.8
1.6
1.4
1.2
1.0
.8
.6
.4
.2
0
G,H
-.40
-.35
-.30
-.25
-.20
-.15
-.10
-.05
0
.05
.10
GH,U2 0.0327, 0.1632, 0.0288, 0.1632
INF-1
VEL1
5

Figure 5a

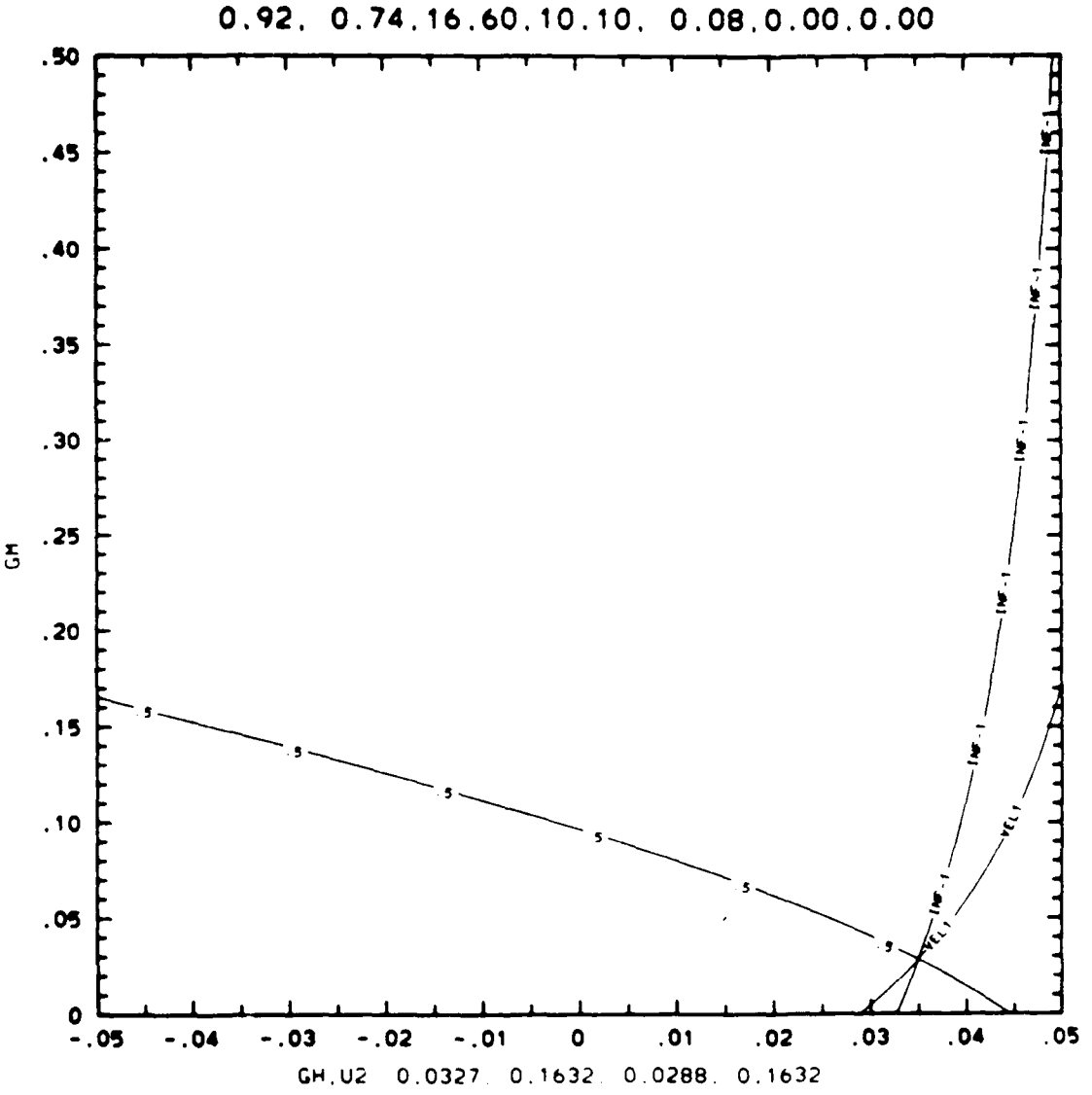
0.92, 0.74,16.60,10.10, 0.08,0.00,0.00
.50
.45
.40
.35
.30
.25
.20
.15
.10
.05
0
GM
-.05
-.04
-.03
-.02
-.01
0
.01
.02
.03
.04
.05
GH,U2 0.0327 0.1632 0.0288 0.1632

Figure 4b

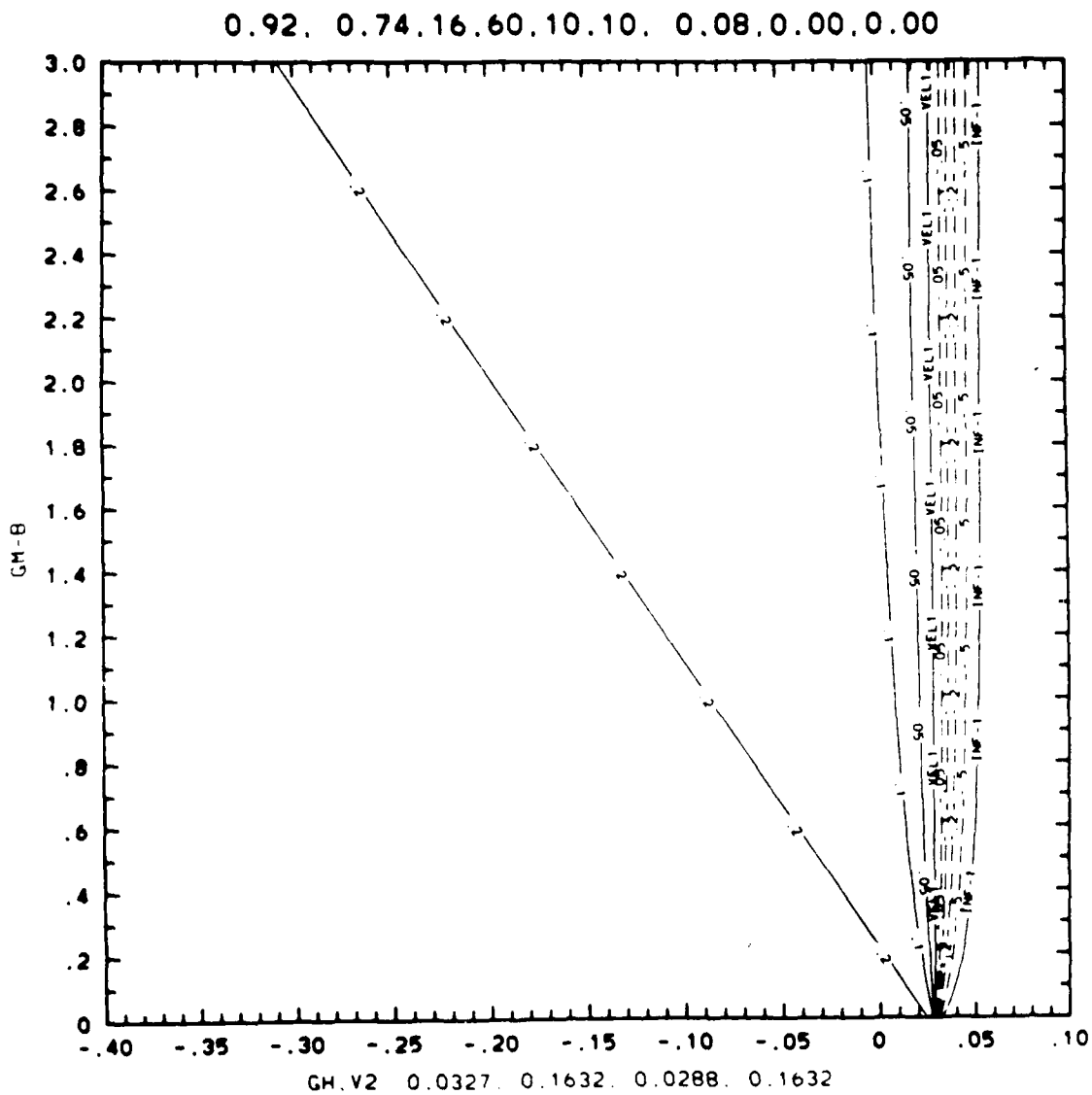
0.92, 0.74,16.60,10.10, 0.08,0.00,0.00
GM-B
3.0
2.8
2.6
2.4
2.2
2.0
1.8
1.6
1.4
1.2
1.0
.8
.6
.4
.2
0
-.40
-.35
-.30
-.25
-.20
-.15
-.10
-.05
0
.05
.10
GH,V2 0.0327, 0.1632, 0.0288, 0.1632

Figure 5a

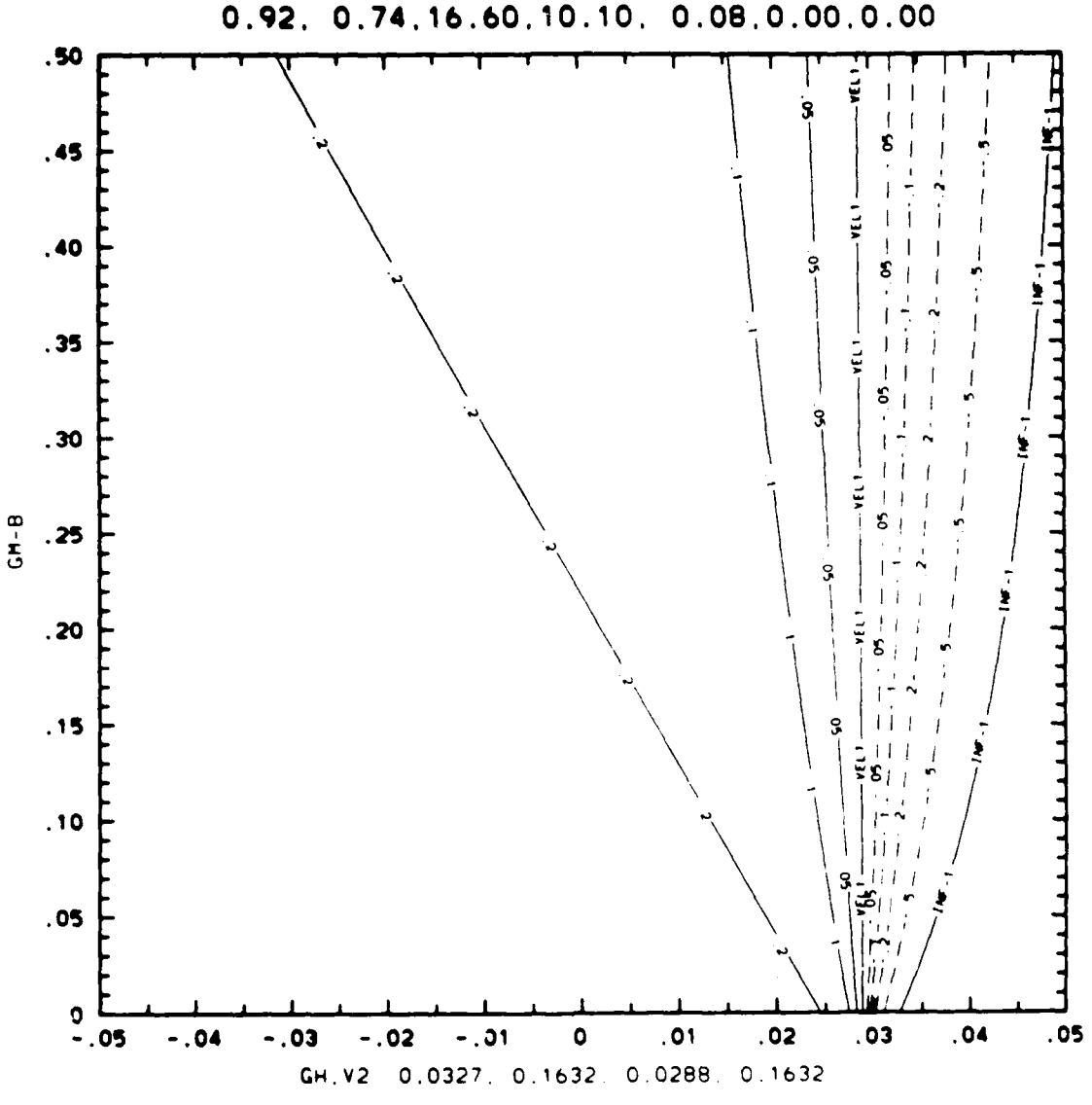
0.92, 0.74,16.60,10.10, 0.08,0.00,0.00
GM-B
.50
.45
.40
.35
.30
.25
.20
.15
.10
.05
0
-.05
-.04
-.03
-.02
-.01
0
.01
.02
.03
.04
.05
GH.V2 0.0327, 0.1632, 0.0288, 0.1632

Figure 5b

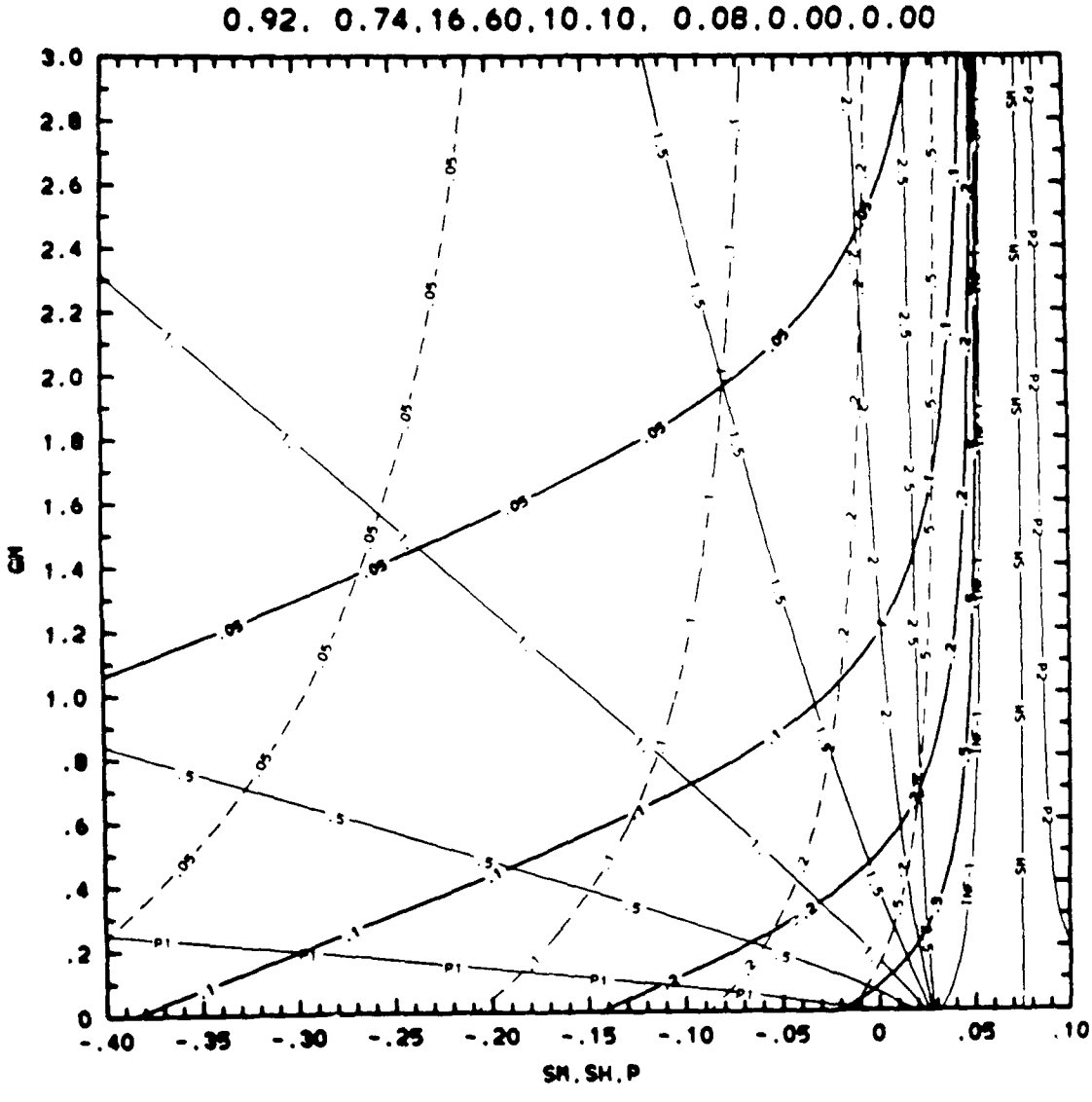
0.92. 0.74.16.60.10.10. 0.08.0.00.0.00
3.0
2.8
2.6
2.4
2.2
2.0
1.8
1.6
1.4
1.2
1.0
.8
.6
.4
.2
0
SH
-.40
-.35
-.30
-.25
-.20
-.15
-.10
-.05
0
.05
.10
SM.SH.P

Figure 6

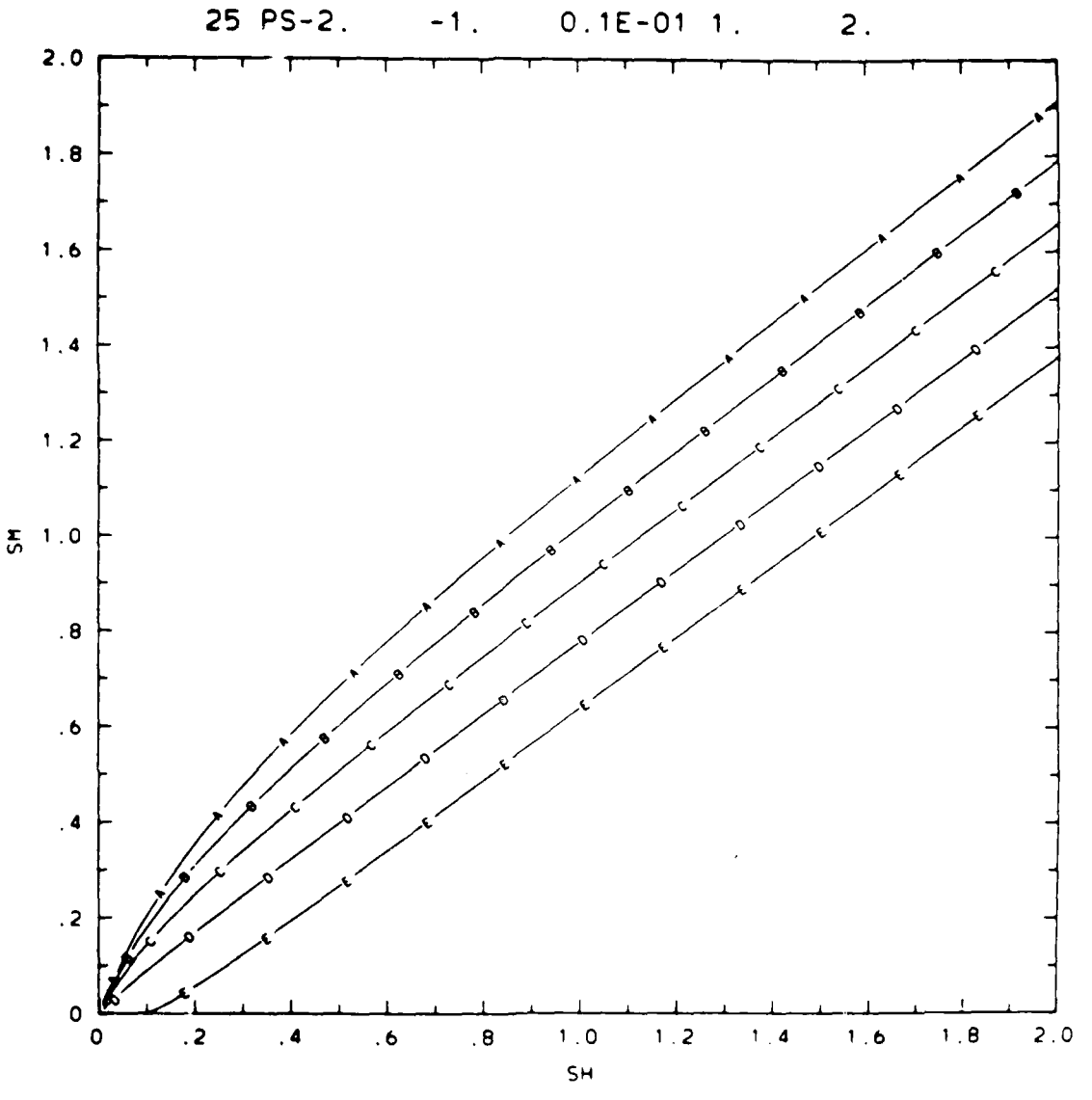

Figure 7

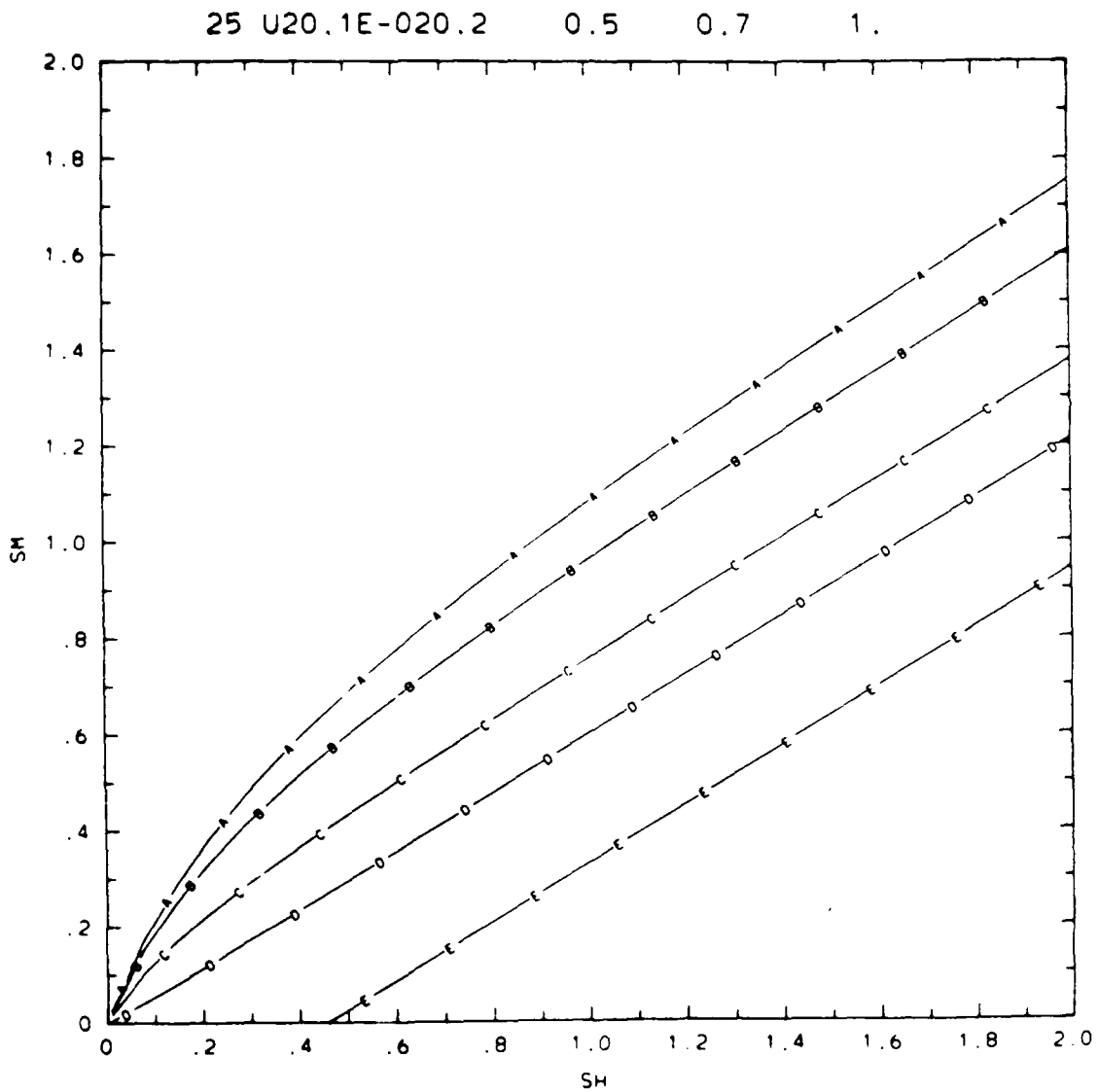

Figure 8

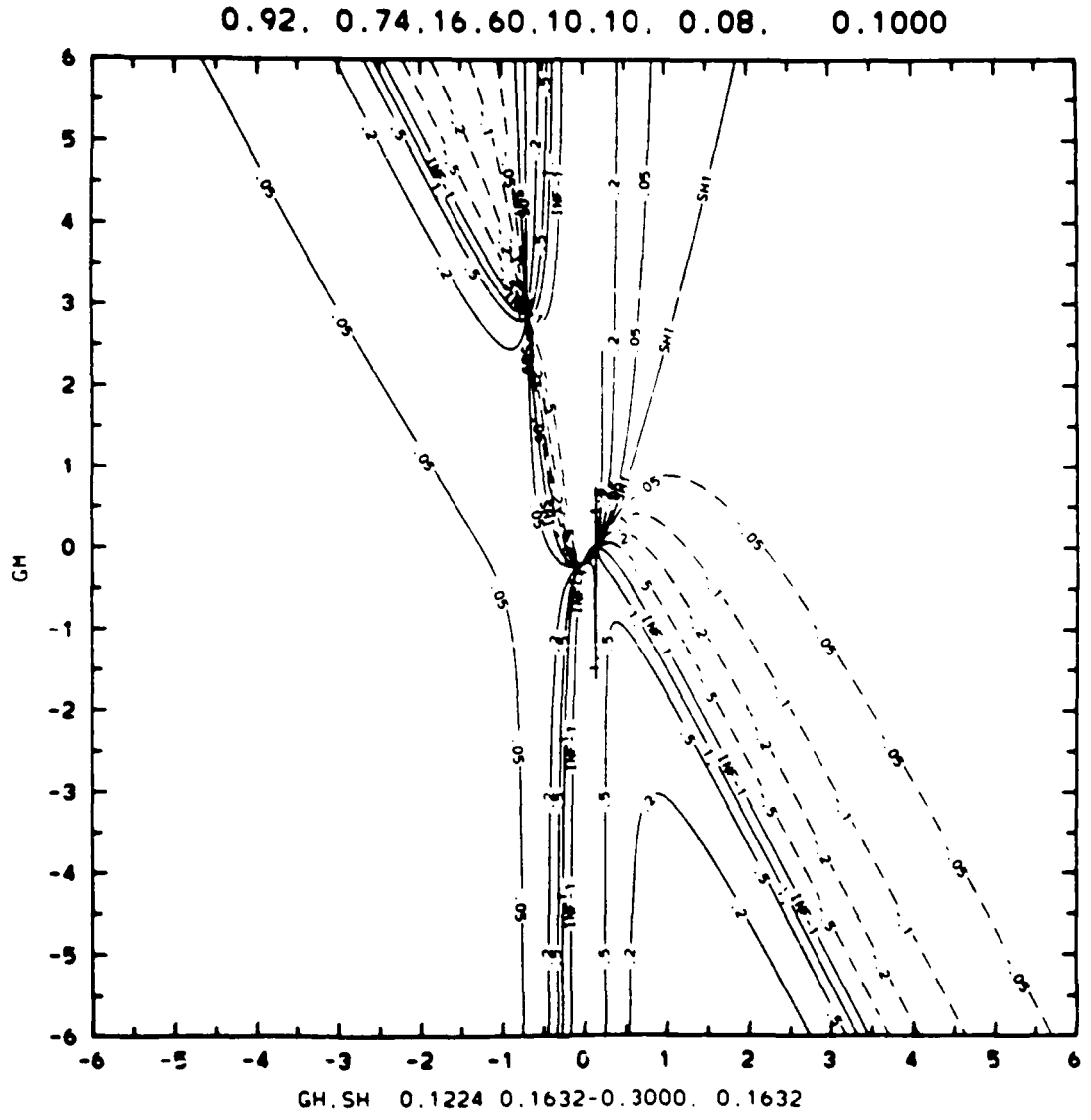

Figure 9

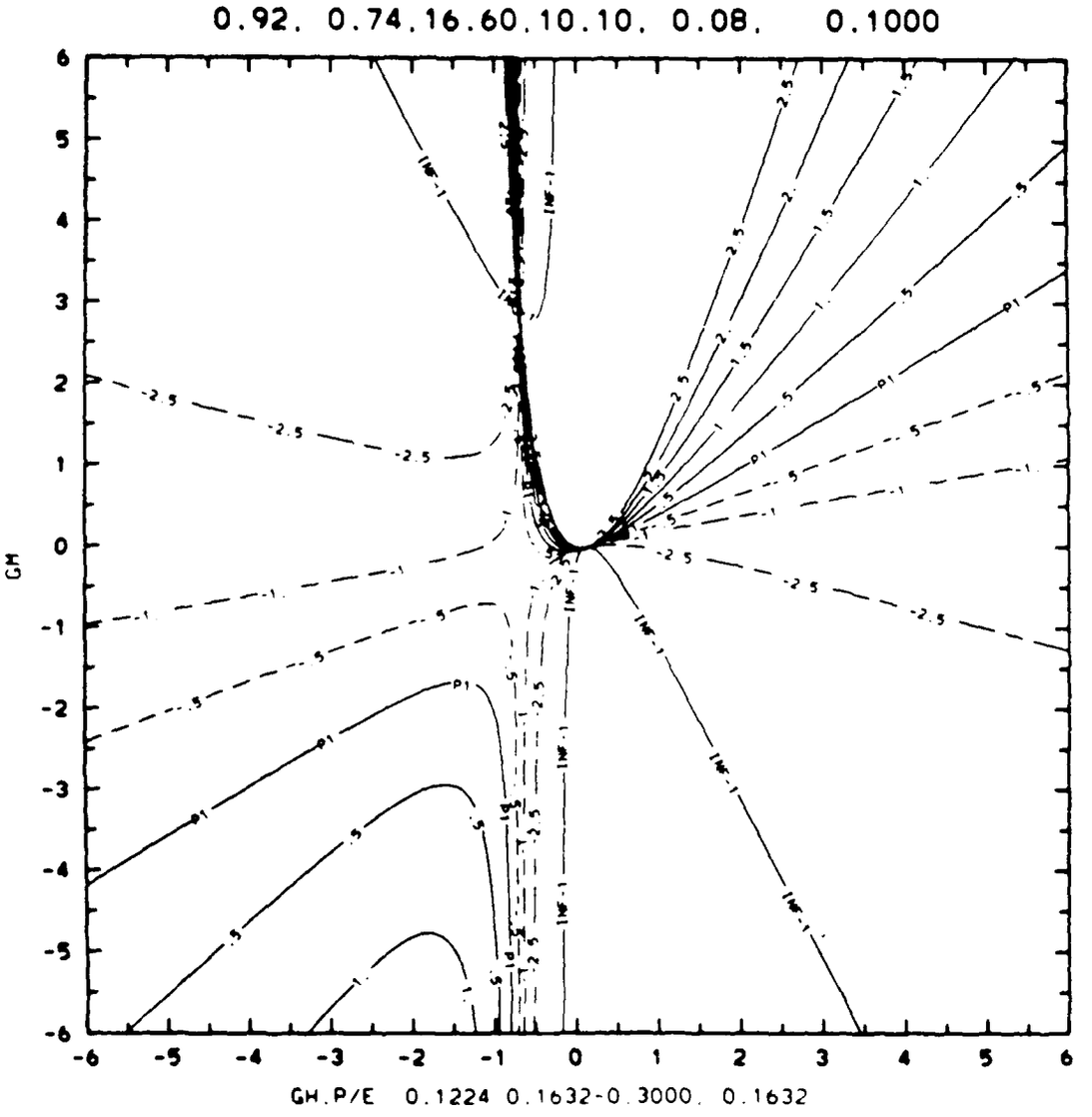

Figure 10a

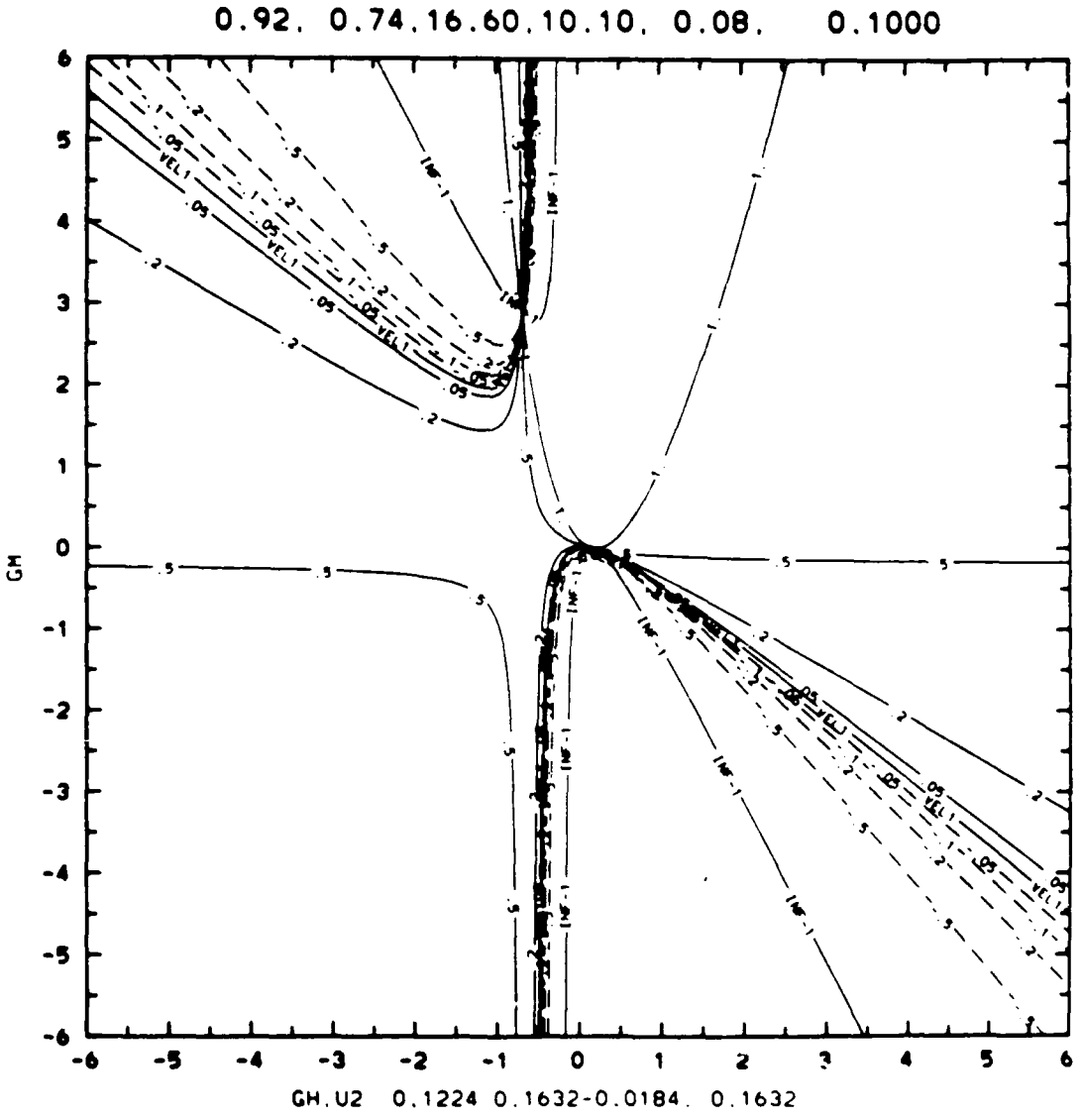

Figure 10b

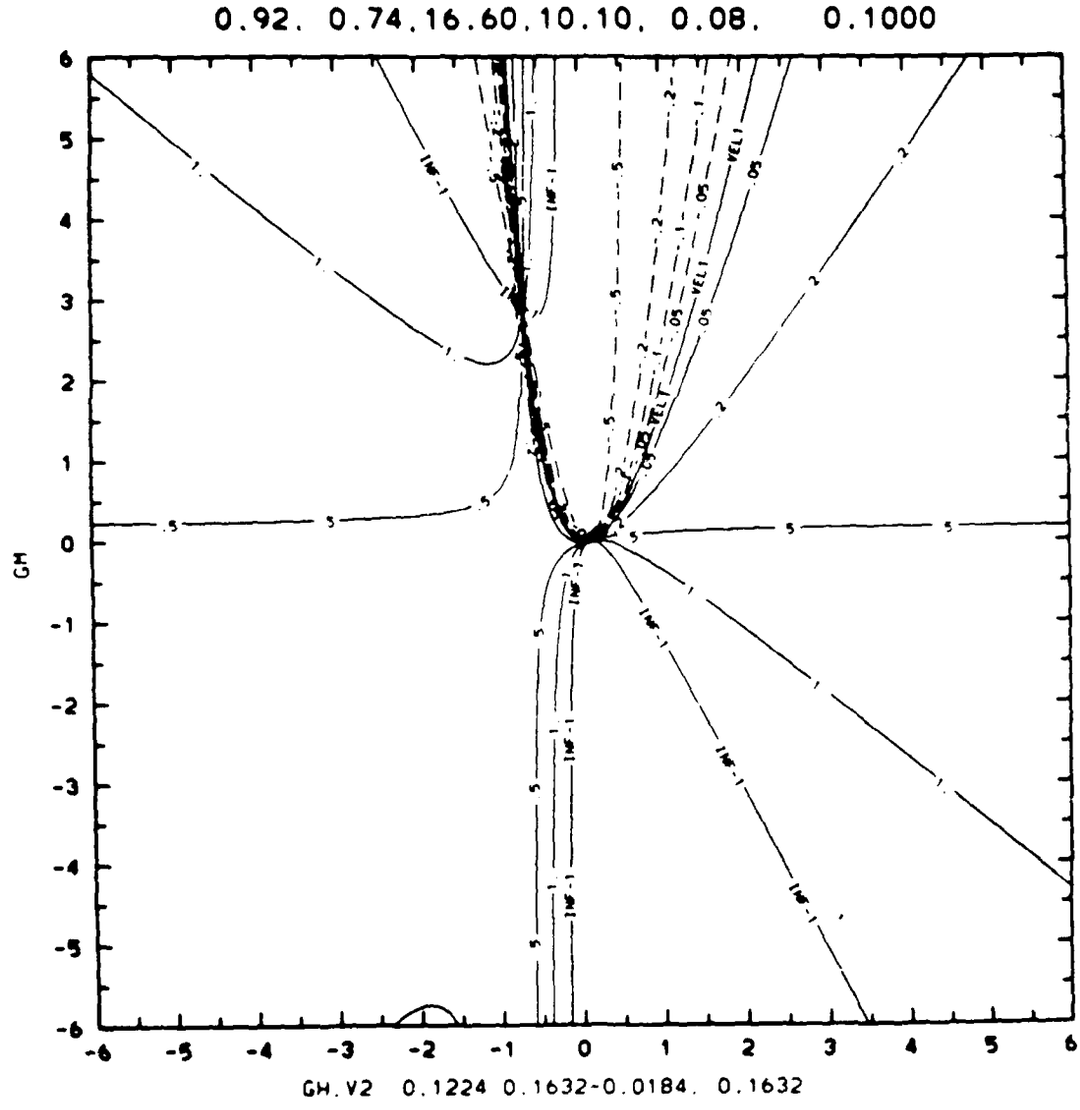

Figure 11a

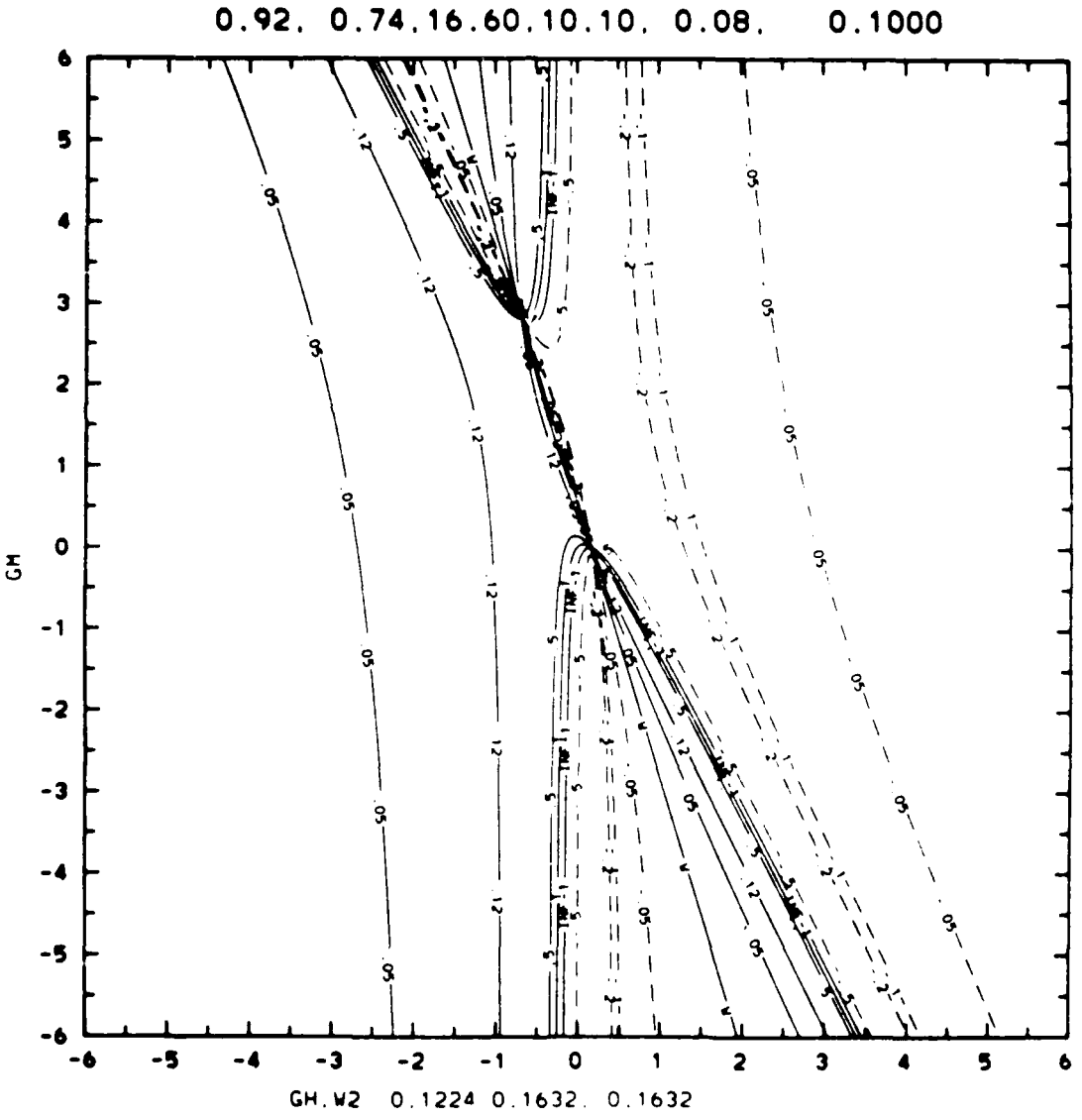

Figure 11b

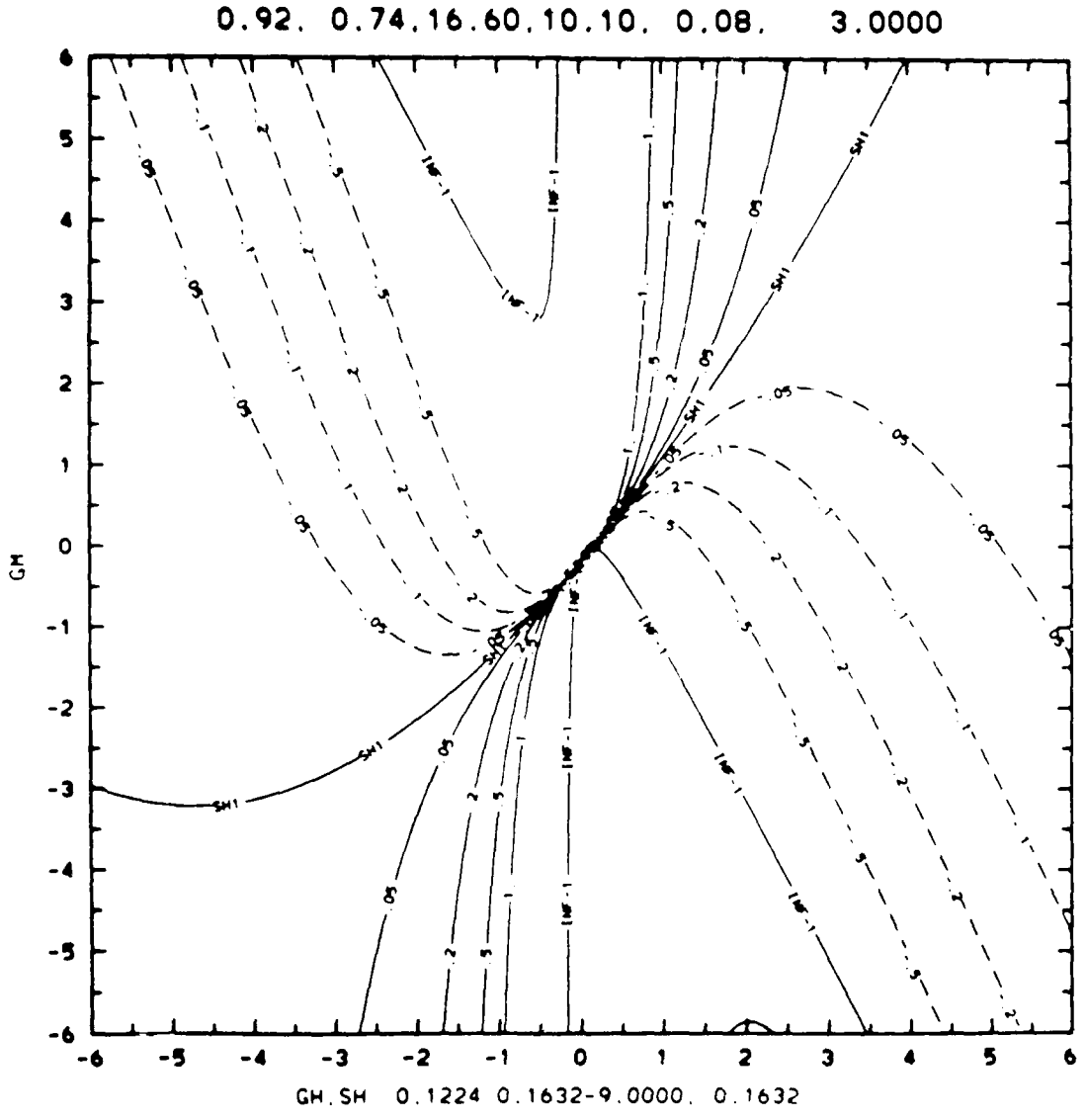

Figure 12

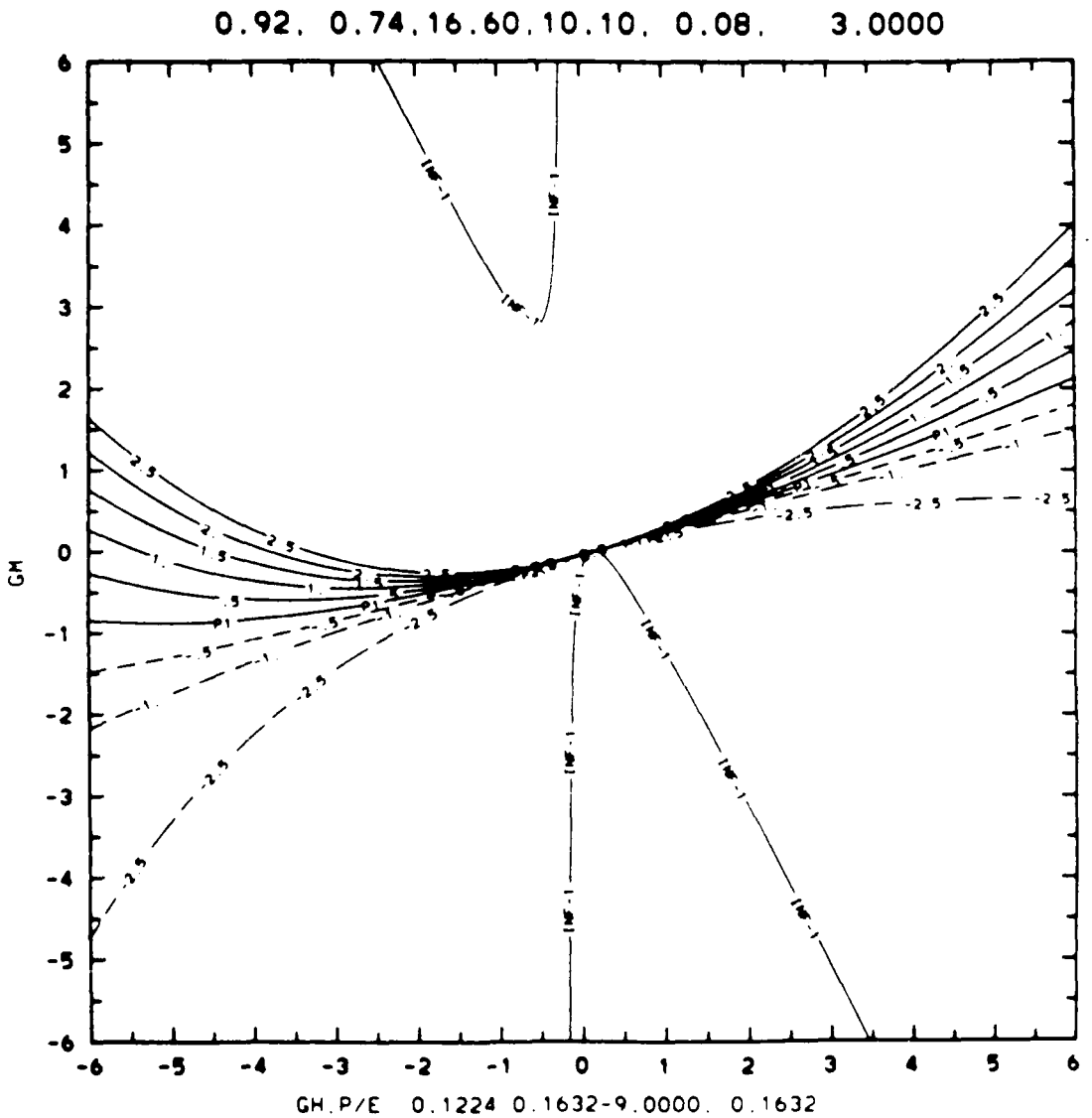

Figure 13a

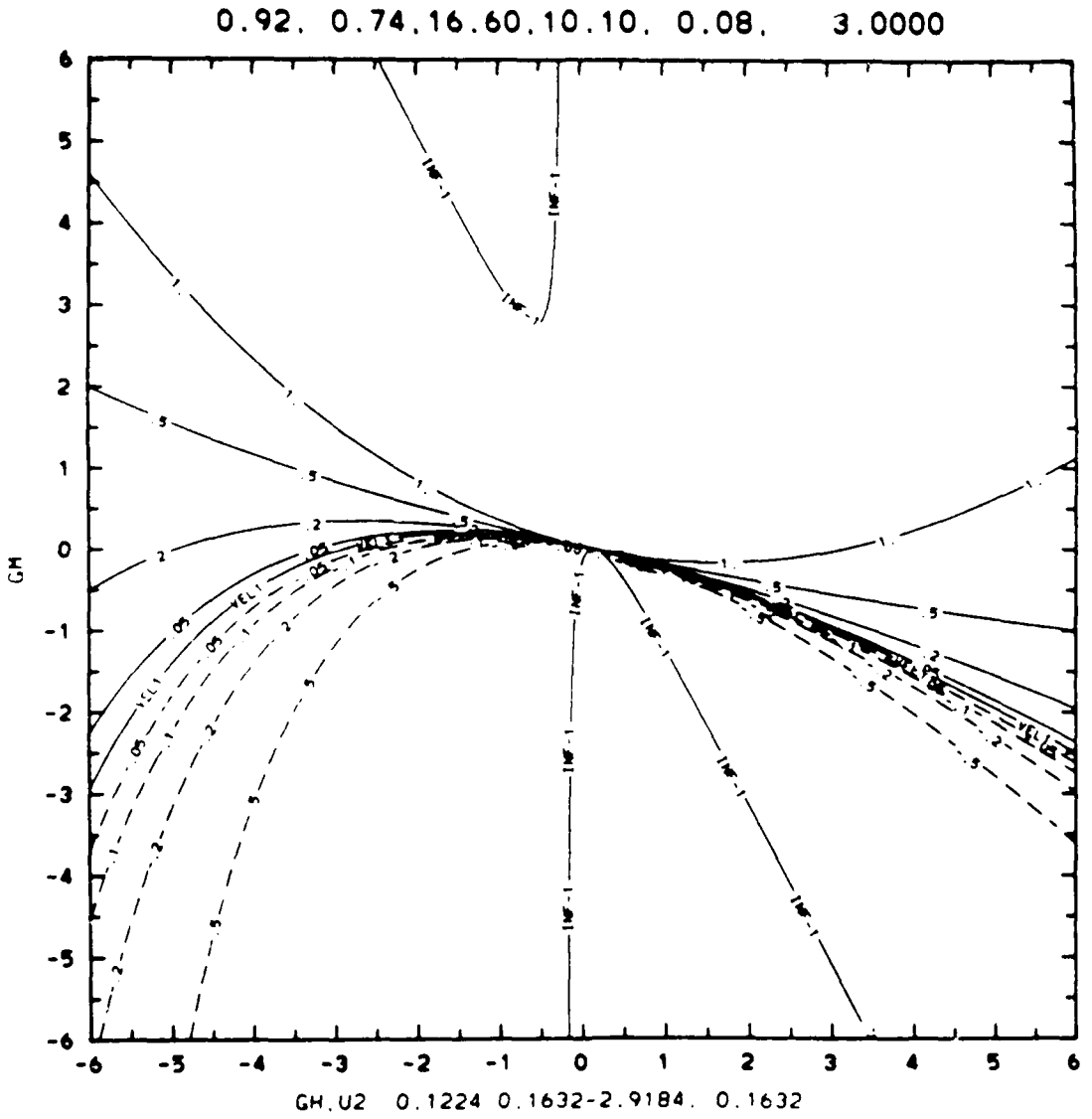

Figure 13b

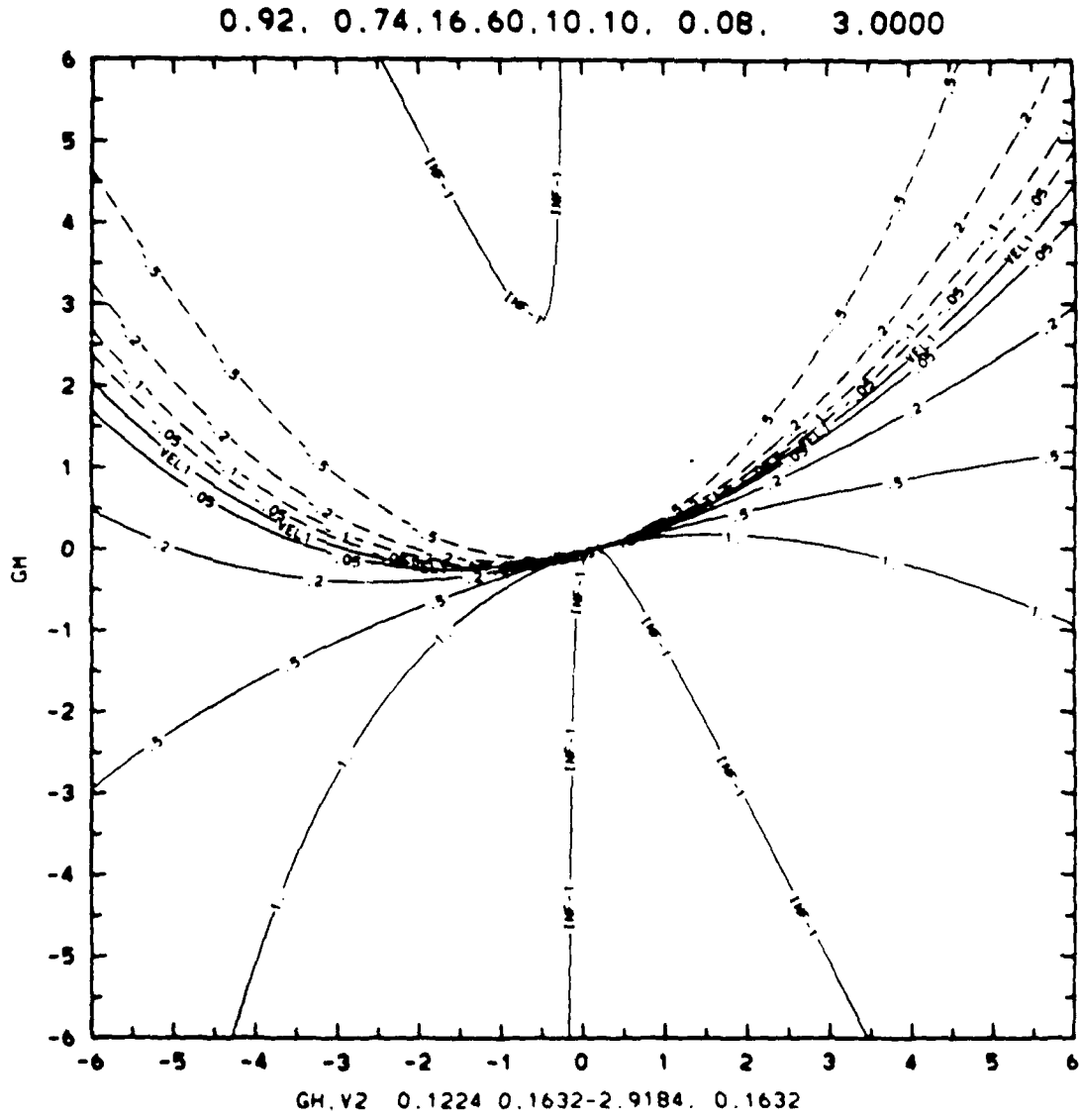

Figure 14a

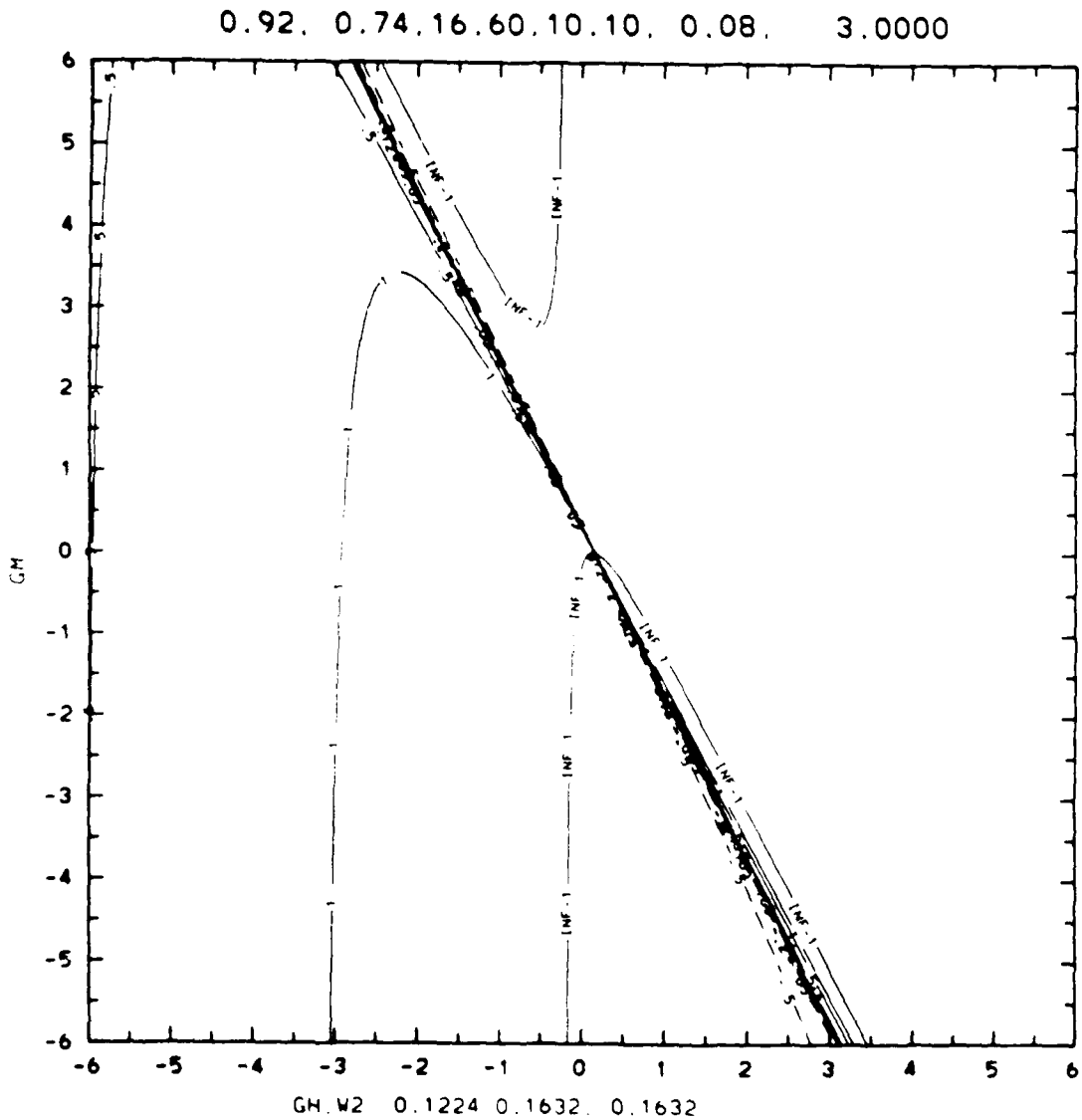

Figure 14b

APPENDIX 2

In proceedings, International Conf. on Development and Application of Computer Techniques to Environmental Studies, November 1986, Los Angeles, CA, USA.

THE REGIONAL ATMOSPHERIC MODELING SYSTEM

C. Tremback. G. Tripoli, R. Arritt, W.R. Cotton and R.A. Pielke

Department of Atmospheric Science, Colorado State University, Fort Collins, Colorado 80523

INTRODUCTION

The numerical atmospheric models developed independently under the direction of William R. Cotton and Roger A. Pielke have recently been combined into the CSU Regional Atmospheric Modelling System (RAMS). RAMS is a general and flexible modelling system rather than a single purpose model. For example, current research using RAMS includes atmospheric scales ranging from large eddy simulations ($\Delta x \approx 100$ m) to mesoscale simulations of convective systems ($\Delta x \approx 100$ km). This paper will discuss the options available in RAMS, the engineering aspects of the system and how the flexibility is attained.

RAMS OPTIONS

RAMS is a merging of basically three models that were designed to simulate different atmospheric circulations. These were a non-hydrostatic cloud model (Tripoli and Cotton[1]) and two hydrostatic mesoscale models (Tremback, et al.[2] and Mahrer and Pielke[3]). Because of this, the modelling system contains many options for various physical and numerical processes. These options are listed below.

1) Basic equations:

   Option 1 - non-hydrostatic time split compressible, (Tripoli and Cotton[1]).
   Option 2 - hydrostatic time split compressible or incompressible, (Tremback et al.[2]).
   Option 3 - quasi-hydrostatic incompressible, (Song et al.[4]).
   Option 4 - hydrostatic incompressible, (Mahrer and Pielke[3]).

2) Dimensionality:

1, 2, or 3 spatial dimensions.

3) Vertical coordinate:

Option 1 - Cartesian
Option 2 - sigma - z

4) Horizontal coordinate:

Option 1 - Cartesian
Option 2 - latitude/longitude

5) Grid stagger:

"Arakawa - C grid"

6) Finite differencing:

Option 1 - leapfrog on long timestep, forward-backward on small timestep, 2nd or 4th order flux conservative advection.
Option 2 - forward-backward time split, 6th order flux conservative (Tremback et al.[5]) or cubic spline advection.

7) Turbulence closure:

Option 1 - Smagorinsky - type eddy viscosity with Richardson number dependence.
Option 2 - eddy viscosity as a function of a prognostic turbulent kinetic energy.
Option 3 - eddy viscosity from O'Brien profile function.

8) Condensation:

Option 1 - grid points fully saturated or unsaturated.
Option 2 - Kuo - type convective parameterization.
Option 3 - Fritsch/Chappell - type convective parameterization.
Option 4 - no condensation.

9) Cloud microphysics:

Option 1 - warm rain processes, (Tripoli and Cotton[6]).
Option 2 - option 1 plus pristine crystals and graupel, (Cotton et al.[7]).
Option 3 - option 2 plus aggregates.
Option 4 - no microphysics.

10) Radiation:

a. Shortwave:
   Option 1 - parameterization described in Chen and Cotton[8].
   Option 2 - parameterization described in Mahrer and Pielke[3].

b. Longwave:
   Option 1 - parameterization described in Chen and Cotton[8].
   Option 2 - parameterization described in Mahrer and Pielke[3].

11) Lower boundary

Option 1 - specified surface temperature and moisture values or fluxes with surface layer similarity parameterization.
Option 2 - surface values obtained from surface energy balance using a prognostic soil model, (Mahrer and Pielke[3]).
Option 3 - modified form of option 2 with prognostic surface equations, (Tremback and Kessler[9]).
Option 4 - option 2 or 3 with vegetation parameterization, (McCumber and Pielke[10]).

12) Upper boundary conditions:

Option 1 - rigid wall.
Option 2 - gravity wave radiative condition.
Option 3 - Raylegh function layer.
Option 4 - prognostic surface pressure (hydrostatic options).

13) Lateral boundary conditions:

Option 1 - Klemp/Wilhelmson radiative boundary.
Option 2 - Orlanski radiative boundary.
Option 3 - Klemp/Lilly radiative boundary.
Option 4 - option 1,2, or 3 with a "mesoscale compensation region" (Tripoli and Cotton[1]).
Option 5 - Perkey and Kreitzberg[11] sponge boundary condition when simulation is run with non-horizontally homogeneous initial conditions.

14) Initialization:

Option 1 - horizontally homogeneous.
Option 2 - option 1 plus variations to force cloud initiation.
Option 3 - NMC data and/or soundings objectively analyzed on isentropic surfaces and

interpolated to the model grid.
Option 4 - NMC data interpolated to the model grid.

As one can see, RAMS is a versatile modelling system. It has been applied to a variety of weather phenomena including:

a) towering cumuli and their modification
b) tropical and mid-latitude cumulonimbi
c) mountain slope and valley circulations
d) orographic cloud formation
e) marine statocumulus
f) mountain wave flow
g) large eddy simulations of power plant plume dispersal
h) mountain generated convective systems
i) mid-latitude convective systems
j) mesoscale transport and dispersion
k) low-level jet simulations
l) atmosphere - soil/vegetation interactions
m) sea breeze simulations

ENGINEERING ASPECTS

Because of the large number of options in RAMS, the structuring of the code needs to be carefully considered. This section will discuss various aspects of the code structure of the system.

Pre-processor The code of RAMS is written in as close to the FORTRAN 77 standard as possible. However, with a program as large as this, the FORTRAN standard is lacking in several features such as global PARAMETER and COMMON statements and conditional compilation. To remedy these insufficiences, the RAMS code takes advantage of a pre-processor written as part of the RAMS package. This pre-processor then produces standard code which can be then compiled on a FORTRAN 77 compatible machine. The pre-processor itself is written in the 77 standard so that the package as a whole is highly portable. It takes full advantage of the character features of FORTRAN and has executed successfully on a number of machines including a VAX, CRAY-1, CRAY-XMP, and CYBER 205 without modification. Some of the features of the pre-processor are described below:

1) By including a character in the first column of a line of code, that line can be "activated" or "eliminated" from the compile file. This allows for conditional compilation of single lines or entire sections of code.

2) A pre-processor variable can be set to a value. This variable can then be used in other expressions including a pre-processor IF or block IF to conditionally set other pre-processor variables. These variables also can be converted to FORTRAN PARAMETER statements which can be inserted anywhere in the rest of the code.

3) A group of statements can be delineated as a "global" which then can be inserted anywhere in the code. This is very useful for groups of COMMON and PARAMETER statements.

4) DO loops can be constructed in a DO/ENDDO syntax, eliminating the need for statement labels on the DO loops.

I/O structure For those machines with limited central memory and a "non-virtual" operating system or for efficiency on virtual systems, RAMS is constructed with a disk I/O scheme. When the scheme is operating, a subset of the model's three-dimensional variables will reside in central memory at any one time. Computations then can be performed with this subset. When these computations are finished, a new subset of three-dimensional variables are requested and computations performed with these. The RAMS structure, thus, is dependent on this I/O scheme and consists of a series of calls to the I/O scheme then the routines which do the calculations.

Modularity For flexibility, RAMS is written as modular as possible. Each individual physical parameterization or numerical process is put in a separate subroutine so that the routines can easily be replaced for different options or with new developments.

Computational routines The routines that do the actual computations for the model are written so that the implementor of a new or replacement routine does not need to be concerned with most of the details of the rest of the model computations. All three-dimensional variables are "passed" to the subroutines through the call statement with other variables passed through COMMON. The implementor then has the flexibility to structure his routine in whatever manner he wishes to produce the desired result. This concept will also make the implementation of routines from other models and programs easier with less modification required.

CONCLUSION

RAMS has been developed at Colorado State University to provide a general and flexible framework for many scales of atmosheric flow simulation. A pre-processor is used to extend the capabilities of standard FORTRAN while the structure of the model allows the implementor much freedom in the developing of individual portions of the model.

RAMS is a research tool and, as such, is not a static program. Some of the developments planned for the system in the near future are two-way interaction nesting capabilities and sixth order leapfrog advection.

ACKNOWLEDGEMENTS

Thanks to Amie Hedstrom for preparing this paper. This work was funded in part by National Science Foundation grant ATM 8312077 and Air Force Geophysics Laboratory contract F19628-84-C-0005.

REFERENCES

1. Tripoli, G.J. and W.R. Cotton (1982), The Colorado State University Three-Dimensional Cloud/Mesoscale Model - 1981. Part I: General Theoretical Framework and Sensitivity Experiments. Journal de Recherches Atmospheriques. Vol. 16, pp. 185-220.

2. Tremback, C.J., G.J. Tripoli and W.R. Cotton (1985), A Regional Scale Atmospheric Numerical Model Including Explicit Moist Physics and a Hydrostatic Time-Split Scheme, pp. 355-358, Preprints of 7th Conference on Numerical Weather Prediction AMS, Montreal, June 17-20.

3. Mahrer, Y. and R.A. Pielke (1977), A Numerical Study of the Airflow Over Irregular Terrain, Beitrage zur Physik der Atmosphare, Vol. 50, pp. 98-113.

4. Song, J.L., R.A. Pielke, M. Segal, R. Arritt and R.C. Kessler (1985), A Method to Determine non-Hydrostatic Effects Within Subdomains of Hydrostatic Model, Journal of Atmospheric Sciences, Vol. 42, pp. 2110-2120.

5. Tremback, C.J., J. Powell, W.R. Cotton and R.A. Pielke (1985), The Forward in Time Upstream Advection Scheme: Extension to Higher Orders, Monthly Weather Review (to be published).

6. Tripoli, G.J. and W.R. Cotton (1980), A Numerical Investigation of Several Factors Contributing to the Observed Variable Intensity of Deep Convection Over South Florida, Journal of Applied Meteorology, Vol. 19, pp. 1037-1063.

7. Cotton, W.R., M.A. Stephens, T. Nehrkorn and G.J. Tripoli (1983), The Colorado State University Three-Dimensional Cloud/Mesoscale Model - 1982. Part II: An Ice Phase Parameterization. Journal de Recherches Atmospheriques, Vol. 16, in press.

8. Chen, C. and W.R. Cotton (1983), A One-Dimensional Simulation of the Stratocumulus-Capped Mixed Layer, Boundary-Layer Meteorology, Vol. 25, pp. 289-321.

9. Tremback, C.J. and R.C. Kessler (1985), A Surface Temperature and Moisture Parameterization for Use in Mesoscale Numerical Models, pp. 355-358, 7th Conference on Numerical Weather Prediction AMS, Montreal, June 17-20.

10. McCumber, M.C. and R.A. Pielke (1981), Simulation of the Effects of Surface Fluxes of Heat and Moisture in a Mesoscale Numerical Model, Part I: Soil Model Layer, Journal Geophys. Res., Vol. 86, pp. 9929-9978.

11. Perkey, D.J. and C.W. Kreitzberg (1976), A Time-Dependent Lateral Boundary Scheme for Limited-Area Primitive Equation Models, Monthly Weather Review, Vol. 104, pp. 744-755.

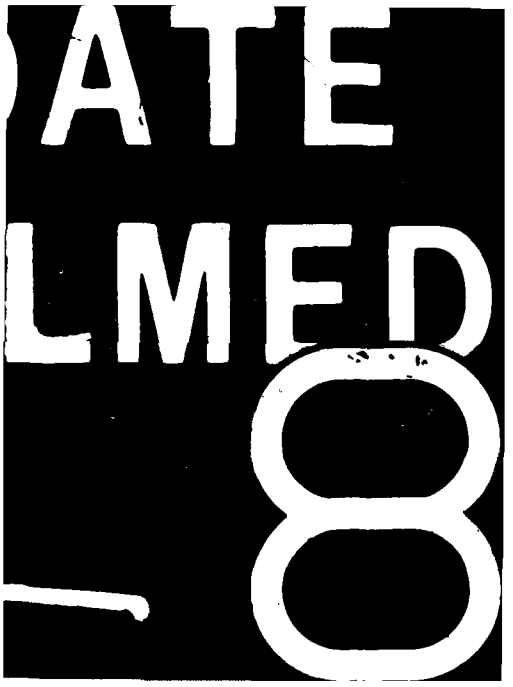
ATE
LMED
8